University of Stavanger

Faculty of Science and Technology

MASTER'S THESIS

Study program/ Specialization: Offshore systems/ Construction	Spring semester, 2010 Open access
Writer: Rasmus Stølsmark	..... (Writer's signature)
Faculty supervisor: Jonas Thor Snæbjørnsson External supervisor(s):	
Titel of thesis: Dynamic Response of a Floating Offshore Wind Turbine	
Credits (ECTS): 30	
Key words: Floating wind turbine Offshore Spar buoy Dynamic response Hywind	Pages: 63 + enclosure: 25 Stavanger, June 14, 2010 Date/year

Dynamic Response of a Floating Offshore Wind Turbine

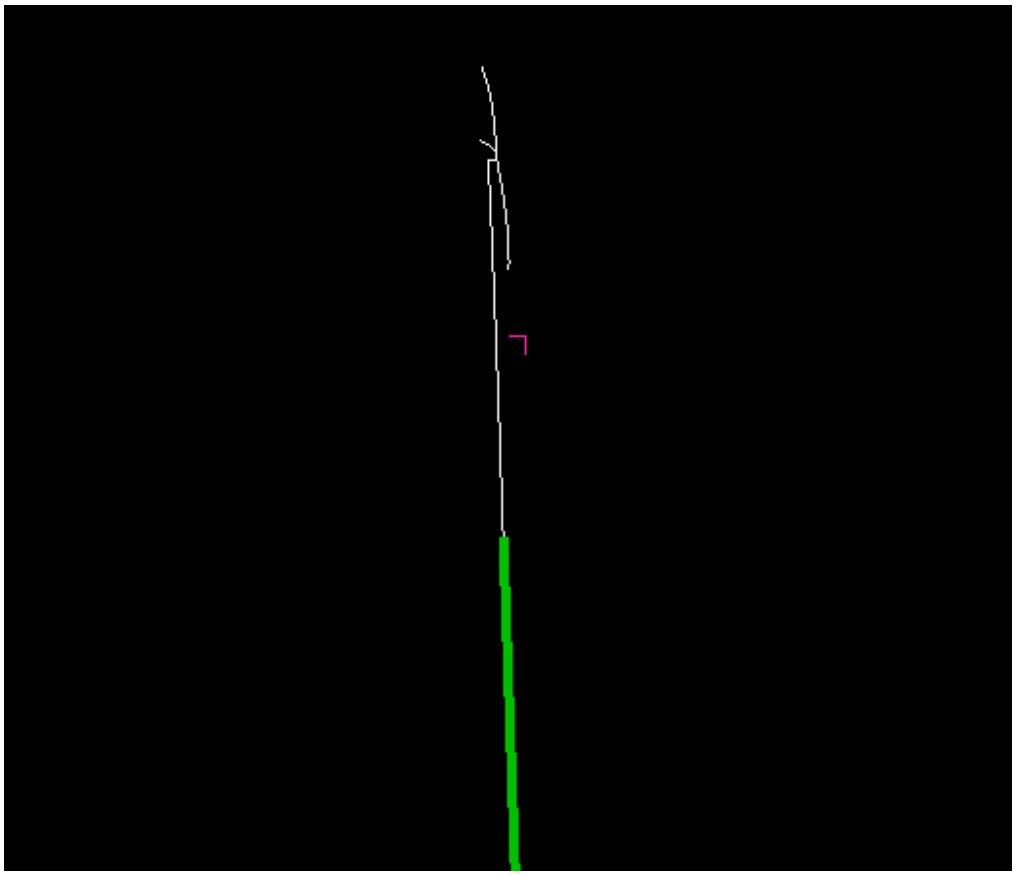

Rasmus Stølsmark

University of Stavanger

June 14, 2010

Abstract

The ever increasing demand for renewable energy, combined with limited areas suitable for large wind farms, has put focus on the development of floating wind turbines. In this thesis the dynamic response of a floating wind turbine, subjected to forces from wind and waves, is analyzed. The wind turbine is of a spar buoy design, similar to Statoil's Hywind project. Simulations with two main type of load cases were run, based on the international offshore wind turbine standard IEC 61400-3. These were normal production, and parked turbine exposed to extreme wind and waves. The results show that the peak response coincides with the largest wave events under production conditions, for all the observed parameters. In extreme conditions the wind and waves have a more equal contribution to the total response. Furthermore, the results indicate that the production load cases governs the design of the rotor blades, while the extreme conditions load cases yields the highest loads in the tower and substructure.

Acknowledgements

First I want to express my gratitude towards my supervisor, Professor Jonas Thor Snæbjørnsson. He willingly spent time on guidance and discussions, even though I often came unannounced. On a couple of occasions my work had come to a complete standstill, but got off to a new start after enlightening discussions with Jonas. Professor Jasna Bogunovic Jakobsen also contributed with some guidance.

Furthermore it was very kind of Risø DTU, the Danish National Laboratory for Sustainable Energy, to let me have a free version of their HAWC2 software. Without its aeroelastic code the dynamic analyses in my thesis would have been virtually impossible to perform. I should also thank the University of Stavanger for sending me on a HAWC2 introduction course in Trondheim, which was crucial to get started with the simulations.

Finally I want to thank my twin brother, Ragnar Stølsmark, who has helped me with feedback on both the layout and the writing of this thesis.

List of symbols and units

a	axial induction factor, [-]
a'	angular induction factor, [-]
a_g	horizontal distance to weight (rotor), [m]
A	wave amplitude, [m]
A_{swept}	rotor swept area, $[\mathrm{m}^2]$
B	number of rotor blades, [-]
BM	distance from centre of buoyancy to metacentre, [m]
c	cord length, [m]
C_d	aerodynamic drag coefficient, [-]
C_D	hydrodynamic drag coefficient, [-]
C_I	hydrodynamic inertia coefficient, [-]
C_l	aerodynamic lift coefficient, [-]
C_L	hydrodynamic lift coefficient, [-]
C_p	power coefficient, [-]
dT	thrust force on annular stream tube, [N]
dQ	torque on annular stream tube, [N]
D	diameter, [m]
$f(z,t)$	hydrodynamic force per unit length, [N/m]
f_I	hydrodynamic inertia force per unit length, [N/m]
f_D	hydrodynamic drag force per unit length, [N/m]
F_d	drag force, [N]
F_l	lift force, [N]
F_x^{moor}	mooring force in global x-direction, [N]
F_y^{moor}	mooring force in global y-direction, [N]
F_z^{moor}	mooring force in global z-direction, [N]
$F_X(x)$	cumulative distribution function, [-]
GM	metacentric height, [m]
I	turbulence intensity, [-]
I_T, I_g	mass moment of inertia about an axis through the centre of gravity, $[\mathrm{kgm}^2]$
k	wave number, $[\mathrm{m}^{-1}]$
k_v	von Karman constant, [-]
KB	distance from keel to centre of buoyancy, [m]
KG	distance from keel to centre of gravity, [m]
l	airfoil span, [m]
L	wave length, [m]

M_z^{moor}	mooring moment in yaw-direction, [Nm]
p	Prandtl tip loss factor, [-]
P	rotor power, [W]
r_h	hub radius, [m]
R	outer blade radius, [m]
Re	Reynolds number, [-]
T_{roll}	roll period, [s]
u	water particle velocity, [m/s]
V	wind speed, [m/s]
$\bar{V}$	mean wind speed, [m/s]
V^*	friction velocity for logarithmic wind profile, [m/s]
$V(z)$	wind speed at height z, [m/s]
$V(z_r)$	wind speed at reference height, [m/s]
V_{rel}	relative wind velocity, [m/s]
V_{Rotor}	wind speed at rotor
W_g	weight of body (rotor), [N]
z_0	surface roughness for logarithmic wind profile, [m]
z_i	initial vertical position of the mooring connection point, [m]
z_r	reference height, [m]
α	wind shear power law exponent, [-]
β	shape parameter in 3-p Weibull distribution, [-]
γ	location parameter in 3-p Weibull distribution, [same as stochastic variable]
δ	logarithmic decrement, [-]
Δ	weight of displaced water, [N]
ζ	damping ratio, [-]
$\eta(x,t)$	water surface profile, [m]
θ_z	yaw position, [rad]
λ	scale parameter in 3-p Weibull distribution, [-]
ν	kinematic viscosity, $[\mathrm{m}^2/\mathrm{s}]$
ρ_{air}, ρ_w	density of air and water respectively, $[\mathrm{kg}/\mathrm{m}^3]$
σ	wind speed standard deviation, [m/s]
σ'	local solidity, [-]
φ	angle of relative wind,[rad]
ω	angular velocity of the wind, [rad/s]
ω_g	angular velocity of precession, [rad/s]
ω_w	wave frequency, [rad/s]
Ω, Ω_g	angular velocity of the wind turbine rotor, [rad/s]

Contents

1 Introduction

Global warming and dwindling oil reserves have increased the focus on development of renewable energy sources, without the large CO2-emmissions associated with combustion of fossil fuels. One of the solutions to this challenge is wind energy. Wind turbines have been used to commercially produce electricity for more than one hundred years [1], with considerable investments in research and development until present day. Hence wind energy is more mature than many of its renewable energy competitors, for example wave energy.

One problem with wind turbines is the large amount of area required to construct a so-called wind farm, a site with multiple wind turbines. To minimize the effect of turbulence from other turbines, a spacing of 10 times the rotor diameter parallel to the prevailing wind direction, and 3-4 rotor diameters perpendicular to the wind, is advised [1]. A large wind farm may then occupy several hundred square kilometers, although this area in many cases might be combined with agriculture. When noise and visual impact from the wind turbines are included, the number of land sites available for large wind farms are limited, especially in Europe. This makes room for development of wind farms offshore, where large areas with, in general, more favorable wind conditions are available.

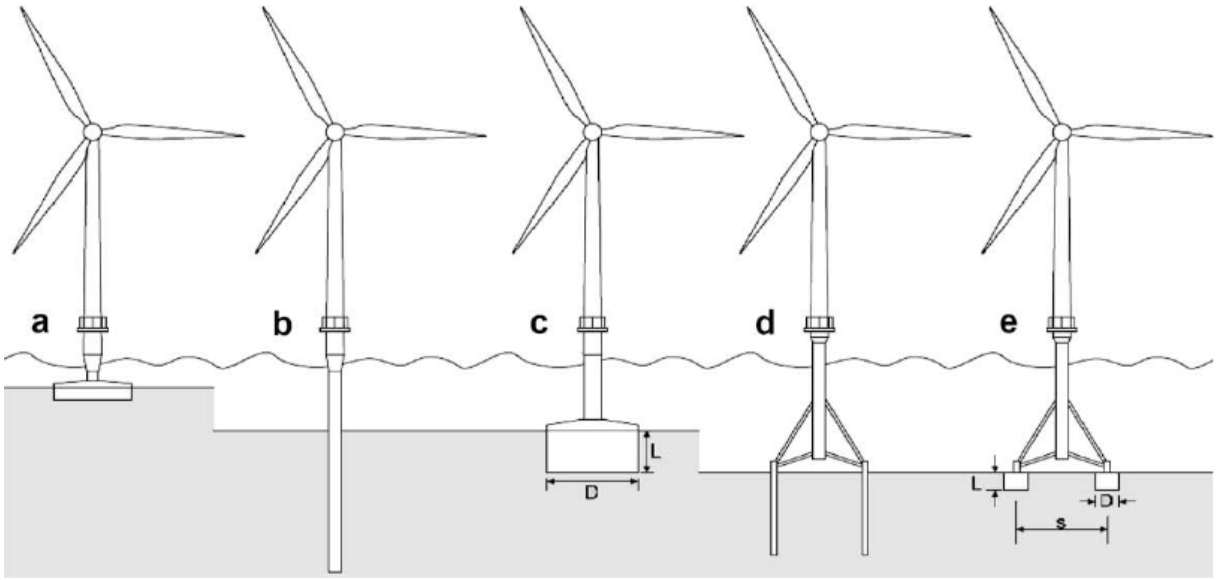

Figure 1: Various foundations for bottom-fixed offshore wind turbines [2].

Until recently, virtually all offshore wind turbines have been installed in shallow water depths up to 30 m, using monopile or gravity based foundations [2] (illustrated in figure 1 as a and b respectively). However in many countries, like Norway, China and the United states, most of the offshore wind resources are associated with deeper waters [3]. For water depths up to 60 m or so, space frame substructures with multiple footings are necessary to provide sufficient stability at a reasonable cost [2]. They can be fixed to the bottom by piles (fig. 1d) or suction piles (fig. 1e). At even deeper waters, bottom-fixed structures do not seem to become economically feasible, and floating solutions must be deployed.

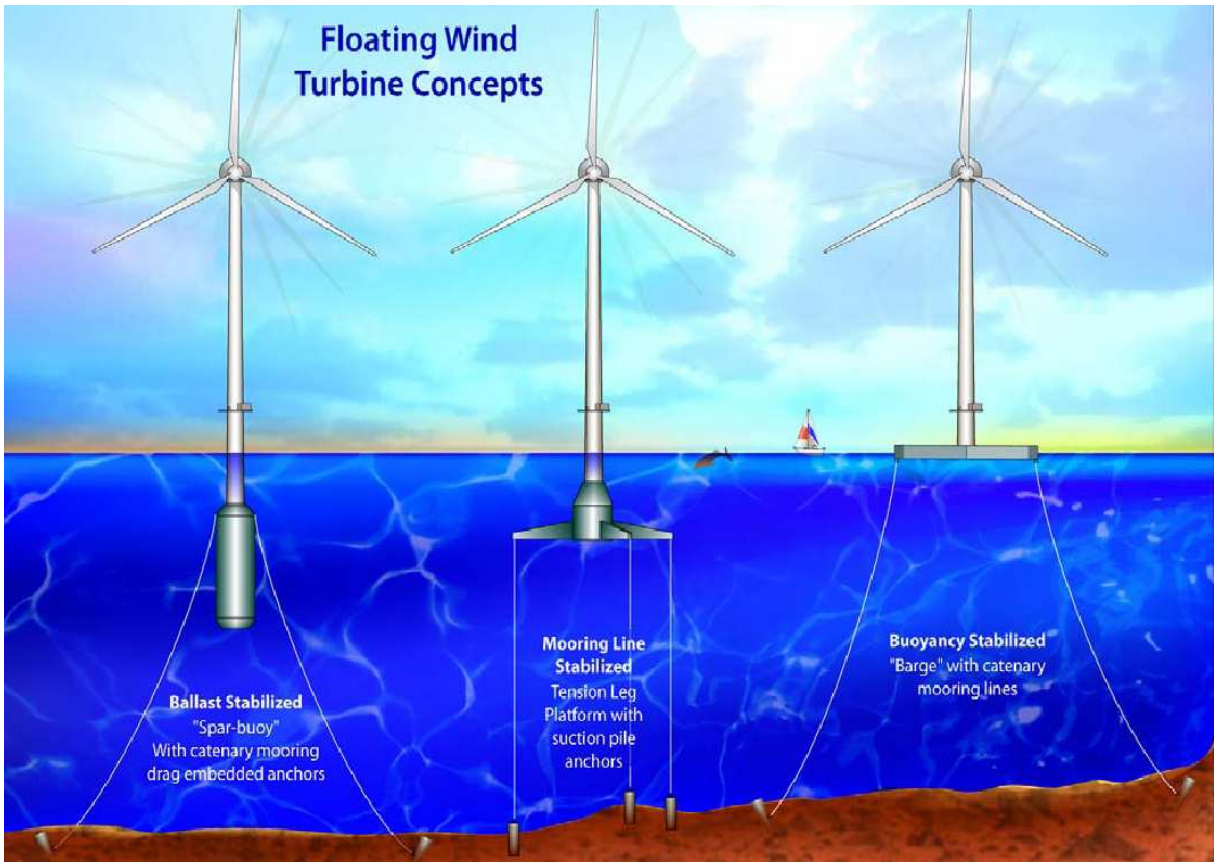

Figure 2: Proposed floating wind turbine concepts [3].

The three main floating wind turbine concepts being evaluated for deep water sites are shown in figure 2. The ballast stabilized concept to the right uses ballast to lower the centre of gravity below the centre of buoyancy, thus ensuring stability. Then there is the tension leg concept, where the wind turbine is placed on a hollow substructure with a large buoyancy surplus. The structure is kept stable by tensioned steel pipes, anchored to the seabed using suction piles. The concept to the right in figure 2 simply places the wind turbine on a sufficiently stable moored barge. Hybrids of these concepts are also a possibility, e.g. the Norwegian Sway project which might be described as a ballast stabilized tension leg concept [4]. Solutions with multiple wind turbines on a single floating platform have also been proposed [5]. Common for most of these concepts are that they are still on the drawing board. Currently the world's only installed full scale floating wind turbine is Statoil's Hywind [6].

1.1 Hywind

Hywind is a 2.3 MW prototype floating wind turbine, placed in the North Sea 10 km west of Karmøy, Norway. The intention of the Hywind project is to test how waves and wind affects the structure, allowing optimization of the design to reduce costs. This is essential to reach Statoil's goal of making floating wind turbines commercially viable.

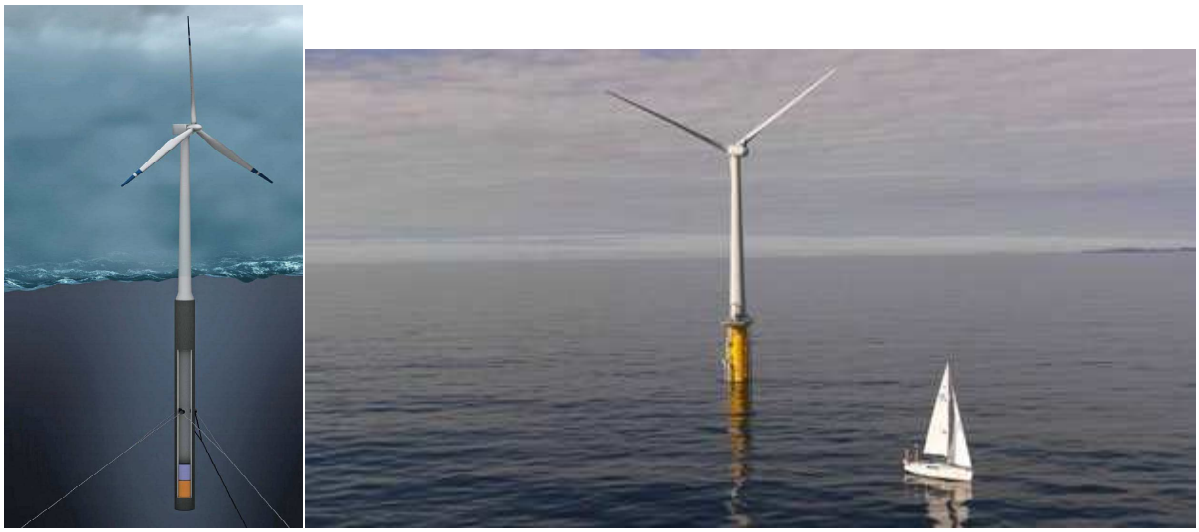

Figure 3: The Hywind floating wind turbine concept [6].

Hywind is of a ballast stabilized design, designed to operate in 120-700 m water depth. The rotor diameter is 82.4 m, and the nacelle is 65 m above mean sea level. It is kept in place by three slack anchored mooring lines, connected to the hull by "crowfoots" to increase yaw stiffness [7]. The term "crowfoot" implies that each mooring line has two connection points, as illustrated in figure 3.

One of the most innovating features of Hywind is the active damping pitch control system [7]. Normal procedure for pitch controlled fixed wind turbines is to adjust the blade pitch to generate constant power, for relative wind speed above the turbine's rated wind speed. However for floating wind turbines this tends to introduce negative damping of the tower motion. The active damping system uses measurements of the tower's velocity to optimize the pitch, both with respect to damping of the tower motion and keeping the power output at constant level.

It is also worth noting the assembly and installation of Hywind [6]. The substructure was manufactured in Finland and towed to Åmøyfjorden, near Stavanger, where it was upended in April 2009. The tower, nacelle and rotor were assembled onshore in Dusavika. The final assembly was completed inshore in Åmøyfjorden, before the complete structure in June 2009 was towed to the offshore test site in upright position. Besides the towing, the only offshore work needed were connection of mooring lines and the electric cable. Considering the large costs associated with offshore work, this might be an important advantage for the Hywind concept.

The wind turbine analyzed in this thesis is of the same spar buoy concept as Hywind. However, the properties of the turbine are based on a benchmark wind turbine from the American NREL. While a detailed description of the NREL turbine is available [8], are only the gross properties of the Hywind project made public.

1.2 Outline

Chapter 2 gives a brief summary of some of the theoretical background that is essential to understand floating wind turbines. It also explains parts of the theory behind some of the techniques used in this thesis, including the HAWC2 code.

In chapter 3 the wind turbine model, and the different load cases, are described in detail. Some limitations of the analysis are also listed here.

Chapter 4 presents the results of the simulations, mainly in the form of tables. Most of these show the maximum value of the observed parameters during each simulation, and also the mean maximum values for load cases that includes stochastic wind or waves.

Chapter 5 evaluates and discusses the results of the simulations. The conclusions are then presented in chapter 6, along with a suggestion of modification for possible future analyses.

2 Theory

2.1 Wind

The wind resource is of a fluctuating nature, with large variations of wind speed in both time and space. On a global scale the geographical variation is caused by differences in the solar radiation hitting the earth, resulting in largest surface heating on land masses near the equator [9]. The heated air rises in the atmosphere and returns to the surface in cooler areas. The rotation of the earth enhances the effect of this phenomenon, creating a worldwide circulation pattern. On a continental scale this pattern is disturbed by the distribution of land and oceans, which results in somewhat unpredictable changes of the weather.

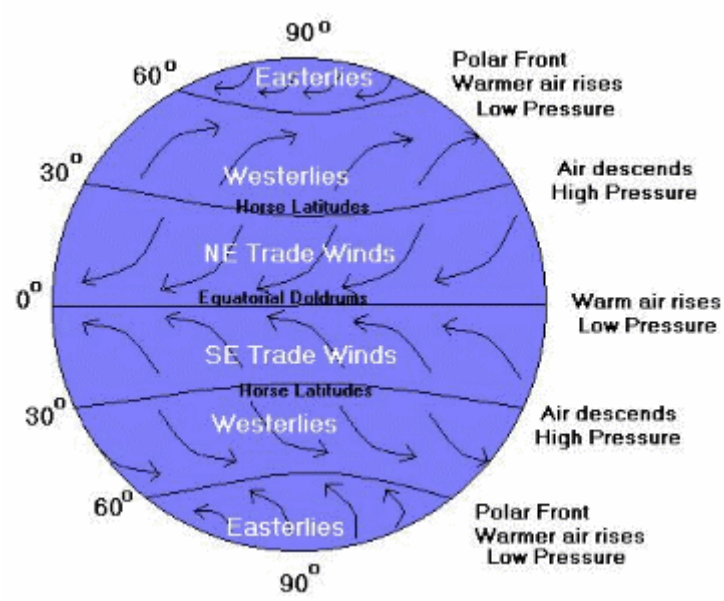

Figure 4: Sketch illustrating global wind patterns [10].

On a more local scale, the wind is greatly influenced of topographical features like mountains, hills and valleys. The wind speed increases when the air is forced over a hill or through narrow mountain passes, in addition to the wind speed generally increasing with height above ground. Local thermal effects also add to the complexity. This is e.g. seen in coastal areas, where cool sea air replaces hot air rising over land during sunny days. During the night the land cools down quicker than the sea, and the wind reverses.

A regular change in wind speed at specific times of day, such as the sea breeze of coastal areas, is called diurnal variation. On a somewhat longer timescale of several days, are the so-called synoptic variations. These are associated with the passing of high and low pressures, which temporarily increases the wind speed. Then there are the seasonal variations, for example in temperate latitudes the winter months tend to be significantly windier than the summer months [9]. Seasonal variations are in general more predictable than synoptic variations, which have a more random nature.

2.2 Turbulence

The highest frequency wind variations are called turbulence. The term in general covers all random variation of wind speed with a period of less than 10 minutes [11]. These fluctuations occur in the longitudinal (prevailing wind direction), vertical and horizontal direction. Turbulence can be seen as random variation about the mean wind speed, and have a zero mean when averaged over 10 minutes. The two main sources of turbulence are friction with the earth's surface, and thermal effects that moves the air vertically.

For calculating design loads on structures affected by wind, turbulence is usually described by the turbulence intensity. Turbulence intensity is defined as the ratio between the standard deviation of the wind speed and the mean [11]:

$$I = \frac{\sigma}{\bar{V}} \tag{1}$$

Typical values are between 0.1-0.4. In general, the turbulence intensity is highest at low wind speeds, and is limited downwards by the terrain features and surface roughness at the given location. For example one can expect higher turbulence intensity in cities than over open waters.

There are several methods that can be used to model turbulence. In this thesis the Mann turbulence model is chosen, which is also recommended in the international wind turbine standard IEC 61400-1 [12]. The theoretical background of the Mann turbulence model is quite comprehensive and will not be presented here, but a detailed description of the model is given in Annex B of IEC 61400-1, third edition.

2.3 Vertical wind shear

Vertical wind shear, or vertical profile of the wind speed, is the variation of horizontal wind speed with height above the ground. This is important for wind turbines primarily of reasons; the first being that the wind energy potential changes at different hub heights. And secondly that wind shear continuously changes the aerodynamic loading on the rotating turbine blades, resulting in additional fatigue damage. There are two main mathematical models used to describe this phenomenon; the logarithmic profile and the power law [11].

The equation describing the logarithmic wind profile is:

$$V(z) = \frac{V^*}{k_v} \ln\left(\frac{z}{z_0}\right) \tag{2}$$

where the surface roughness z_0 describes the roughness of the terrain on the ground. The friction velocity $V^*$and z_0 can be calculated from experimental data. z_0 for different types of terrain is also typically given in standards.

The power law is of the form:

$$\frac{V(z)}{V(z_r)} = \left(\frac{z}{z_r}\right)^{\alpha} \tag{3}$$

where the wind speed can be calculated based on the wind speed at a reference height z_r. The exponent α is highly variable, and must be determined empirically. Typical values of α are around 0.1-0.2, but it changes with parameters like altitude, temperature, season etc.

As recommended in the international offshore wind turbine standard IEC-61400-3 [13], a power law profile with an exponent of 0.14 is used in the simulations in this thesis. Some exceptions occur in load cases involving certain gust events and extreme wind speed, in compliance with the standard.

2.4 Energy potential

The power output P from a wind turbine with rotor swept area A_{swept} is proportional to the cube of the wind speed, and can be calculated from the following equation [11]:

$$P = \frac{1}{2} C_p \rho_{air} A_{swept} V^3 \tag{4}$$

The power coefficient C_p describes the fraction of the power in the wind that is converted into rotor power. It can be shown that the theoretical maximum C_p for a wind turbine is 0.593. This is also known as the Betz limit [9]. In practice, including mechanical losses in the generator etc., a maximum of about 45 % of the available energy in the wind is harvested by modern horizontal axis wind turbines [11].

From eq. (4) it is obvious that relatively small changes in the mean wind speed will have a significant impact on the overall energy production. For example a wind speed increase of 14 % from 7 to 8 m/s, will lead to a 49 % increase in the power output. Clearly enough to make or break the economic potential of an otherwise promising wind farm site.

2.5 Airfoil

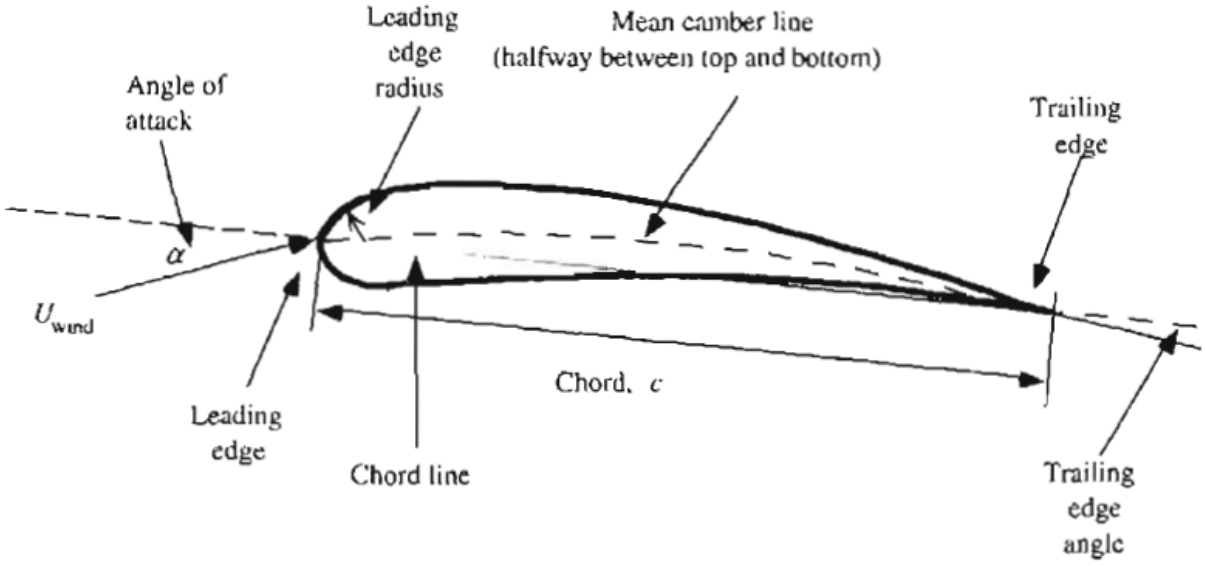

Figure 5: Sketch showing key parameters in airfoil design [11].

The cross section of a wind turbine blade has the shape of an airfoil, as shown in figure 5. The air hits the blade with the so-called relative wind velocity (U_{wind} in figure 5), the resultant of the wind velocity and the tangential velocity due to the rotation of the blade. When a stream of air passes an airfoil, air flowing over its upper side travels a longer distance than air flowing on its lower side due to the geometry of the airfoil. This increases the flow velocity on the upper surface of the blade, thus reducing the static pressure according to Bernoulli's theorem [1]. The pressure differential creates a net upwards force on the blade. The component of this force perpendicular to the relative wind direction is called lift force. The component parallel to the relative wind direction is called drag force, which also has contribution from viscous friction [11]. The lift force is given by:

$$F_l = \frac{1}{2} C_l \rho_{air} c l V_{rel}^2 \tag{10}$$

where c is the chord length and l is the airfoil span.

Similarly the drag force is given by:

$$F_d = \frac{1}{2} C_d \rho_{air} c l V_{rel}^2 \tag{11}$$

For a given airfoil, the lift and drag coefficients are functions of the angle of attack, α, and the Reynolds number, Re [11]. The angle of attack is the angle between the relative wind direction and the chord line, as shown in figure 5. The Reynolds number is a non-dimensional parameter describing the characteristics of fluid flow conditions, and is defined as:

$$Re = \frac{Vc}{\nu} = \frac{Inertial\ force}{Viscous\ force} \tag{12}$$

The lift coefficient increases approximately linearly with increasing angle of attack, until it reaches a critical value where the lift is reduced and drag increases rapidly. This phenomenon is known as stall, and its effect on lift and drag coefficients for a typical airfoil is shown in figure 6. When stall occurs the boundary layer on the upper surface is separated, and a turbulent wake forms above the airfoil [9].

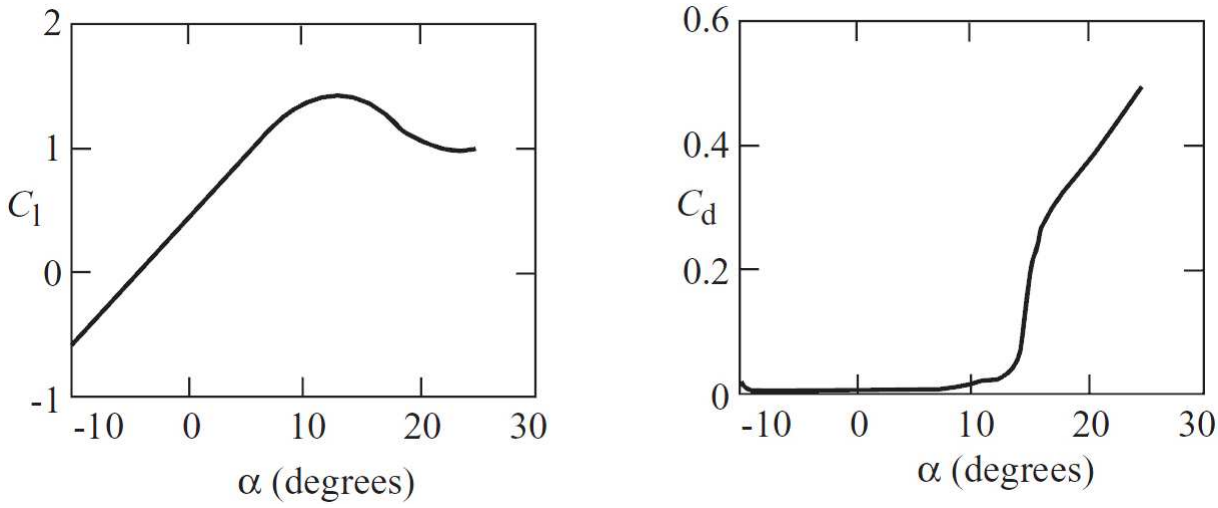

Figure 6: Lift and drag coefficient as a function of angle of attack for a typical Airfoil, with critical angle of attack (stall angle) at approximately 13 degrees. The Reynolds number is kept constant [9].

Another important parameter is the axial induction factor, a. It describes the fractional decrease in wind velocity between the undisturbed wind and the wind at the rotor [11]:

$$a = \frac{V - V_{Rotor}}{V} \tag{13}$$

Similarly, an angular induction factor a' describes the change of tangential velocity the air flow experience as it passes the rotating blades:

$$a' = \frac{\omega}{2\Omega} \tag{14}$$

2.6 Blade element momentum theory

The blade element momentum theory is a widespread model for calculating wind turbine aerodynamics, and is included in the HAWC2 code used in this thesis. It is basically a combination of the momentum theory and the blade element theory.

The momentum theory utilizes conservation of momentum to calculate forces and flow conditions on a rotor with infinite number of blades, since force equals the rate of change of momentum [11]. By considering an ideal rotor placed in a stream tube, and applying the Bernoulli's equation and basic algebra, the thrust force experienced on an annular stream tube of thickness dr and radius r can be expressed as [11]:

$$dT = 4a(1-a)\rho_{air}V^2\pi r dr \tag{15}$$

Similarly, an expression for the torque acting on the stream tube can be developed:

$$dQ = 4a'(1-a)\rho_{air}V\pi r^3\Omega dr \tag{16}$$

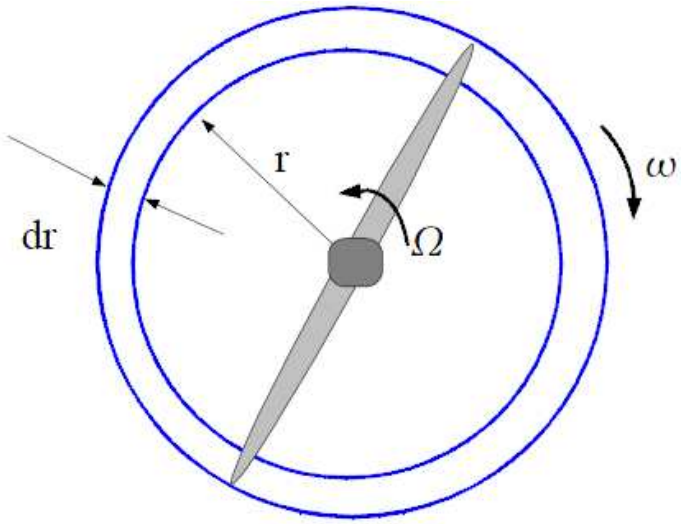

Figure 7: Notation used in describing a rotating annular stream tube [14].

As illustrated in figure 8, the blade element theory is based on dividing the blades into *N* elements in the span wise direction. Two key assumptions are made [11]:

- There is no aerodynamic interaction between blade elements.
- The forces on the blades are determined solely by the lift and drag characteristics of the airfoil shape of the blades.

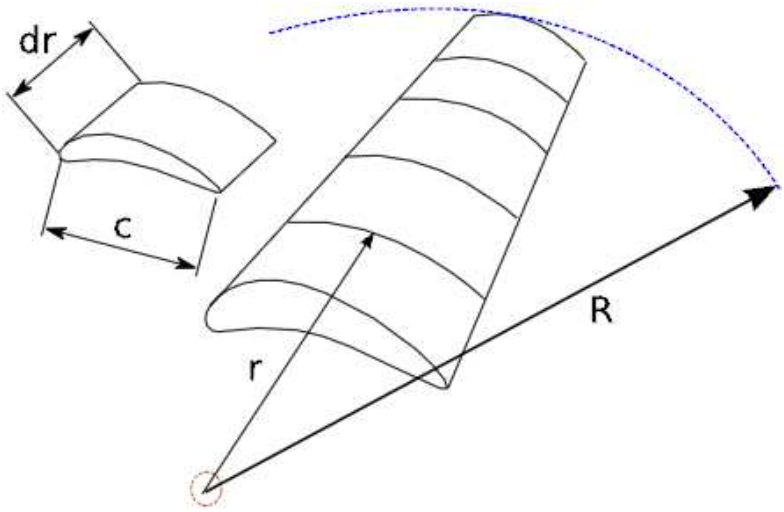

Figure 8: Illustration of the blade element model[14].

The tangential speed of the rotor is proportional with the radius, r, thus the relative wind velocity increases towards the blade tip. And as the cord length and angle of attack in modern wind turbines typically varies along the blade, the forces on two separate elements may differ significantly. As for the momentum theory, expressions for torque and thrust force can be established. For a turbine with total number of blades B, it can be shown that

the thrust force on a section at a distance, r, from the centre is [11]:

$$dT = \frac{1}{2} B \rho_{air} V_{rel}^2 (C_l \cos\varphi + C_d \sin\varphi) c dr \tag{17}$$

where φ is the angle of relative wind, which is the angle between the plane of rotation and the relative wind.

The torque on a section at a distance, r, from the centre is [11]:

$$dQ = \frac{1}{2} B \rho_{air} V_{rel}^2 (C_l \sin\varphi - C_d \cos\varphi) c r dr \tag{18}$$

To express dT and dQ as functions of the free wind velocity, V, it is convenient to introduce the local solidity σ', defined as the total blade chord length at a given radius divided by the circumferential length at that radius [9]:

$$\sigma' = \frac{Bc}{2\pi r} \tag{19}$$

After some geometric considerations, equation (17) may be written as [11]:

$$dT = \sigma' \pi \rho_{air} \frac{V^2(1-a)^2}{\sin^2\varphi} (C_l \cos\varphi + C_d \sin\varphi) r dr \tag{20}$$

Similarly, equation (18) becomes:

$$dQ = \sigma' \pi \rho_{air} \frac{V^2(1-a)^2}{\sin^2\varphi} (C_l \sin\varphi - C_d \cos\varphi) r^2 dr \tag{21}$$

The blade element momentum theory is then based on combining equation (15) and (20), and (16) and (21), respectively. It is then possible to e.g. calculate the total power output from the rotor, using the equation [14]:

$$P = \int_{r_h}^{R} \Omega dQ dr \tag{22}$$

where r_h is the hub radius.

As the blade element momentum theory is based on ideal flow conditions around the rotor, calculated values may deviate significantly from measured data. Therefore several correction factors to improve the accuracy have been introduced [1]. The most commonly used is probably the Prandtl tip loss factor, p, that compensates for the reduced lift due to air flowing around the tip of the blade [11]. Its value varies from 0 to 1 and characterizes the

reduction in forces along the blade. The factor is calculated using the formula

$$p = \frac{2}{\pi}\cos^{-1}\left(e^{-\frac{B(R-r)}{2r\sin\varphi}}\right) \tag{23}$$

and is then multiplied into the equations (15) and (16) from the momentum theory.

2.7 Gyroscopic effects

The rotating wind turbine rotor generates a gyroscopic effect. The system can be modeled as a rigid body with moment of inertia I_g rotating at an angular velocity Ω_g about a horizontal axis, as shown in figure 9. W_g is the weight of the body (rotor), and a_g is the horizontal distance to the weight (from the centre of the tower). The moment $W_g a_g$ then induces a secondary rotation with angular velocity ω_g about a vertical axis, a phenomenon called precession [11]. A couple $I_g \Omega_g \omega_g$ acts on the body about an axis perpendicular to both the horizontal rotation axis, and the vertical precession axis, in opposite direction of Wa. Then the angular velocity of precession becomes:

$$\omega_g = \frac{W_g a_g}{I_g \Omega_g} \tag{24}$$

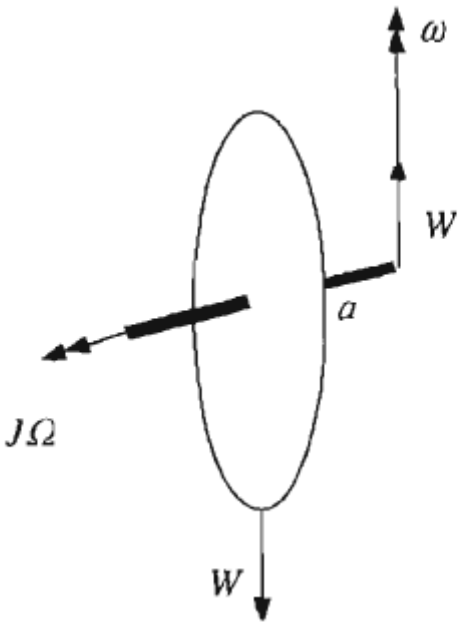

Figure 9: Sketch illustrating the gyroscopic principle [11]. The symbols used are the same as in the text, but without the subscript "g".

It is however in many cases possible to neglect gyroscopic effects [15], as the angular yaw velocity of the turbine usually is rather small. Gyroscopic loads are therefore not included in the HAWC2 code, and hence neglected in the simulations in this thesis.

2.8 Regular and irregular waves

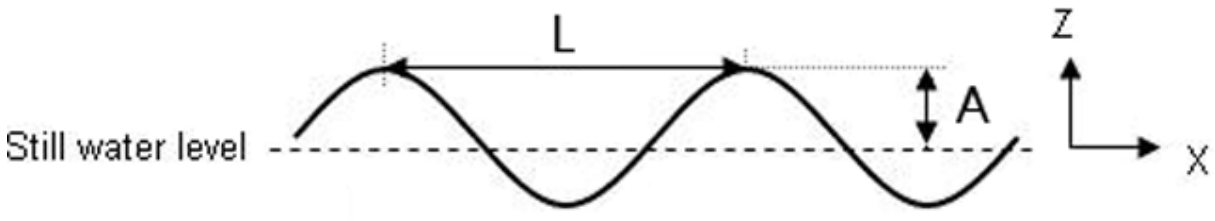

Figure 10: Surface profile of a regular sinusoidal wave.

Two types of waves are used in the simulations in this thesis; regular and irregular waves. Regular, or linear, waves have a sinusoidal surface profile [16]:

$$\eta(x,t) = A\,sin(\omega_w t - kx) \tag{25}$$

where the wave amplitude *A* equals half the wave height, ω_w is the wave frequency, and *x* is the horizontal position. The wave number *k* is related to the wavelength *L* as

$$k = \frac{2\pi}{L} \tag{26}$$

A set of equations describing water particle velocity and acceleration, in both horizontal and vertical direction, can be derived for this wave type. Different equations are used for deep, intermediate and shallow waters, but these are too comprehensive to be presented here.

The perfect sinusoidal surface profile of regular waves does not correspond well with observations of a real sea surface. A better approximation is achieved by the use of irregular waves. These can be seen as the superposition of a large number of individual regular waves, of different height, frequency and direction [17]. The energy content in different frequencies of the sea state is described by a wave spectrum. In this thesis the Jonswap wave spectrum is used, which was developed from wave measurements in the southern North Sea.

2.9 Hydrodynamic forces

All structures floating in open sea are to some degree exposed to forces from waves and currents, also known as hydrodynamic forces. Currents generate water particle velocities, while waves are associated with both water particle velocity and acceleration. The magnitude of forces from waves and currents vary with height above seabed, and is usually largest at the surface. The force per unit length acting in the direction of the flow on a submerged cylinder can be found using the Morison's equation [16]:

$$f(z,t) = f_I + f_D = \frac{\pi D^2}{4}\rho_w C_I \dot{u} + \frac{1}{2}\rho_w C_D D u|u| \tag{27}$$

where f_I and f_D are inertia and drag force respectively. The formula is only valid when the diameter of the cylinder is small compared to the wavelength, so that the water particle acceleration over the cylinder may be considered constant. Similarly a lift force acting perpendicular to the direction of the flow can be calculated. This is found using the same equation as for f_D, but with a different lift coefficient C_L. Morison's equation may also be used on other shapes than a cylinder, provided the inertia and drag coefficients are known. The hydrodynamic model in the HAWC2 code is based on Morison's equation.

2.10 Mooring forces

Mooring forces are in general quite complex, and specialized software are often required to make accurate dynamic calculations of the forces in each mooring line. In this thesis however, a more simple approach have been chosen. Instead of calculating the forces in each mooring line, functions that represent the resulting mooring force from all the lines are set up. The calculations are based on the global position of the mooring connection point. The horizontal mooring forces are calculated using hyperbolic sine functions, and an exponential function is used in the vertical direction. A linear function to represent yaw stiffness is also included.

Given the global x, y, z and θ_z (yaw) positions of the mooring connection point, the mooring forces are calculated from the following functions:

$$F_x^{moor} = -100\,000\sinh(0.2x) \tag{28}$$

$$F_y^{moor} = -100\,000\sinh(0.2y) \tag{29}$$

$$F_z^{moor} = 900\,000e^{-0.1(z-z_i)} \tag{30}$$

$$M_z^{moor} = -125\,000\,000\theta_z \tag{31}$$

where z_i is the initial vertical position of the mooring connection point. Equations 28 and 29 are based on the wind turbine model being placed in the global horizontal origin, such that the initial x- and y-positions of the mooring connection point equals zero. The horizontal mooring force in both x- and y-direction will then be zero, as sinh(0)=0. From equation 30, the initial vertical mooring force becomes 900 kN downwards (positive z-direction). Similarly, the yaw moment from equation 31 is initially zero (θ_z=0).

In the simulations the mooring forces is handled by a Dynamic Link Library (DLL), that gets the position of the mooring connection point from the HAWC2 simulation. It then calculates the mooring forces, and returns them to HAWC2 as external forces on the structure. This procedure is repeated for every time step.

In addition to the forces from equation 28-31, the mooring DLL is also used to apply additional linear damping to the wind turbine model. This is done both because there

normally will be a certain amount of damping from the mooring lines, and for practical reasons. Once the DLL-procedure is established, it is simpler to expand it to take care of both mooring forces and additional damping for the entire wind turbine model, instead of creating a separate damping DLL. The numerical values of the damping are from an presentation by NREL [18], as presented in table 2.

Additional linear damping in surge	100 000 N/(m/s)
Additional linear damping in sway	100 000 N/(m/s)
Additional linear damping in heave	130 000 N/(m/s)
Additional linear damping in yaw	13 000 000 Nm/(rad/s)

Table 2: Additional linear damping applied through the mooring DLL.

The additional damping term is particularly important for heave motions, which would otherwise be completely undamped in the HAWC2 code.

2.11 Stability

To have sufficient stability is essential for all floating constructions. A body is called initially stable if it returns to its original position after being exposed to a small angular displacement [16]. When a vessel is tilted the centre of gravity remains at the same position relative to the vessel, while the centre of buoyancy moves to the new centre of the volume of water which the hull displaces. This creates an uprighting moment that forces the vessel back to its original position, as illustrated in figure 11. The initial stability is described by the metacentric height GM, which is the distance between the centre of gravity and the metacentre. The metacentre is where a vertical line through the new centre of buoyancy intersects the vertical through the original centre of buoyancy, after a small angle of rotation. The stability of a vessel increases with increasing GM. In general, GM can be calculated using the equation:

$$GM = KB + BM - KG \tag{32}$$

based on distances from the keel K.

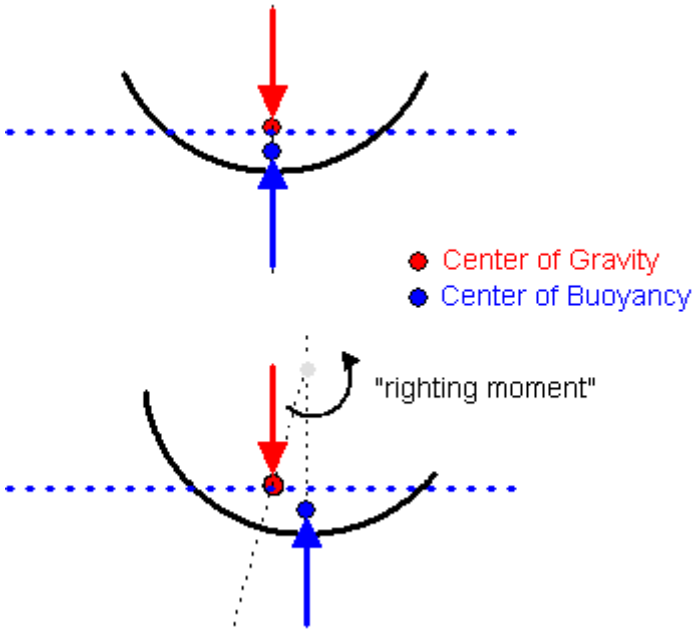

Figure 11: Sketch illustrating the principle of stability for a vessel.

The GM also governs the vessels roll period. The roll period is given by [17]:

$$T_{roll} = 2\pi\sqrt{\frac{I_T}{\Delta \cdot GM}} \tag{32}$$

Hence a large GM results in a low roll period, while a vessel with low stability/GM get a high (slow) roll period.

2.12 Logarithmic decrement

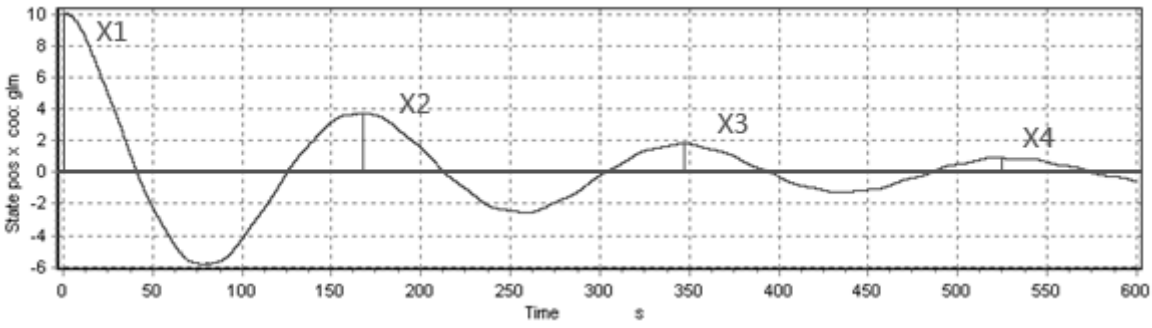

Figure 12: Time series of a damped oscillating motion, with the peak amplitudes 1 through 4 indicated.

Logarithmic decrement, δ, can be used to determine the damping ratio of an underdamped oscillating system. It is based on the amplitudes of successive peaks in a free decay test, and is calculated using the formula [19]:

$$\delta = \frac{1}{m} ln \frac{x_1}{x_{m+1}} \tag{33}$$

where x_1 has the greatest amplitude, and x_{m+1} is the amplitude m periods away. The damping ratio ζ is then given by:

$$\zeta = \frac{1}{\sqrt{1+\left(\frac{2\pi}{\delta}\right)^2}} \tag{34}$$

The method of logarithmic decrement becomes less and less accurate as the damping ratio increases, and should be used with caution for values of ζ>0.5.

2.13 Statistical load response extrapolation

The offshore wind turbine standard IEC 61400-3 requires some load response results to be extrapolated to 50 years extreme values [13]. This can be done using a method described in [17]. The data are divided into suitable intervals, and plotted in a graph with axis-values adapted to the probability distribution of choice. If the data follow a straight line in the graph, then they may be assumed to follow this distribution.

For load response extrapolation in association with IEC 61400-1, the 3-parameter Weibull seems to give the most accurate results [20, 21]. The cumulative distribution function of the 3-parameter Weibull distribution is defined as:

$$F_X(x) = 1 - \mathrm{e}^{-\left(\frac{x-\gamma}{\lambda}\right)^{\beta}} \tag{35}$$

where the location parameter γ is what separates it from an ordinary Weibull distribution.

For the data to follow a 3-parameter Weibull distribution, they should approximate a straight line in a graph with $\ln(x-\gamma)$ along the horizontal axis, and $\ln\left(-\ln\left(1-F_X(x)\right)\right)$ along the vertical axis. While the ordinary Weibull distribution ($\gamma = 0$) tends to give a convex curve when plotted in the graph, a straight line can be achieved by adjusting the location parameter in a 3-parameter Weibull distribution.

The 50 years response value may then be found by using the $F_X(x)$ value that corresponds to the response being exceeded once during a 50 years period. When the extrapolation is based on maximum values from simulations over a limited time period, this value can be calculated from:

$$F_X(x_{50}) = 1 - \frac{1}{n_{50}} \tag{36}$$

where n_{50} is the number of simulation periods in 50 years. If 10 minute simulations are used, there are 2 628 000 10 minute periods in 50 years, so the 50 years response has an probability of exceedance of 3.8×10^{-7}in a single simulation. Then the value

$F_X(x_{50})$=0.999999619 can be plotted in the above mentioned chart. The 50 years response is found from the intersection point between $\ln\left(-\ln\left(1-F_X(x_{50})\right)\right)$ and the line fitted to the observed data.

2.14 HAWC2

The HAWC2 code is a tool for simulation of wind turbine response in time domain, developed at the aeroelastic design program at Risø National Laboratory in Denmark. It has been used for all the simulations in this thesis. A short, but accurate description of the code is given in the HAWC2 user's manual [22]:

"*The structural part of the code is based on a multibody formulation where each body is an assembly of timoshenko beam elements. The formulation is general which means that quite complex structures can be handled and arbitrary large rotations of the bodies can be handled. The turbine is modeled by an assembly of bodies connected with constraint equations, where a constraint could be a rigid coupling, a bearing, a prescribed fixed bearing angle etc. The aerodynamic part of the code is based on the blade element momentum theory, but extended from the classic approach to handle dynamic inflow, dynamic stall, skew inflow, shear effects on the induction and effects from large deflections. Several turbulence formats can be used. Control of the turbine is performed through one or more DLL's (Dynamic Link Library). The format for these DLL's is also very general, which means that any possible output sensor normally used for data file output can also be used as a sensor to the DLL. This allows the same DLL format to be used whether a control of a bearing angle, an external force or moment is placed on the structure*."

The coordinate systems shown in figure 13 are used throughout the simulations in this thesis. The global origin is placed in the centre of the substructure, at mean water level. The global z-axis points vertically downwards, while the global y-direction is horizontal in the downwind direction. The x-axis is horizontal, perpendicular to the y- and z-axis, as defined by a right-hand coordinate system. All the main bodies, like the tower or blades, have their own coordinate system. The orientation of these may be chosen in whatever way the user finds convenient. In figure 13 the main body coordinate systems are the ones colored in red and blue. The subscripts T, S, H and B denote tower, shaft, hub and blade respectively.

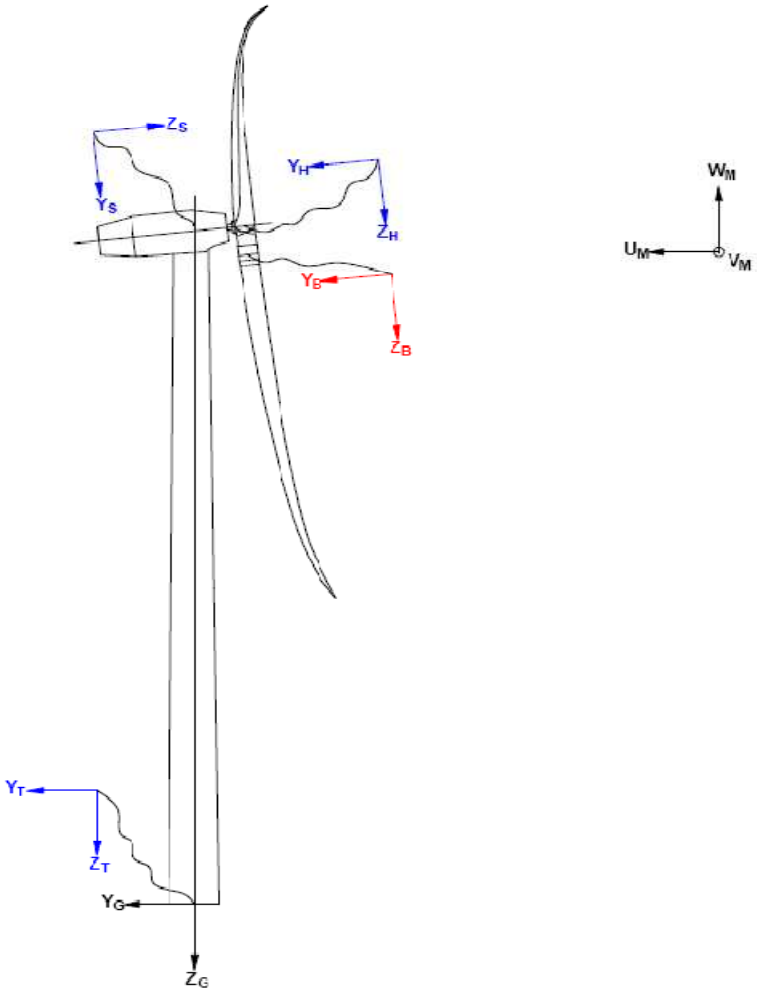

Figure 13: Sketch showing the coordinate system used in the simulations [22]. Default coordinate systems of global reference ($\boldsymbol{X_G}$, $\boldsymbol{Y_G}$, $\boldsymbol{Z_G}$) and wind speed ($\boldsymbol{U_M}$, $\boldsymbol{V_M}$, $\boldsymbol{W_M}$) in black.

3 Methods

3.1 Model description

The turbine model considered in this thesis is based on the "NREL offshore 5-MW baseline wind turbine" [8]. The turbine specifications were developed by the American National Renewable Energy Laboratory (NREL) to support concept studies aimed at assessing offshore wind technology.

It is in essence a three bladed pitch controlled turbine with hub height at 90 m and a rotor diameter of 126 m. The gross properties of the turbine are presented in table 1. Detailed information about the structural inputs used in the simulations is given in the appendix.

Rating	5 MW
Rotor Orientation, Configuration	Upwind, 3 Blades
Control	Variable Speed, Collective Pitch
Drivetrain	High Speed, Multiple-Stage Gearbox
Rotor, Hub Diameter	126 m, 3 m
Hub Height	90 m
Cut-In, Rated, Cut-Out Wind Speed	3 m/s, 11.4 m/s, 25 m/s
Cut-In, Rated Rotor Speed	6.9 rpm, 12.1 rpm
Rated Tip Speed	80 m/s
Overhang, Shaft Tilt, Precone	5 m, 5°, 2.5°
Rotor Mass	110,000 kg
Nacelle Mass	240,000 kg

Table 1: Gross properties of the NREL offshore 5-MW baseline wind turbine.

The wind turbine's substructure is of a floating, ballast stabilized design, similar to the Hywind project. The submerged diameter is 10.3 m, and the water crossing diameter is 6.0 m, as shown in figure 14. The overall height of the substructure is 110 m, of which 10 m is above the mean water level. A tower of 80 m is then used to achieve the total hub height of 90 m.

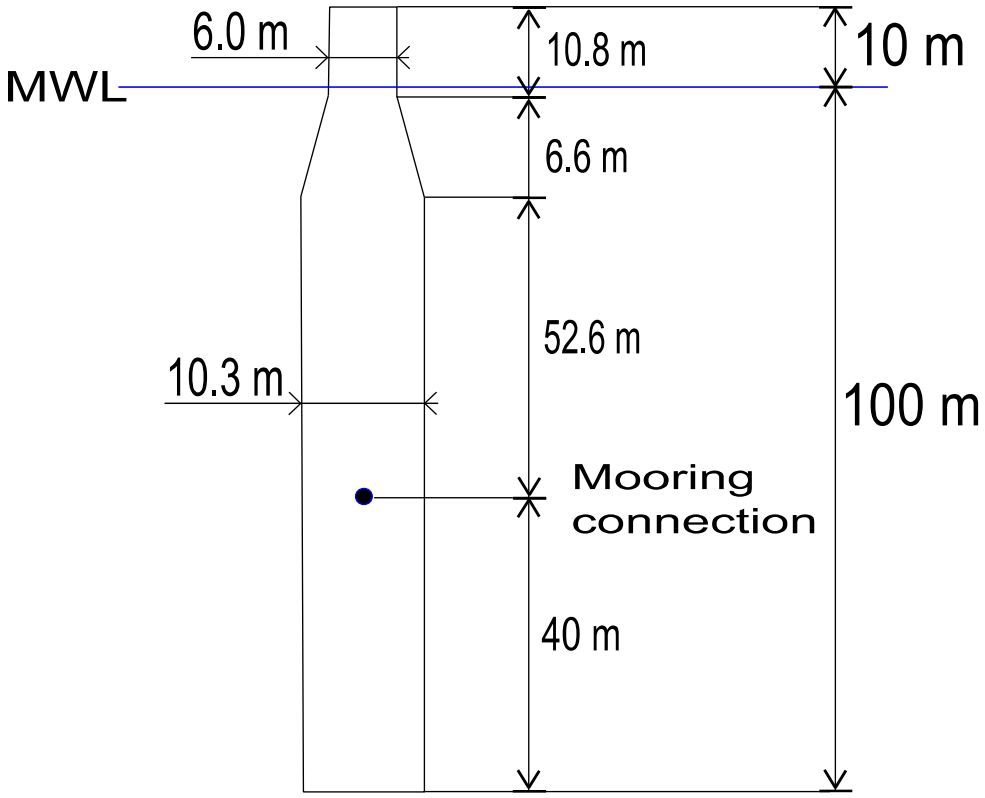

Figure 14: Sketch showing the dimensions of the cylindrical substructure.

The connection points of the mooring lines are placed 60 m below mean water level, near the model's pitch center. In the simulations these are treated as a single point, in the centre of the substructure. Its initial global xyz-position is (0, 0, 60).

To get the required stability, roughly 6500 tons of ballast is added to the bottom of the substructure. In comparison the 2.3 MW Hywind demonstration turbine is loaded with approximately 3500 tons of ballast.

3.2 Load cases

The load cases used it the simulations are based on the international wind turbine standard IEC 61400 part 1, Design requirements [12], and part 3, Design requirements for offshore wind turbines [13]. This includes the values of any environmental parameters, e.g. the density of air and water, specified in the standard. The magnitudes of the loads are based on the wind turbine satisfying the requirements of wind turbine class I_A [12]. This involves a maximum 10 minute average wind speed of 50 m/s at hub height, and a reference turbulence intensity of 0.16 at a wind speed of 15 m/s. Detailed information about the different load cases can be found in table 2.

DLC 1.1 ONC is simulated with a high frequent pitch control system, designed for bottom fixed/onshore wind turbines. For all other load cases the wind turbine is equipped with a low frequent pitch control system, particularly adapted to minimize motion in floating wind turbines. The key aspect in this matter is that the pitch control natural frequency is lower than the dominating tower motion frequency, to avoid negative damping of the motion [23]. While the offshore pitch control system has a natural frequency of 0.02 Hz, the onshore control system used in DLC 1.1 ONC has a natural frequency of 0.10 Hz. This load case is included in the simulations to verify the effect of the offshore pitch control system.

The wave conditions in DLC 6.1b and 6.1c are set to regular airy, where the standard specifies a single extreme design wave. This is done because of difficulties with implementing a single wave in the simulations. The other load cases are in compliance with the load cases described in IEC 61400-3.

All load cases that include turbulent wind are run ten times each, with 10 minutes simulations. DLC 1.4 and 1.5 have steady wind, but irregular waves. For these load cases three different wave data sets have been generated, based on the given sea state. All the different simulations within the load case have been run with the same three wave sets. This is done because the main focus of these load cases are the effect of a sudden change in the wind condition, not the sea state. However, running the simulations with three distinct wave sets reveal the impact of a moderate sea state on top of extreme wind conditions. DLC 6.1b and 6.1c have no random components in either wind or waves, and are run once per yaw misalignment direction.

Load case	Wind conditions	Wave conditions	Current conditions	Wave/wind directionality	Other information
DLC 1.1	Turbulent wind, V_{hub}=11.4 m/s, I=0.199	Irregular airy, H_s=5 m, T_p=12 s	U_0=0.114 m/s	Waves, wind and current aligned	Normal production conditions
DLC 1.1 ONC	Turbulent wind, V_{hub}=11.4 m/s, I=0.199	Irregular airy, H_s=5 m, T_p=12 s	U_0=0.114 m/s	Waves, wind and current aligned	High frequent, "onshore" pitch control syst.
DLC 1.3	Turbulent wind, V_{hub}=11.4 m/s, I=0.308	Irregular airy, H_s=5 m, T_p=12 s	U_0=0.114 m/s	Waves, wind and current aligned	Extreme turbulence
DLC 1.4	Steady wind, V_{hub}=9.4, 11.4, 13.4 m/s	Irregular airy, H_s=5 m, T_p=12 s	U_0=0.094, 0.114, 0.134 m/s	Wind direction change: +-76.6°, +- 63.2°, +-53.7°	Extreme coherent gust (15 m/s) with direction change
DLC 1.5	Steady wind, V_{hub}=11.4 m/s	Irregular airy, H_s=5 m, T_p=12 s	U_0=0.114 m/s	Waves, wind and current aligned	Extreme wind shear, positive/negative, vertical/horizontal
DLC 1.6a	Turbulent wind, V_{hub}=11.4 m/s, I=0.199	Irregular airy, H_s=12 m, T_p=13 s	U_0=0.114 m/s	Waves, wind and current aligned	Severe sea state, 50 years return period
DLC 6.1a	Turbulent wind, V_{hub}=50 m/s, I=0.11	Irregular airy, H_s=14 m, T_p=14 s	Extreme current, U_0=1.00 m/s	Yaw misalignment: 0°, +-8°	Extreme wind speed, extreme sea state
DLC 6.1b	Steady wind, V_{hub}=70 m/s	Regular airy, H=12 m, T =12 s	Extreme current, U_0=1.00 m/s	Yaw misalignment: 0°, +-15°	Extreme wind speed, reduced regular waves
DLC 6.1c	Steady wind, V_{hub}=55 m/s	Regular airy, H=20 m, T =14 s	Extreme current, U_0=1.00 m/s	Yaw misalignment: 0°, +-15°	Reduced wind speed, extreme regular waves

Table 2: Description of the load cases used in the simulations.

The following parameters are evaluated for all the load cases:

- Shear force between nacelle and tower (in global y-direction)
- Bending moment between the substructure and the tower, 10 m above still water level
- Out-of-plane blade tip deflection (measured at "blade1")
- Out-of-plane blade root bending moment (measured at "blade1")
- Axial acceleration at nacelle level
- Horizontal displacement at hub height (global y-direction)
- Tower pitch angle (measured at hub height)

In addition the following parameters are evaluated for the load cases with the turbine in production (DLC 1.x):

- In-plane blade root bending moment (measured at "blade1")
- Rotor power
- Rotor power standard deviation

For load case 6.1a, with turbulent wind and irregular extreme sea state, maximum wind speed and wave amplitude (maximum water surface level) are measured.

In all load cases the mean wind speed is increased from zero to the value specified in table 2 over a period of 50 seconds. This is done to avoid large impact loads at the start of the simulation. To avoid the results being disturbed by this initiation period, gust events in DLC 1.4 and 1.5 occurs after t=200 s, and the max loads are collected from t=200 s to t=300s. Similarly ten minute periods with turbulent wind conditions are measured from t=200 s to t=800 s.

IEC 61400 specify a load safety factor of 1.35 for all design situations classified as "Normal", which apply for all load cases that is run in this thesis. For the purpose of internal comparison of the load cases the safety factor will have no influence, and is therefore neglected throughout the analysis in this thesis.

The offshore wind turbine standard IEC 61400-3 requires the load response results from DLC 1.1, with normal production conditions, to be extrapolated to 50 years extreme values. IEC 61400-1 specify that this extrapolation should at least include the maximum in- and out-of-plane blade root bending moments, as well as the out-of-plane blade tip deflection. In this thesis these three parameters are extrapolated to 50 years return periods for DLC 1.1 and DLC 1.1 ONC, assuming a 3-parameter Weibull distribution. To get enough data points, all three rotor blades are assumed to be independent, so a total of 30 maxima are collected from the 10 simulations.

In the other load cases the turbine model is already exposed to extreme conditions equivalent to a 50 year return period, and mean values of maximum loads are used.

Free decay test

In addition to the load cases from IEC 61400-3, free decay tests to determine the turbine model's motion period and damping in heave, surge, sway, yaw, pitch and roll have been run. These simulations are performed with a parked turbine in still water without any wind, but with an initial displacement in the degree of freedom that is being evaluated. Both the damping and the period have been determined based on the first four motion amplitudes. The results are compared to data from Statoil's simulations of the conceptual 5 MW Hywind turbine [18], which is of a different design, but based on the same principles.

3.3 Limitations

In the simulations several load types or phenomenons are ignored. Some of the most significant are:

- Icing on blades
- Sea ice
- Marine growth on substructure
- Power transmission line loads
- Fault conditions
- Transportation and assembly
- Turbine is modeled without yaw bearing
- Gyroscopic loads
- Fatigue

In addition to the list above, the mooring loads are subject to coarse approximations. While an accurate simulation of these would require use of specialized software, the mooring loads in this thesis are calculated from simple functions.

Calculation of stresses is not included in the HAWC2 code, and the evaluation of these is therefore left out of the analysis in this thesis. The main focus is instead put on the motion and internal forces of the wind turbine model.

4 Results

4.1 Free decay test

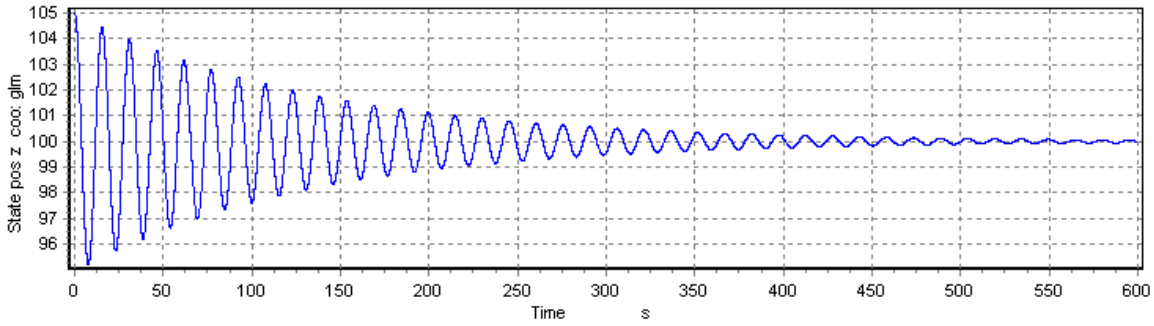

Figure 15: Heave motion free decay test.

Figure 15 shows a time series from the heave motion free decay test, with an initial vertical displacement of 5 meters downwards (positive z-direction). The damping ratio in heave is 0.018, which is about half of the damping found in a free decay simulation performed by Statoil on a 5 MW version of the Hywind concept [18], as seen in figure 21. Also the heave motion period is only 15.4 seconds, while the 5 MW Hywind model had a period of about 30

seconds. This could disturb the results from the simulations, especially in load cases that include large waves with long periods.

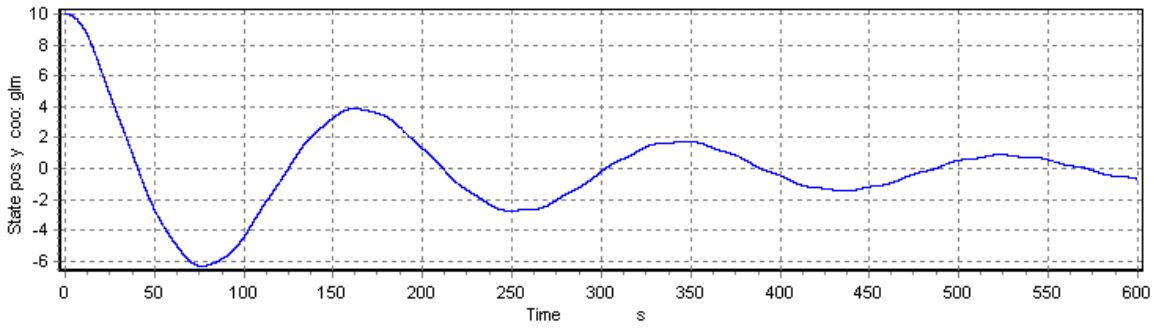

Figure 16: Surge motion free decay test.

Figure 16 shows a time series from the surge motion free decay test, with an initial horizontal displacement of 10 meters in the positive y-direction. The surge damping ratio is 0.126, which matches the results from Statoil's simulations. The surge period is 174 seconds, where the result from Statoil was about 132 seconds. The slightly longer surge period will probably not have a large impact on the results, as it anyway is much longer than the dominating periods of wind and wave loading.

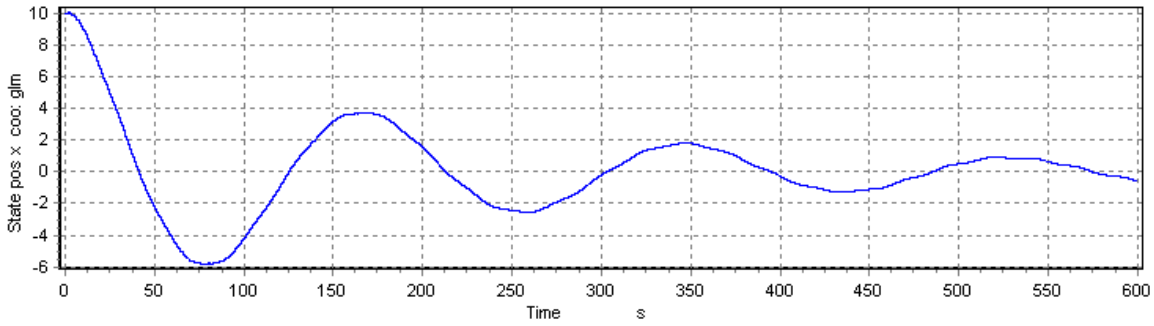

Figure 17: Sway motion free decay test.

Figure 17 shows a time series from the sway motion free decay test, with an initial horizontal displacement of 10 meters in the positive x-direction. As in Statoil's simulations, surge and sway motion results are almost identical. The damping ratio in sway is 0.125, and the period is 174 seconds.

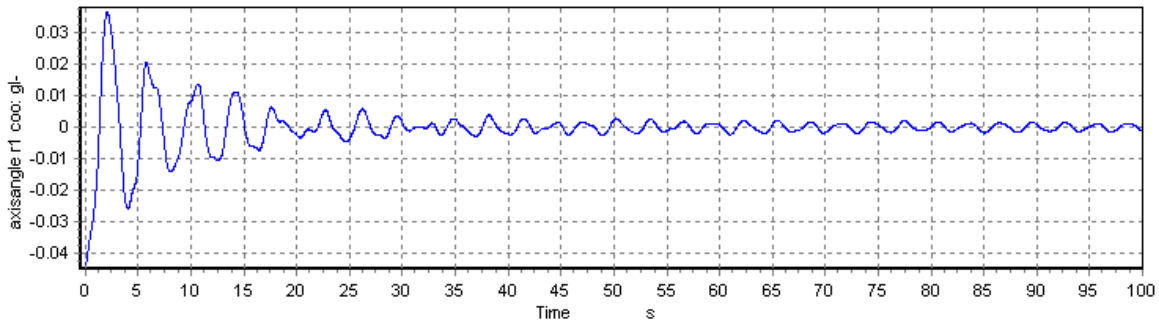

Figure 18: Yaw motion free decay test. Angles are in radians.

Figure 18 shows a time series from the yaw motion free decay test, with an initial displacement of 0.0436 radians (2.5°) in the negative θ_z-direction. The model comes out with a yaw period of 4.2 seconds, about half the period from Statoil's data. The damping ratio of 0.074 is somewhat larger than in Statoil's model.

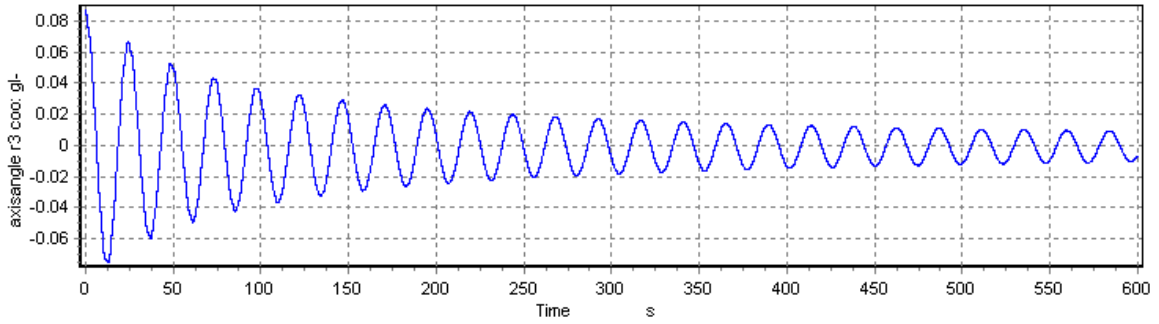

Figure 10: Pitch motion free decay test. Angles are in radians.

Figure 19 shows a time series from the pitch motion free decay test, with an initial displacement of 0.0873 radians (5.0°) in the positive θ_x-direction. Pitch is the dominating motion for a floating wind turbine of the spar buoy (Hywind) concept, and it is essential for the simulations that this motion is of a satisfying character. The pitch period is 24.2 seconds, which is well above the dominating ocean wave periods, and close to Statoil's results. However, the damping ratio of 0.037 is about two thirds of the damping ratio in Statoil's model.

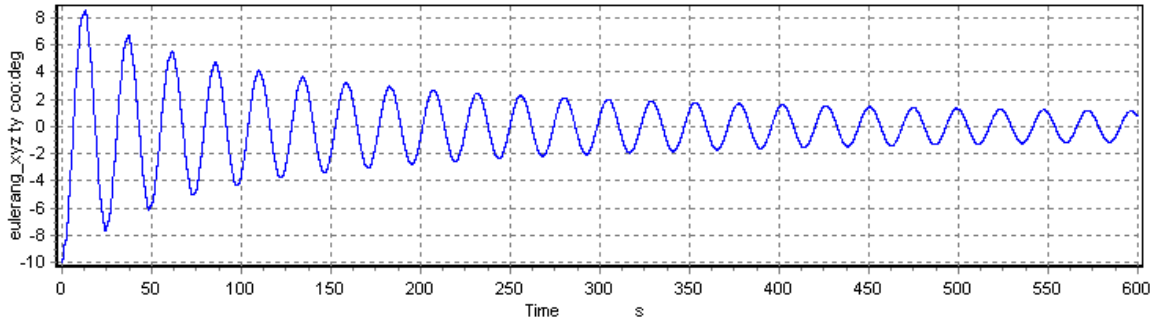

Figure 11: Roll motion free decay test. Angles are in degrees.

Figure 20 shows a time series from the roll motion free decay test, with an initial rotation of 10.0° in the negative θ_y-direction. The roll period is 24.2 seconds, and the damping ratio is 0.036. Both the roll and pitch motion tests yields pretty much exactly the same results, which corresponds well to the data from Statoil's simulations.

		Heave	Surge	Sway	Yaw	Pitch	Roll
Turbine in this thesis	Damping ratio	0.018	0.126	0.125	0.074	0.037	0.036
	Period [s]	15.4	174.3	173.5	4.2	24.2	24.2
Statoil's data	Damping ratio	0.037	0.104	0.103	0.043	0.053	0.054
	Period [s]	31.1	131.3	130.1	8.3	28.1	28.5

Table 3: Results from the free decay tests.

The results from the free decay tests are summarized in table 3 above. The values from Statoil's data are estimated from the time series in figure 21. The heave motion period of 15.4 seconds versus Statoil's model 31.1 seconds, is probably the most critical difference between the two models. The damping ratio in heave, pitch and roll are also somewhat lower than in Statoil's model. It must however be stressed that the results from the free decay test performed in this thesis and Statoil's data are based on two distinct wind turbines, and some differences must be expected.

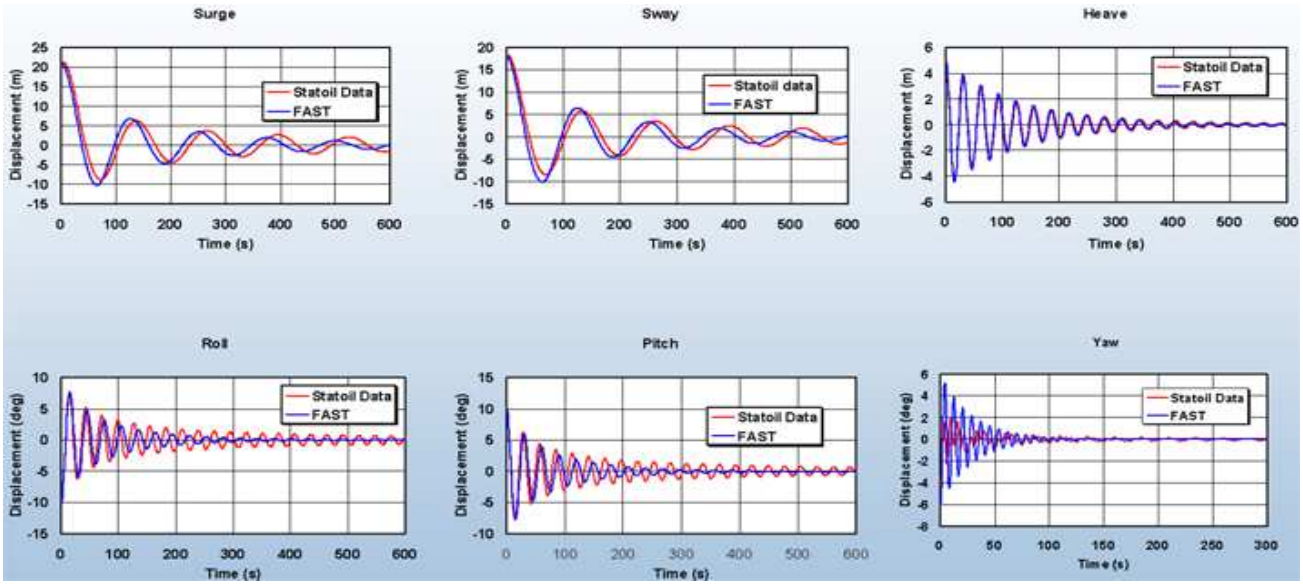

Figure 21: Time series of displacement during free decay tests of a conceptual 5 MW Hywind model performed by NREL (FAST) and Statoil.

4.2 DLC 1.1

Design load case 1.1 is meant to simulate normal production conditions, with turbulent wind and irregular waves. The mean wind speed at hub height is 11.4 m/s, with a turbulence intensity of 0.199. The significant wave height is set to 5 m, with a peak period of 12 seconds. The ocean current is set to 0.114 m/s. Wave, wind and current directions are aligned. A total of 10 simulations were run, each covering a 10 minute period. The maximum values of each parameter that was registered are presented in table 4a and 4b.

	Shear force nacelle/tower [kN]	Bending moment substruc./tower [MNm]	Out-of-plane blade tip deflection [m]	Out-of-plane blade root bend. moment [kNm]	In-plane blade root bend. moment [kNm]
Simulation 1	1 815	158.8	8.28	14 880	7 842
Simulation 2	1 598	139.2	9.81	17 240	7 803
Simulation 3	1 697	143.4	8.67	13 450	7 778
Simulation 4	1 578	135.4	8.23	14 030	6 653
Simulation 5	1 771	151.7	8.98	15 300	7 176
Simulation 6	1 648	143.0	8.76	15 470	7 621
Simulation 7	1 972	172.5	8.78	14 750	7 989
Simulation 8	2 083	177.0	9.39	15 580	7 573
Simulation 9	1 778	152.7	9.47	16 090	8 304
Simulation 10	1 592	141.0	8.77	15 010	7 425
Mean value	**1 753**	**151.5**	**8.91**	**15 180**	**7 616**

Table 4a: Results from the simulations of DLC 1.1.

	Axial acc. at nacelle $[m/s^2]$	Horiz. displacement at hub height [m]	Tower pitch angle [deg]	Rotor power [kW]	Rotor power stdev. [kW]
Simulation 1	2.216	27.22	2.92	11 130	1 661
Simulation 2	2.132	26.05	2.59	11 130	1 695
Simulation 3	2.070	27.00	2.86	9 870	1 565
Simulation 4	2.153	26.59	2.56	10 430	1 527
Simulation 5	2.318	26.13	2.58	10 240	1 522
Simulation 6	1.978	26.25	2.67	10 410	1 557
Simulation 7	2.313	28.27	3.10	11 280	1 577
Simulation 8	2.649	25.80	2.92	11 380	1 561
Simulation 9	2.354	28.37	2.76	12 340	1 615
Simulation 10	1.808	27.98	2.59	9 560	1 532
Mean value	**2.199**	**26.97**	**2.76**	**10 780**	**1 581**

Table 4b: Results from the simulations of DLC 1.1.

Compared to the other load cases with the turbine in production (DLC 1.x), the results from DLC 1.1 seems fairly moderate. For example both the average maximum blade tip deflection of 8.91 m and the tower pitch angle of 2.76° are amongst the lowest of all the load cases. One should however be aware of that the results in table 4 are from 10 minute simulations, and the standard requires these values to be extrapolated to a 50 years return period. So the mean values from DLC 1.1 should not be compared directly with the mean values from the other load cases.

50 year response extrapolation

The out-of-plane blade tip deflection, and in- and out-of-plane blade root bending moments are extrapolated to 50 years return periods. In addition to the maximum values for from blade 1, the values gathered from blade 2 and 3 are also used to get a more accurate 50 years response extrapolation. This gives a total of 30 maximums for each parameter under consideration. All the data used in the response extrapolation are shown in table 5.

	Out-of-plane blade tip deflection [m]			Out-of-plane blade root bend. moment [kNm]			In-plane blade root bend. moment [kNm]		
	Blade 1	Blade 2	Blade 3	Blade 1	Blade 2	Blade 3	Blade 1	Blade 2	Blade 3
Simulation 1	8.28	9.43	9.80	14 880	16 780	17 000	7 842	8 479	7 760
Simulation 2	9.81	9.09	8.90	17 240	16 410	16 440	7 803	7 746	7 201
Simulation 3	8.67	9.09	8.66	13 450	14 560	15 050	7 778	8 745	8 063
Simulation 4	8.23	8.22	8.62	14 030	13 920	13 920	6 653	6 668	6 288
Simulation 5	8.98	8.43	9.96	15 300	14 520	16 650	7 176	7 240	7 727
Simulation 6	8.76	9.11	8.19	15 470	15 360	14 560	7 621	7 210	7 141
Simulation 7	8.78	8.43	10.19	14 750	14 770	17 830	7 989	8 188	8 317
Simulation 8	9.39	9.52	9.20	15 580	17 160	15 390	7 573	7 404	7 373
Simulation 9	9.47	9.21	9.26	16 090	15 460	15 590	8 304	8 447	7 938
Simulation 10	8.77	9.16	8.94	15 010	15 800	15 140	7 425	7 488	7 378

Table 5: Data used in the 50 years response extrapolation.

Using the method described in the theory section, the extrapolated 50 years responses becomes as presented in table 6. On average the extrapolated values are about 40 % higher than the mean values of the ten minute simulations. There is of course a large uncertainty in these estimates, but assuming they are correct they are considerably higher than most other results from production load cases. For example is the extrapolated blade tip deflection of 12.3 m almost 2 m more than the highest value from the other load cases (excluding DLC 1.1 ONC), and would make the blade tip crash into the tower.

50 years out-of-plane blade tip deflection [m]	50 years out-of-plane blade root bend. moment [kNm]	50 years in-plane blade root bend. moment [kNm]
12.3	21 600	10 700

Table 6: A selection of parameters from **DLC 1.1** extrapolated to a 50 years return period.

Further details about the load extrapolation, including plot of the data, can be found in the appendix.

4.3 DLC 1.1 ONC

Design load case 1.1 ONC is identical to DLC 1.1, but the turbine model is set up with a high frequent, "onshore" pitch control system. The mean wind speed at hub height is 11.4 m/s, with a turbulence intensity of 0.199. The significant wave height is set to 5 m, with a peak period of 12 seconds. The ocean current is set to 0.114 m/s. Wave, wind and current directions are aligned. A total of 10 simulations were run, each covering a 10 minute period. The maximum values of each parameter that was registered are presented in table 7a and 7b.

	Shear force nacelle/tower [kN]	Bending moment substruc./tower [MNm]	Out-of-plane blade tip deflection [m]	Out-of-plane blade root bend. moment [kNm]	In-plane blade root bend. moment [kNm]
Simulation 1	1 831	158.8	9.56	15 400	7 718
Simulation 2	1 917	169.8	9.48	16 560	7 248
Simulation 3	2 450	217.9	10.76	18 710	6 969
Simulation 4	1 779	152.9	8.83	14 880	6 994
Simulation 5	1 973	168.8	9.78	16 250	6 512
Simulation 6	1 933	169.1	9.24	16 560	7 492
Simulation 7	2 384	212.3	8.99	15 060	6 293
Simulation 8	1 707	146.5	9.17	15 550	6 606
Simulation 9	2 055	185.0	9.50	15 430	6 980
Simulation 10	2 083	185.6	9.16	16 400	6 767
Mean value	**2 011**	**176.7**	**9.45**	**16 080**	**6 958**

Table 7a: Results from the simulations of DLC 1.1 ONC.

	Axial acc. at nacelle $[m/s^2]$	Horiz. displacement at hub height [m]	Tower pitch angle [deg]	Rotor power [kW]	Rotor power stdev. [kW]
Simulation 1	2.481	31.62	4.19	10 590	1 644
Simulation 2	2.249	37.22	5.10	10 390	1 675
Simulation 3	2.773	40.80	6.33	15 340	2 096
Simulation 4	2.200	31.13	3.80	9 581	1 430
Simulation 5	2.224	34.05	4.51	12 470	1 686
Simulation 6	2.206	34.11	4.34	12 050	1 595
Simulation 7	2.400	41.59	5.72	11 170	1 637
Simulation 8	1.732	26.22	2.73	11 170	1 432
Simulation 9	2.279	34.97	4.89	11 590	1 658
Simulation 10	2.682	38.00	5.16	11 630	1 792
Mean value	**2.323**	**34.97**	**4.68**	**11 600**	**1 665**

Table 7b: Results from the simulations of DLC 1.1 ONC.

The average forces and deflections acquired from DLC 1.1 ONC, with "onshore" controller, are in general higher than the values from DLC 1.1. One exception is the average maximum in-plane blade root bending moment, which is somewhat lower for DLC 1.1 ONC. It is also worth noting that the rotor power standard deviation is higher, so the turbine with onshore controller would provide less constant electrical power to the grid.

50 year response extrapolation

The out-of-plane blade tip deflection, and in- and out-of-plane blade root bending moments are extrapolated to 50 years return periods. In addition to the maximum values for from blade 1, the values gathered from blade 2 and 3 are also used to get a more accurate 50 years response extrapolation. This gives a total of 30 maximums for each parameter under consideration. All the data used in the response extrapolation are shown in table 8.

	Out-of-plane blade tip deflection [m]			Out-of-plane blade root bend. moment [kNm]			In-plane blade root bend. moment [kNm]		
	Blade 1	Blade 2	Blade 3	Blade 1	Blade 2	Blade 3	Blade 1	Blade 2	Blade 3
Simulation 1	9.56	9.47	9.73	15 400	15 670	16 630	7 718	7 856	7 378
Simulation 2	9.48	10.13	9.17	16 560	16 510	15 270	7 248	6 710	6 652
Simulation 3	10.76	10.40	9.39	18 710	18 130	16 730	6 969	7 013	7 183
Simulation 4	8.83	9.07	9.53	14 880	15 570	15 580	6 994	6 549	6 648
Simulation 5	9.78	9.47	9.21	16 250	16 380	15 960	6 512	7 080	6 685
Simulation 6	9.24	9.43	8.98	16 560	16 820	16 260	7 492	6 925	7 232
Simulation 7	8.99	9.70	9.29	15 060	16 500	16 460	6 293	7 010	6 711
Simulation 8	9.17	8.46	8.92	15 550	16 030	15 400	6 606	6 590	6 314
Simulation 9	9.50	10.93	9.29	15 430	18 980	16 210	6 980	7 159	7 827
Simulation 10	9.16	10.30	8.78	16 400	18 950	15 030	6 767	6 973	6 789

Table 8: Data used in the 50 years response extrapolation.

Using the method described in the theory section, the extrapolated 50 years responses becomes as presented in table 9. Relative to the mean values from the simulations, the extrapolated values are pretty similar to the ones from DLC 1.1. With a 50 years out-of-plane blade tip deflection of 13.7 m, it would only be a matter of hours before the critical tip deflection of about 11 m was exceeded under the given conditions.

50 years out-of-plane blade tip deflection [m]	50 years out-of-plane blade root bend. moment [kNm]	50 years in-plane blade root bend. moment [kNm]
13.7	26 300	10 100

Table 9: A selection of parameters from **DLC 1.1 ONC** extrapolated to a 50 years return period.

Further details about the load extrapolation, including plot of the data, can be found in the appendix.

On- vs offshore controller verification

In addition to the ordinary load case simulations, a test setup was run to verify the difference between the on- and offshore controller. Models with both controllers were exposed to identical wind conditions as shown in figure 22. The wind was increasing up to 15 m/s over a period of 50 seconds, and then kept constant. No waves or currents were included in the simulations. With pitch being the dominating motion, the global pitch angle of the wind turbine tower is a good indicator of the model's stability, and this parameter was measured.

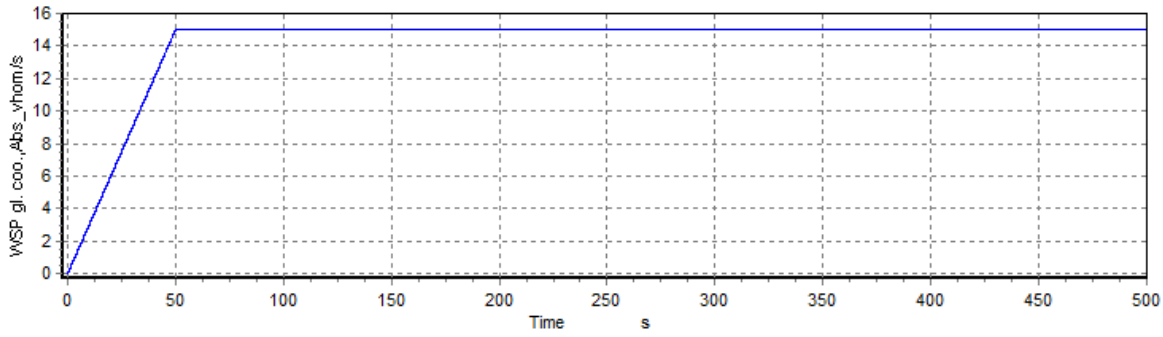

Figure 22: Graph showing the wind speed profile used in the on- vs offshore controller verification simulations.

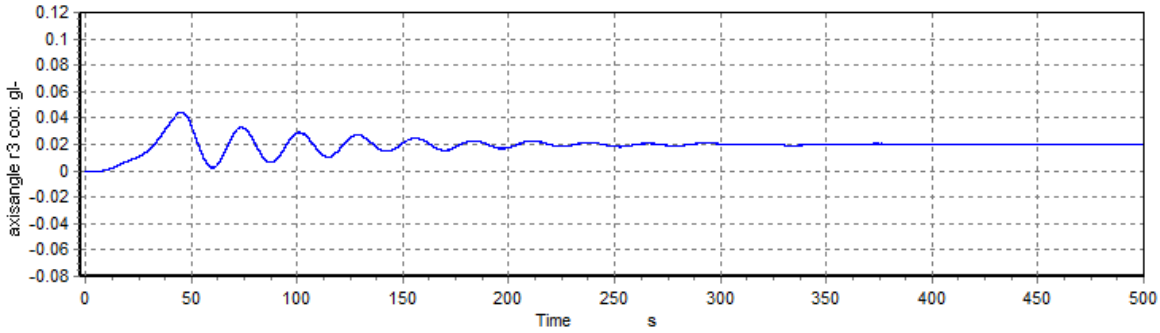

Figure 23: Time series of the pitch motion with offshore controller.

As seen in figure 23, the model with offshore controller experiences some initial oscillations, but these are eventually dampened out. As expected, this controller is effective in minimizing pitch motion.

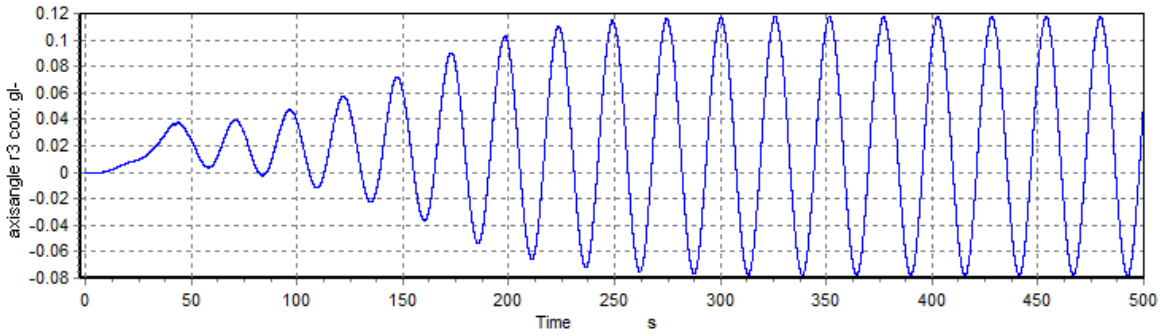

Figure 24: Time series of the pitch motion with onshore controller.

Where the offshore controller manages to dampen the pitch motion, the onshore controller enhances it, as seen in figure 24. The turbine ends up oscillating heavily back and forth, with motions too large for any efficient power production.

4.4 DLC 1.3

Design load case 1.3 is meant to simulate production conditions, but with extreme turbulence corresponding to a 50 years return period. The mean wind speed at hub height is 11.4 m/s, with a turbulence intensity of 0.308. Irregular airy waves are used, with a significant wave height of 5 m, and a peak period of 12 seconds. The ocean current is set to 0.114 m/s. Wave, wind and current directions are aligned. A total of 10 simulations were run, each covering a 10 minute period. The maximum values of each parameter that was registered are presented in table 10a and 10b.

	Shear force nacelle/tower [kN]	Bending moment substruc./tower [MNm]	Out-of-plane blade tip deflection [m]	Out-of-plane blade root bend. moment [kNm]	In-plane blade root bend. moment [kNm]
Simulation 1	1 939	176.3	9.41	16 900	8 080
Simulation 2	1 787	157.9	10.43	18 700	11 810
Simulation 3	1 726	147.7	10.40	16 420	13 530
Simulation 4	1 477	132.5	9.49	17 270	12 810
Simulation 5	1 967	168.7	10.46	19 350	11 270
Simulation 6	1 676	144.6	8.42	15 160	8 050
Simulation 7	2 001	171.8	10.86	18 630	11 330
Simulation 8	1 748	149.2	9.77	17 280	9 650
Simulation 9	1 785	154.0	9.44	17 180	13 020
Simulation 10	1 645	144.2	8.94	16 270	11 960
Mean value	**1 775**	**154.7**	**9.76**	**17 316**	**11 150**

Table 10a: Results from the simulations of DLC 1.3.

	Axial acc. at nacelle $[m/s^2]$	Horiz. displacement at hub height [m]	Tower pitch angle [deg]	Rotor power [kW]	Rotor power stdev. [kW]
Simulation 1	2.997	28.40	3.49	10 800	1 723
Simulation 2	2.453	30.35	3.28	12 120	1 820
Simulation 3	2.142	27.53	3.33	11 640	1 997
Simulation 4	2.309	26.47	2.71	9 930	1 750
Simulation 5	2.617	28.12	3.17	11 480	1 801
Simulation 6	2.153	29.51	3.30	12 480	1 759
Simulation 7	2.514	28.31	3.14	12 410	1 889
Simulation 8	2.166	27.54	2.97	11 770	1 685
Simulation 9	2.012	26.42	2.99	13 610	1 912
Simulation 10	2.241	26.39	2.83	12 360	1 913
Mean value	**2.360**	**27.90**	**3.12**	**11 860**	**1 825**

Table 10b: Results from the simulations of DLC 1.3.

The mean maximum tower loading, shear force between nacelle/tower and bending moment between substructure and tower, are almost identical to the unextrapolated mean values from DLC 1.1. But while the tower is not much affected by the increased turbulence, the blade loads are significantly larger. The mean maximum in-plane blade root bending moment of 11 150 kNm is the largest of all the load cases, even higher than the extrapolated 50 years return period value from DLC 1.1. The mean blade tip deflection is 9.76 m, which is well below the critical value of 11 m, and 2.5 m less than the 50 years value from DLC 1.1

4.5 DLC 1.4

Design load case 1.4 is sudden gusts of 15 m/s with wind direction change, imposed on a steady wind speed while the wind turbine is in production. An example of the wind profile used in DCL 1.4 is shown in figure 25. Simulations with three different initial hub height wind speeds are run; 9.4 m/s, 11.4 m/s and 13.4 m/s, corresponding to rated wind speed (11.4

m/s) +-2.0m/s. Their respective direction changes are +-76.6°, +-63.2° and +-53.7°. Irregular airy waves are used, with a significant wave height of 5 m, and a peak period of 12 seconds. The same three wave data realizations are used throughout the load case, so for example the waves from wave set 1 is identical for all the simulations, regardless of wind speed and direction. The ocean current velocity is set to 1 % of the wind velocity before the gust event. Wave, wind and current directions are aligned prior to the gust with direction change.

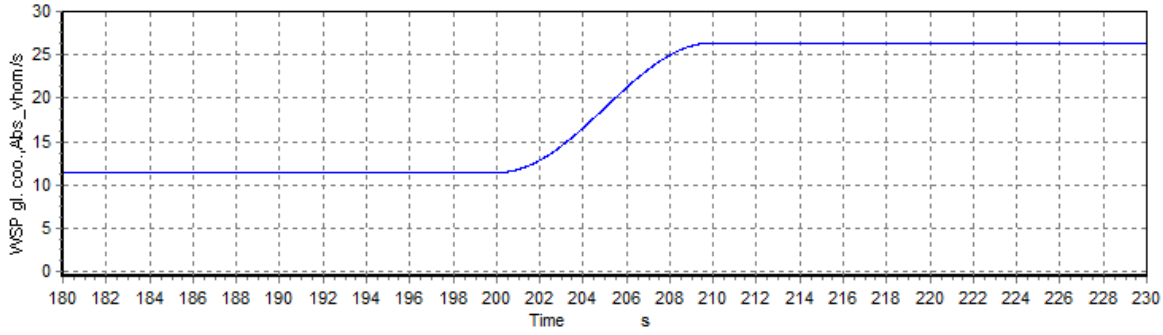

Figure 25: Absolute horizontal wind speed profile for DLC 1.4.

V_{hub}=9.4 m/s, V_{gust}=15 m/s, wind direction change=-76.6°

	Shear force nacelle/tower [kN]	Bending moment substruc./tower [MNm]	Out-of-plane blade tip deflection [m]	Out-of-plane blade root bend. moment [kNm]	In-plane blade root bend. moment [kNm]
Wave set 1	1 315	118.5	10.39	15 370	6 044
Wave set 2	1 217	111.7	9.44	13 720	6 588
Wave set 3	1 346	114.9	8.93	13 410	5 907
Mean value	**1 292**	**115.0**	**9.58**	**14 167**	**6 180**

Table 11a: Results from simulations of DLC 1.4, V_{hub}=9.4 m/s, wind direction change=-76.6°.

	Axial acc. at nacelle $[m/s^2]$	Horiz. displacement at hub height [m]	Tower pitch angle [deg]	Rotor power [kW]	Rotor power stdev. [kW]
Wave set 1	1.687	23.30	2.32	7 734	1 515
Wave set 2	1.748	22.61	2.17	7 938	1 634
Wave set 3	1.439	22.98	2.27	5 946	1 130
Mean value	**1.625**	**22.96**	**2.25**	**7 206**	**1 426**

Table 11b: Results from simulations of DLC 1.4, V_{hub}=9.4 m/s, wind direction change=-76.6°.

The maximum values of each parameter that was registered from V_{hub}=9.4 m/s and wind direction change=-76.6° are presented in table 11a and 11b. Most of the parameters have moderate values compared to other load cases, also compared to other wind speed/direction scenarios within DLC 1.4.

V_{hub}=9.4 m/s, V_{gust}=15 m/s, wind direction change=76.6°

	Shear force nacelle/tower [kN]	Bending moment substruc./tower [MNm]	Out-of-plane blade tip deflection [m]	Out-of-plane blade root bend. moment [kNm]	In-plane blade root bend. moment [kNm]
Wave set 1	1 234	97.0	10.10	15 920	5 517
Wave set 2	1 076	91.1	10.00	15 910	5 458
Wave set 3	1 401	113.5	9.34	12 660	5 307
Mean value	**1 237**	**100.5**	**9.81**	**14 830**	**5 427**

Table 12a: Results from simulations of DLC 1.4, V_{hub}=9.4 m/s, wind direction change=76.6°.

	Axial acc. at nacelle $[m/s^2]$	Horiz. displacement at hub height [m]	Tower pitch angle [deg]	Rotor power [kW]	Rotor power stdev. [kW]
Wave set 1	1.329	23.18	1.73	7 965	2 170
Wave set 2	1.530	21.19	1.78	8 554	2 362
Wave set 3	1.578	23.99	2.24	6 571	1 801
Mean value	**1.479**	**22.79**	**1.92**	**7 697**	**2 111**

Table 12b: Results from simulations of DLC 1.4, V_{hub}=9.4 m/s, wind direction change=76.6°.

The maximum values of each parameter that was registered from V_{hub}=9.4 m/s and wind direction change=76.6° are presented in table 12a and 12b. It should be emphasized that the simulations of this wind speed/direction scenario crashed about 35 second after the start of the gust event. The large wind direction change combined with the turbine model's lack of yaw bearing, resulted in the rotor being blown to a complete standstill. The results are therefore not entirely comparable to the others of DLC 1.4. None of the values, however, are amongst the highest within the load case.

V_{hub}=11.4 m/s, V_{gust}=15 m/s, wind direction change= -63.2°

	Shear force nacelle/tower [kN]	Bending moment substruc./tower [MNm]	Out-of-plane blade tip deflection [m]	Out-of-plane blade root bend. moment [kNm]	In-plane blade root bend. moment [kNm]
Wave set 1	1 580	143.1	10.47	19 270	6 590
Wave set 2	1 300	111.9	10.56	16 910	6 505
Wave set 3	1 406	117.9	9.57	15 150	6 633
Mean value	**1 429**	**124.3**	**10.20**	**17 110**	**6 576**

Table 13a: Results from simulations of DLC 1.4, V_{hub}=11.4 m/s, wind direction change=-63.2°.

	Axial acc. at nacelle $[m/s^2]$	Horiz. displacement at hub height [m]	Tower pitch angle [deg]	Rotor power [kW]	Rotor power stdev. [kW]
Wave set 1	1.677	26.51	2.73	12 070	2 902
Wave set 2	1.234	23.16	2.14	11 410	2 899
Wave set 3	1.558	24.60	2.37	10 550	2 150
Mean value	**1.490**	**24.76**	**2.41**	**11 340**	**2 650**

Table 13b: Results from simulations of DLC 1.4, V_{hub}=11.4 m/s, wind direction change=-63.2°.

The maximum values of each parameter that was registered from V_{hub}=11.4 m/s and wind direction change=-63.2° are presented in table 13a and 13b. The values of bending moment between substructure/tower, blade tip deflection, out-of-plane blade root bending moment, horizontal displacement at hub height and tower pitch angle are all the highest within DLC 1.4, and this seems to be the most critical wind speed/direction change combination. This is despite the fact that some of the others have 2 m/s higher wind speeds. Compared to the other production load cases most of the values are still fairly moderate, with the exception of blade tip deflection and out-of-plane blade root bending moments. These values are only surpassed by DLC 1.6a with extreme sea state, and the extrapolated 50 years return period values from DLC 1.1 and DLC 1.1 ONC.

V_{hub}=11.4 m/s, V_{gust}=15 m/s, wind direction change= 63.2°

	Shear force nacelle/tower [kN]	Bending moment substruc./tower [MNm]	Out-of-plane blade tip deflection [m]	Out-of-plane blade root bend. moment [kNm]	In-plane blade root bend. moment [kNm]
Wave set 1	1 586	134.9	10.33	16 530	6 458
Wave set 2	1 367	111.6	8.89	14 220	6 514
Wave set 3	1 477	118.2	8.40	13 370	6 041
Mean value	**1 477**	**121.6**	**9.21**	**14 710**	**6 338**

Table 14a: Results from simulations of DLC 1.4, V_{hub}=11.4 m/s, wind direction change=63.2°.

	Axial acc. at nacelle [m/s^2]	Horiz. displacement at hub height [m]	Tower pitch angle [deg]	Rotor power [kW]	Rotor power stdev. [kW]
Wave set 1	1.773	24.90	2.64	11 610	2 166
Wave set 2	1.566	22.56	2.08	11 140	2 051
Wave set 3	1.919	24.66	2.42	11 060	1 681
Mean value	**1.753**	**24.04**	**2.38**	**11 270**	**1 966**

Table 14b: Results from simulations of DLC 1.4, V_{hub}=11.4 m/s, wind direction change=63.2°.

The maximum values of each parameter that was registered from V_{hub}=11.4 m/s and wind direction change=63.2° are presented in table 14a and 14b. The mean maximum shear force between nacelle/tower is the highest of DLC 1.4, but 1 477 kN is a moderate value compared to other load cases. Most of the other values are exceeded by the simulations with the same wind speed, but opposite direction change.

V_{hub}=13.4 m/s, V_{gust}=15 m/s, wind direction change= -53.7°

	Shear force nacelle/tower [kN]	Bending moment substruc./tower [MNm]	Out-of-plane blade tip deflection [m]	Out-of-plane blade root bend. moment [kNm]	In-plane blade root bend. moment [kNm]
Wave set 1	1 383	122.0	7.38	10 960	6 662
Wave set 2	1 247	104.5	6.61	11 760	6 700
Wave set 3	1 260	107.4	5.89	10 580	6 556
Mean value	**1 297**	**111.3**	**6.63**	**11 100**	**6 639**

Table 15a: Results from simulations of DLC 1.4, V_{hub}=13.4 m/s, wind direction change=-53.7°.

	Axial acc. at nacelle $[m/s^2]$	Horiz. displacement at hub height [m]	Tower pitch angle [deg]	Rotor power [kW]	Rotor power stdev. [kW]
Wave set 1	1.806	23.49	2.27	17 150	3 090
Wave set 2	1.354	21.15	1.73	14 100	2 895
Wave set 3	1.535	23.38	2.09	17 600	2 510
Mean value	**1.565**	**22.67**	**2.03**	**16 280**	**2 832**

Table 15b: Results from simulations of DLC 1.4, V_{hub}=13.4 m/s, wind direction change=-53.7°.

The maximum values of each parameter that was registered from $\mathrm{V_{hub}}$=13.4 m/s and wind direction change=-53.7° are presented in table 15a and 15b. Most values are below those of $\mathrm{V_{hub}}$=11.4 m/s and wind direction change=-63.2, in particular the blade tip deflection at 6.63 m and the out-of-plane blade root bending moment of 11 100 kNm, which are amongst the lowest of all the load cases. It is worth noting the high average maximum rotor power at 16 280 kW, which could potentially damage the electrical system.

V_{hub}=13.4 m/s, V_{gust}=15 m/s, wind direction change=53.7°

	Shear force nacelle/tower [kN]	Bending moment substruc./tower [MNm]	Out-of-plane blade tip deflection [m]	Out-of-plane blade root bend. moment [kNm]	In-plane blade root bend. moment [kNm]
Wave set 1	1 464	127.7	6.63	12 350	6 621
Wave set 2	1 265	105.0	6.35	11 840	6 330
Wave set 3	1 244	110.1	6.13	11 140	6 553
Mean value	**1 324**	**114.3**	**6.37**	**11 780**	**6 501**

Table 16a: Results from simulations of DLC 1.4, V_{hub}=13.4 m/s, wind direction change=53.7°.

	Axial acc. at nacelle $[m/s^2]$	Horiz. displacement at hub height [m]	Tower pitch angle [deg]	Rotor power [kW]	Rotor power stdev. [kW]
Wave set 1	2.116	23.03	2.26	12 810	2 614
Wave set 2	1.708	21.56	1.86	13 170	2 554
Wave set 3	1.762	23.48	2.15	12 610	2 153
Mean value	**1.862**	**22.69**	**2.09**	**12 860**	**2 440**

Table 16b: Results from simulations of DLC 1.4, V_{hub}=13.4 m/s, wind direction change=53.7°.

The maximum values of each parameter that was registered from V_{hub}=13.4 m/s and wind direction change=53.7° are presented in table 16a and 16b. The mean axial acceleration at the nacelle of 1.862 m/s^2 is the highest value of DLC 1.4, but is still small compared to some of the other load cases. The average blade tip deflection of 6.37 is the lowest value registered, regardless of load case.

4.6 DLC 1.5

Design load case 1.5 is sudden extreme wind shear events, imposed on a steady wind speed while the wind turbine is in production. Over a period of 12 seconds the wind speed changes rapidly in the horizontal or vertical direction, positive or negative, and returns to normal wind shear. Examples of the wind profiles used in DCL 1.5 are shown in figure 26 and figure 27. The initial wind speed at hub height equals the rated wind speed of 11.4 m/s. As for DLC 1.4, the same three wave data realizations are used throughout the load case, so for example the waves from wave set 1 is identical for all the simulations within DLC 1.5. The ocean current is set to 0.114 m/s. Wave, wind and current directions are aligned.

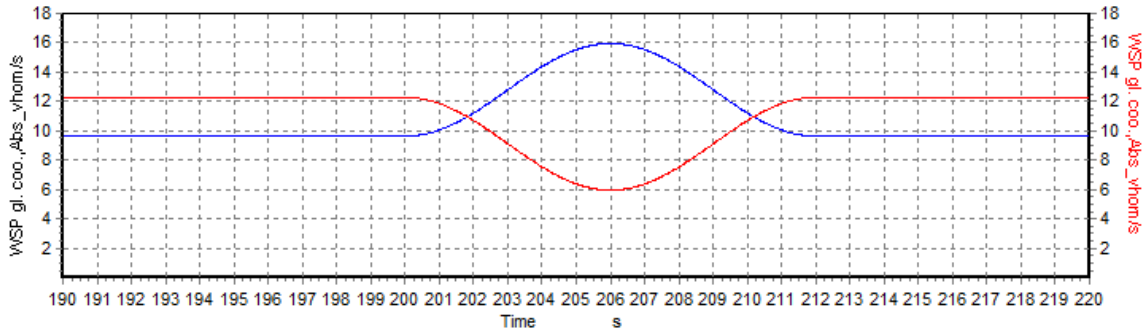

Figure 26: Extreme negative vertical wind shear, wind speed at rotor top in red, rotor bottom in blue.

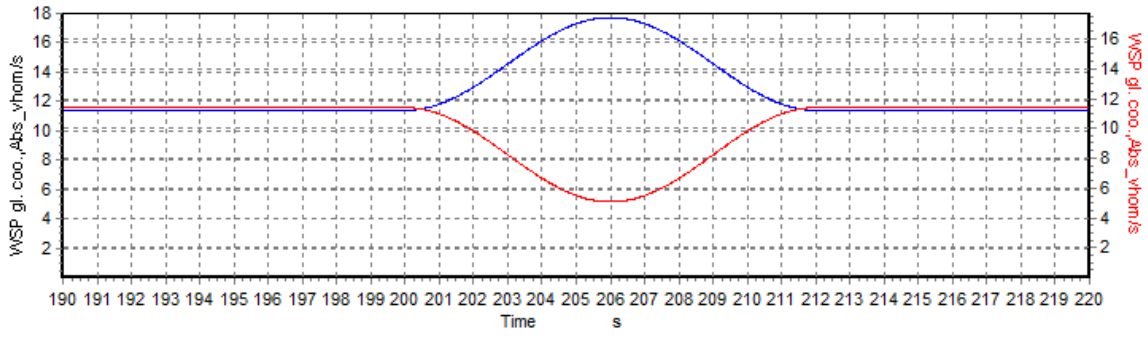

Figure 27: Extreme horizontal wind shear. The two lines are the wind speeds at the left/right edge of the rotor area.

Extreme negative vertical wind shear

	Shear force nacelle/tower [kN]	Bending moment substruc./tower [MNm]	Out-of-plane blade tip deflection [m]	Out-of-plane blade root bend. moment [kNm]	In-plane blade root bend. moment [kNm]
Wave set 1	1 390	120.3	7.03	11 870	4 680
Wave set 2	1 429	130.0	7.31	12 290	5 122
Wave set 3	1 455	124.9	7.57	12 580	4 883
Mean value	**1 425**	**125.1**	**7.30**	**12 247**	**4 895**

Table 17a: Results from simulations of DLC 1.5, extreme negative vertical wind shear.

	Axial acc. at nacelle $[m/s^2]$	Horiz. displacement at hub height [m]	Tower pitch angle [deg]	Rotor power [kW]	Rotor power stdev. [kW]
Wave set 1	1.129	23.85	1.67	7 320	983
Wave set 2	1.226	26.02	2.54	7 550	1 204
Wave set 3	1.300	24.89	2.20	7 480	988
Mean value	**1.218**	**24.92**	**2.14**	**7 450**	**1 058**

Table 17b: Results from simulations of DLC 1.5, extreme negative vertical wind shear.

The maximum values of each parameter that was registered from extreme negative vertical wind shear are presented in table 17a and 17b. The values are in general relatively low compared to those of other production load cases. Most of the key parameters are also at the lowest values of DLC 1.5, but the differences between the various wind shear cases are small.

Extreme positive vertical wind shear

	Shear force nacelle/tower [kN]	Bending moment substruc./tower [MNm]	Out-of-plane blade tip deflection [m]	Out-of-plane blade root bend. moment [kNm]	In-plane blade root bend. moment [kNm]
Wave set 1	1 384	120.6	7.47	12 380	4 843
Wave set 2	1 514	131.8	7.32	12 350	5 179
Wave set 3	1 452	124.7	7.58	12 600	5 025
Mean value	**1450**	**125.7**	**7.46**	**12 440**	**5016**

Table 18a: Results from simulations of DLC 1.5, extreme positive vertical wind shear.

	Axial acc. at nacelle $[m/s^2]$	Horiz. displacement at hub height [m]	Tower pitch angle [deg]	Rotor power [kW]	Rotor power stdev. [kW]
Wave set 1	1.123	23.68	2.20	7 310	996
Wave set 2	1.235	26.36	2.59	7 610	1 236
Wave set 3	1.284	25.26	2.24	7 440	999
Mean value	**1.214**	**25.10**	**2.34**	**7 450**	**1 077**

Table 18b: Results from simulations of DLC 1.5, extreme positive vertical wind shear.

The maximum values of each parameter that was registered from extreme positive vertical wind shear are presented in table 18a and 18b. Most of the values are a fraction larger than those from the negative vertical wind shear, but the difference is not very significant. Nevertheless, positive vertical wind shear is overall the "worst case" amongst DLC 1.5.

Extreme negative horizontal wind shear

	Shear force nacelle/tower [kN]	Bending moment substruc./tower [MNm]	Out-of-plane blade tip deflection [m]	Out-of-plane blade root bend. moment [kNm]	In-plane blade root bend. moment [kNm]
Wave set 1	1 400	121.2	7.16	11 940	5 338
Wave set 2	1 496	130.0	7.39	12 320	5 376
Wave set 3	1 449	124.3	7.59	12 600	5 279
Mean value	**1 448**	**125.2**	**7.38**	**12 290**	**5 331**

Table 19a: Results from simulations of DLC 1.5, extreme negative horizontal wind shear.

	Axial acc. at nacelle $[m/s^2]$	Horiz. displacement at hub height [m]	Tower pitch angle [deg]	Rotor power [kW]	Rotor power stdev. [kW]
Wave set 1	1.145	23.99	2.26	7 330	990
Wave set 2	1.234	26.00	2.52	7 550	1 216
Wave set 3	1.306	24.91	2.20	7 490	992
Mean value	**1.228**	**24.97**	**2.33**	**7 460**	**1 066**

Table 19b: Results from simulations of DLC 1.5, extreme negative horizontal wind shear.

The maximum values of each parameter that was registered from extreme negative horizontal wind shear are presented in table 19a and 19b. The in-plane blade root bending moment is the highest within DLC 1.5, but it is still low compared to other load cases. Most of the other values are approximately the same or a bit lower than those of the positive vertical wind shear.

Extreme positive horizontal wind shear

	Shear force nacelle/tower [kN]	Bending moment substruc./tower [MNm]	Out-of-plane blade tip deflection [m]	Out-of-plane blade root bend. moment [kNm]	In-plane blade root bend. moment [kNm]
Wave set 1	1 376	118.9	7.19	11 920	4 683
Wave set 2	1 508	131.6	7.31	12 320	5 063
Wave set 3	1 458	125.1	7.56	12 580	4 875
Mean value	**1 447**	**125.2**	**7.35**	**12 270**	**4 874**

Table 20a: Results from simulations of DLC 1.5, extreme positive horizontal wind shear.

	Axial acc. at nacelle $[m/s^2]$	Horiz. displacement at hub height [m]	Tower pitch angle [deg]	Rotor power [kW]	Rotor power stdev. [kW]
Wave set 1	1.113	23.58	2.18	7 300	992
Wave set 2	1.212	26.35	2.60	7 600	1 220
Wave set 3	1.283	25.23	2.24	7 440	997
Mean value	**1.203**	**25.05**	**2.34**	**7 450**	**1 070**

Table 20b: Results from simulations of DLC 1.5, extreme positive horizontal wind shear.

The maximum values of each parameter that was registered from extreme positive horizontal wind shear are presented in table 20a and 20b. The mean results are practically identical to those of the negative horizontal wind shear, except for the in-plane blade root bending moment that is the lowest of DLC 1.5.

4.7 DLC 1.6a

Design load case 1.6a is with the wind turbine in production under normal wind speed and turbulence conditions, but with a severe sea state corresponding to a 50 years return period. The significant wave height and peak period shall reflect the worst sea state that could occur at the given hub height wind speed, and is set to 12 m and 13 s respectively. The mean wind speed at hub height is 11.4 m/s, with a turbulence intensity of 0.199. The ocean current is set to 0.114 m/s. Wave, wind and current directions are aligned. A total of 10 simulations were run, each covering a 10 minute period. The maximum values of each parameter that was registered are presented in table 21a and 21b.

	Shear force nacelle/tower [kN]	Bending moment substruc./tower [MNm]	Out-of-plane blade tip deflection [m]	Out-of-plane blade root bend. moment [kNm]	In-plane blade root bend. moment [kNm]
Simulation 1	2 609	229.0	10.38	19 510	8 554
Simulation 2	3 185	281.4	11.86	20 410	6 924
Simulation 3	2 840	254.6	10.75	18 380	7 783
Simulation 4	2 850	260.6	10.43	17 740	7 699
Simulation 5	2 936	266.4	10.37	17 270	7 564
Simulation 6	2 763	250.2	10.20	17 360	10 170
Simulation 7	2 478	222.7	10.22	17 930	7 325
Simulation 8	2 871	258.9	9.51	16 280	8 769
Simulation 9	2 746	250.4	10.15	20 270	9 357
Simulation 10	2 878	255.1	9.91	17 120	7 022
Mean value	**2 816**	**252.9**	**10.38**	**18 230**	**8 117**

Table 21a: Results from the simulations of DLC 1.6a.

	Axial acc. at nacelle $[m/s^2]$	Horiz. displacement at hub height [m]	Tower pitch angle [deg]	Rotor power [kW]	Rotor power stdev. [kW]
Simulation 1	3.787	35.40	3.86	15 990	2 747
Simulation 2	4.175	43.27	5.01	20 130	2 923
Simulation 3	4.293	36.42	4.06	14 470	2 746
Simulation 4	5.037	41.40	4.93	17 430	3 014
Simulation 5	4.425	40.15	4.93	14 390	2 840
Simulation 6	4.665	40.45	4.29	17 540	2 643
Simulation 7	4.203	42.03	3.73	16 290	2 759
Simulation 8	4.706	35.46	4.57	16 130	2 854
Simulation 9	5.718	40.49	4.69	22 020	2 925
Simulation 10	4.310	42.58	4.80	18 520	2 919
Mean value	**4.532**	**39.77**	**4.49**	**17 290**	**2 837**

Table 21b: Results from the simulations of DLC 1.6a.

The mean maximum values from DLC 1.6a are in general amongst the highest of the production cases, only exceeded by the values from DLC 1.1 and DLC 1.1 ONC that is extrapolated to 50 years return period. The axial acceleration at hub height of 4.533 m/s^2 is about the same level as the simulations with a parked turbine exposed to extreme wind and wave conditions. It is also interesting that this load case has by far the highest maximum rotor power, even though the wind conditions are fairly moderate.

4.8 DLC 6.1a

Design load case 6.1 is meant to simulate extreme environmental conditions, where the wind turbine is parked/shut down to insure its survival. DLC 6.1a includes extreme, turbulent wind and extreme, irregular waves, both corresponding to a 50 years return period. The mean wind speed at hub height is set to 50 m/s, with a turbulence intensity of 0.11. The significant wave height is set to 14 m, with a peak period of 14 seconds. The ocean current is also meant to reflect a 50 years return period, and a velocity of 1.00 m/s is chosen. Wave, wind and current directions are aligned, but are simulated with directions of 0° and +-8° relative to the global y-direction, to investigate the effect of yaw misalignment. A total of 10 simulations were run for each yaw misalignment direction, each covering a 10 minute period.

Yaw misalignment 0°

	Shear force nacelle/tower [kN]	Bending moment substruc./tower [MNm]	Out-of-plane blade tip deflection [m]	Out-of-plane blade root bend. moment [kNm]
Simulation 1	4 186	393.3	8.65	19 760
Simulation 2	3 923	366.4	8.64	19 400
Simulation 3	3 695	345.1	8.47	19 500
Simulation 4	3 869	361.1	8.91	20 390
Simulation 5	4 187	394.7	8.36	19 460
Simulation 6	3 647	337.8	9.12	20 800
Simulation 7	4 260	401.0	8.24	19 000
Simulation 8	4 787	450.0	8.87	21 370
Simulation 9	3 586	327.7	9.04	19 650
Simulation 10	4 020	378.8	8.56	19 160
Mean value	**4 016**	**375.6**	**8.69**	**19 850**

Table 22a: Results from the simulations of DLC 6.1a, yaw misalignment 0°.

	Axial acc. at nacelle $[m/s^2]$	Horiz. displacement at hub height [m]	Tower pitch angle [deg]	Max wind speed [m/s]	Max wave amplitude [m]
Simulation 1	4.508	67.67	8.63	67.97	9.43
Simulation 2	4.803	59.29	7.28	67.65	9.60
Simulation 3	4.484	61.85	7.94	69.88	8.21
Simulation 4	4.995	59.20	7.55	68.27	9.30
Simulation 5	5.150	72.31	9.69	71.44	10.18
Simulation 6	4.720	57.74	7.35	68.88	9.43
Simulation 7	5.891	62.06	8.39	68.44	10.39
Simulation 8	6.139	72.70	10.2	67.30	11.39
Simulation 9	4.757	54.50	5.66	67.04	11.20
Simulation 10	5.540	61.47	7.91	67.79	9.177
Mean value	**5.099**	**62.88**	**8.06**	**68.47**	**9.83**

Table 22b: Results from the simulations of DLC 6.1a, yaw misalignment 0°.

The maximum values of each parameter that was registered from yaw misalignment direction 0° are presented in table 22a and 22b. The results are in general higher than those of the production load cases (1.x). Especially the shear force between nacelle/tower, the bending moment between substructure/tower, the horizontal displacement at hub height and the tower pitch angle reach large values. The values are, however, not the highest within DLC 6.1a.

Yaw misalignment -8°

	Shear force nacelle/tower [kN]	Bending moment substruc./tower [MNm]	Out-of-plane blade tip deflection [m]	Out-of-plane blade root bend. moment [kNm]
Simulation 1	3 745	354.2	8.90	19 900
Simulation 2	3 895	369.1	9.56	20 990
Simulation 3	3 963	375.5	8.48	19 060
Simulation 4	3 767	349.6	8.19	17 930
Simulation 5	3 954	362.7	9.24	21 140
Simulation 6	3 866	353.6	9.47	20 390
Simulation 7	4 313	409.9	10.26	24 130
Simulation 8	3 811	346.9	9.64	21 000
Simulation 9	4 340	410.6	9.18	19 820
Simulation 10	3 944	366.9	11.69	24 380
Mean value	**3 960**	**369.9**	**9.46**	**20 870**

Table 23a: Results from the simulations of DLC 6.1a, yaw misalignment -8°.

	Axial acc. at nacelle $[m/s^2]$	Horiz. displacement at hub height [m]	Tower pitch angle [deg]	Max wind speed [m/s]	Max wave amplitude [m]
Simulation 1	4.590	63.40	7.96	65.94	10.95
Simulation 2	4.519	66.48	8.42	67.32	9.46
Simulation 3	5.344	63.41	7.95	68.19	9.13
Simulation 4	4.685	59.69	7.83	72.56	9.91
Simulation 5	5.416	64.02	8.39	67.57	12.33
Simulation 6	5.114	58.78	7.35	68.98	8.23
Simulation 7	5.319	71.45	9.26	70.34	10.49
Simulation 8	4.921	63.30	8.73	67.39	10.07
Simulation 9	4.948	74.89	9.83	69.83	10.36
Simulation 10	4.884	65.58	8.50	69.69	9.74
Mean value	**4.974**	**65.10**	**8.42**	**68.78**	**10.07**

Table 23b: Results from the simulations of DLC 6.1a, yaw misalignment -8°.

The maximum values of each parameter that was registered from yaw misalignment direction -8° are presented in table 23a and 23b. As one could expect, the results are pretty close to those of the other yaw misalignment directions. The most significant difference is in the mean maximum blade tip deflection, which with 9.46 m is the highest within DLC 1.6. The other values are in general high, but a bit lower than the ones from yaw misalignment direction 8°.

Yaw misalignment 8°

	Shear force nacelle/tower [kN]	Bending moment substruc./tower [MNm]	Out-of-plane blade tip deflection [m]	Out-of-plane blade root bend. moment [kNm]
Simulation 1	3 945	378.2	9.43	19 940
Simulation 2	4 277	406.0	8.25	19 430
Simulation 3	3 761	351.7	8.66	19 730
Simulation 4	4 252	319.9	8.82	20 410
Simulation 5	4 663	430.4	9.35	21 270
Simulation 6	3 831	345.1	8.87	20 310
Simulation 7	4 263	396.8	8.34	20 210
Simulation 8	3 887	368.4	8.39	19 620
Simulation 9	4 427	417.4	10.41	22 050
Simulation 10	4 832	446.5	9.73	23 730
Mean value	**4 214**	**386.0**	**9.03**	**20 670**

Table 24a: Results from the simulations of DLC 6.1a, yaw misalignment 8°

	Axial acc. at nacelle $[m/s^2]$	Horiz. displacement at hub height [m]	Tower pitch angle [deg]	Max wind speed [m/s]	Max wave amplitude [m]
Simulation 1	5.162	68.13	8.92	68.49	10.00
Simulation 2	5.731	73.42	9.37	65.93	11.22
Simulation 3	4.714	60.75	8.20	68.22	9.51
Simulation 4	5.553	62.95	8.39	70.00	11.53
Simulation 5	6.303	70.56	9.25	68.27	10.75
Simulation 6	4.644	61.18	8.23	71.74	11.98
Simulation 7	5.698	68.34	8.95	65.46	9.63
Simulation 8	4.506	65.05	8.72	68.76	10.47
Simulation 9	4.892	75.65	10.49	72.20	10.14
Simulation 10	5.010	68.51	9.22	71.14	11.35
Mean value	**5.221**	**67.45**	**8.97**	**69.02**	**10.66**

Table 24b: Results from the simulations of DLC 6.1a, yaw misalignment 8°.

The maximum values of each parameter that was registered from yaw misalignment direction 8° are presented in table 24a and 24b. This is overall the "worst case" scenario within DLC 6.1a, although the difference between the yaw misalignment directions is small. Another observation is that high maximum wind speed and wave amplitude not necessarily correlates with high values of the other parameters. For example, in simulation 6 large measurements are made of both wind and waves, but the rest of the parameters are still all below the mean value. It is more the combination and timing of the two that generates the greatest loads.

4.9 DLC 6.1b

DLC 6.1b includes extreme, steady wind and somewhat reduced extreme regular waves imposed on a wind turbine that is parked/shut down. The steady wind speed at hub height is 70 m/s, corresponding to a 50 years event. The wave height is set to 12 m, with a period of 12 seconds. The ocean current is also meant to reflect a 50 years return period, and a velocity of 1.00 m/s is chosen. Wave, wind and current directions are aligned, but are simulated with directions of 0° and +-15° relative to the global y-direction, to investigate the effect of yaw misalignment. As there are no stochastic variables included in this load case, only one simulation per yaw misalignment direction is performed. The maximum values of each parameter that was registered are presented in table 25a and 25b.

	Shear force nacelle/tower [kN]	Bending moment substruc./tower [MNm]	Out-of-plane blade tip deflection [m]	Out-of-plane blade root bend. moment [kNm]
Yaw mis. 0°	4 131	386.0	10.13	23 240
Yaw mis. -15°	4 012	374.7	10.03	22 520
Yaw mis. 15°	4 025	374.7	9.71	23 150

Table 25a: Results from the simulations of DLC 6.1b.

	Axial acc. at nacelle $[m/s^2]$	Horiz. displacement at hub height [m]	Tower pitch angle [deg]
Yaw mis. 0°	2.762	63.07	8.71
Yaw mis. -15°	2.709	61.98	8.47
Yaw mis. 15°	2.694	61.77	8.46

Table 25b: Results from the simulations of DLC 6.1b.

The head on direction of 0° yields a slightly higher response than the misaligned (+-15°) directions on all the registered parameters. The out of plane blade root bending moment of 23 240 kNm is the highest value from any load case. Compared to the other load cases with a parked turbine under extreme environmental conditions (6.1x), the most distinct parameter is the axial acceleration at nacelle height, which is roughly half the value found in DLC 6.1a and 6.1c.

4.10 DLC 6.1c

DLC 6.1b includes extreme, but reduced, steady wind and extreme regular waves imposed on a wind turbine that is parked/shut down. The steady wind speed at hub height is 55 m/s, which is lower than the 50 years event. The wave height is set to 20 m, with a period of 14 seconds. The ocean current is meant to reflect a 50 years return period, and a velocity of 1.00 m/s is chosen. Wave, wind and current directions are aligned, but are simulated with directions of 0° and +-15° relative to the global y-direction, to investigate the effect of yaw misalignment. As there are no stochastic variables included in this load case, only one simulation per yaw misalignment direction is performed. The maximum values of each parameter that was registered are presented in table 26a and 26b.

	Shear force nacelle/tower [kN]	Bending moment substruc./tower [MNm]	Out-of-plane blade tip deflection [m]	Out-of-plane blade root bend. moment [kNm]
Yaw mis. 0°	4 123	392.5	7.81	18 100
Yaw mis. -15°	3 812	361.4	7.46	16 940
Yaw mis. 15°	3 851	364.3	7.28	17 470

Table 26a: Results from the simulations of DLC 6.1c

	Axial acc. at nacelle $[m/s^2]$	Horiz. displacement at hub height [m]	Tower pitch angle [deg]
Yaw mis. 0°	4.631	68.31	8.45
Yaw mis. -15°	4.222	62.86	7.94
Yaw mis. 15°	4.223	63.32	7.91

Table 26b: Results from the simulations of DLC 6.1c.

As for DLC 6.1b, the head on direction of 0° scores higher than the misaligned (+-15°) directions on all the registered parameters, and the differences are larger for this load case. As one could expect, the blade tip deflection and out-of-plane blade root bending moment are lower for DLC 6.1c than for 6.1a and 6.1b, due to the reduced wind speed. The other results are pretty similar to those of DLC 6.1a.

4.11 Results summary

	Shear force nacelle/tower [kN]	Bending moment substruc./tower [MNm]	Out-of-plane blade tip deflection [m]	Out-of-plane blade root bend. moment [kNm]	In-plane blade root bend. moment [kNm]
DLC 1.1	1 753	151.5	8.91 (12.30)	15 180 (21 600)	7 616 (10700)
DLC 1.1 ONC*	2 011	176.7	9.45 (13.70)	16 080 (22 600)	6958 (10 100)
DLC 1.3	1 775	154.7	9.76	17 316	11 150
DLC 1.4	1 477	124.3	10.20	17 110	6 639
DLC 1.5	1 450	125.7	7.46	12 440	5 331
DLC 1.6a	2 816	252.9	10.38	18 230	8 117
DLC 6.1a	4 214	386.0	9.46	20 870	N/A
DLC 6.1b	4 131	386.0	10.13	23 240	N/A
DLC 6.1c	4 123	392.5	7.81	18 100	N/A
Overall max	**4 214**	**392.5**	**10.38 (12.30)**	**23 240**	**11 150**

Table 27a: Summary of results from all the load cases. Extrapolated values are in brackets. *DLC 1.1 ONC is run with a different control system, and cannot be compared directly with the other load cases.

	Axial acc. at nacelle $[m/s^2]$	Horiz. displacement at hub height [m]	Tower pitch angle [deg]	Rotor power [kW]	Rotor power stdev. [kW]
DLC 1.1	2.199	26.97	2.76	10 780	1 581
DLC1.1 ONC*	2.323	34.97	4.68	11 600	1 665
DLC 1.3	2.36	27.9	3.12	11 860	1 825
DLC 1.4	1.862	24.76	2.41	16 280	2 832
DLC 1.5	1.228	25.1	2.34	7 460	1 077
DLC 1.6a	4.532	39.77	4.49	17 290	2 837
DLC 6.1a	5.221	67.45	8.97	N/A	N/A
DLC 6.1b	2.762	63.07	8.71	N/A	N/A
DLC 6.1c	4.631	68.31	8.45	N/A	N/A
Overall max	**5.221**	**68.31**	**8.97**	**17 290**	**2 832**

Table 27b: Summary of results from all the load cases. Extrapolated values are in brackets. . *DLC 1.1 ONC are performed with a different control system, and are left out of the maximum load considerations.

The results from all the load cases are summarized in table 27a and 27b. For load cases that include several wind/wave directions or scenarios, each parameter is presented with the largest mean value from any scenario.

The structural loading, shear force between nacelle/tower and bending moment between substructure/tower, are considerably higher for the load cases with a parked turbine under extreme conditions (DLC 6.1x), than for the production load cases (DLC 1.x). The same goes for the motion parameters; axial acceleration and horizontal displacement at hub height, and tower pitch angle. For out-of-plane blade tip deflection and blade root bending moment, the results are more mixed. None of the other load cases are even close to the extrapolated blade tip deflection of DLC 1.1.

Of the production load cases, the one with the highest loads are in general DLC 1.6a, with moderate wind, but severe sea state. Only the extrapolated values from DLC 1.1 are higher.

5 Discussion

The motions and internal forces of the wind turbine are the result of a combination of wind and wave loading. To illustrate the contribution from each of these, time series of wind speed and water surface level (waves) from DLC 1.1 (normal production conditions), along with some key parameters, are presented in figure 28. The time series are taken from simulation 8, which had the highest maximum values of DLC 1.1 on several parameters.

During the simulation period there are two incidents with particularly large waves, the first at around 250 seconds, while the other one occurs after about 650 seconds. Both have wave amplitude of roughly 4 m, or 8 m wave height. These wave events coincide with peak values of all the registered parameters. Only the out-of-plane bending moment reaches its maximum value outside these two events.

If the responses to the first wave event are examined closely, one can observe that the peak values of the tower shear force and bending moment precedes the peak values of the parameters associated with the rotor, i.e. the blade tip deflection, the blade root bending moment and the rotor power. This is because the large waves initiate considerable pitch motion of the wind turbine, which results in a fore-aft movement of the rotor disc area. While the peaks of the tower's internal forces corresponds in time with the maximum hub height displacement, are the peaks of the rotor parameters occurring as the turbine is moving forward against the wind direction, after the maximum displacement. This is due to the increased relative wind velocity the rotor experiences, as it moves into the wind with a velocity of approximately 3 m/s.

A similar time series from DLC 6.1a, with a parked turbine under extreme environmental conditions, would draw a more complex picture. As the mean wind speed increases from 11.4 to 50 m/s its relative contribution to the wind turbine response increases significantly, even though the significant wave height also increases from 5 to 14 m. The maximum values of the different parameters becomes more scattered between large waves, strong wind gusts, or unfavorable combinations of the two.

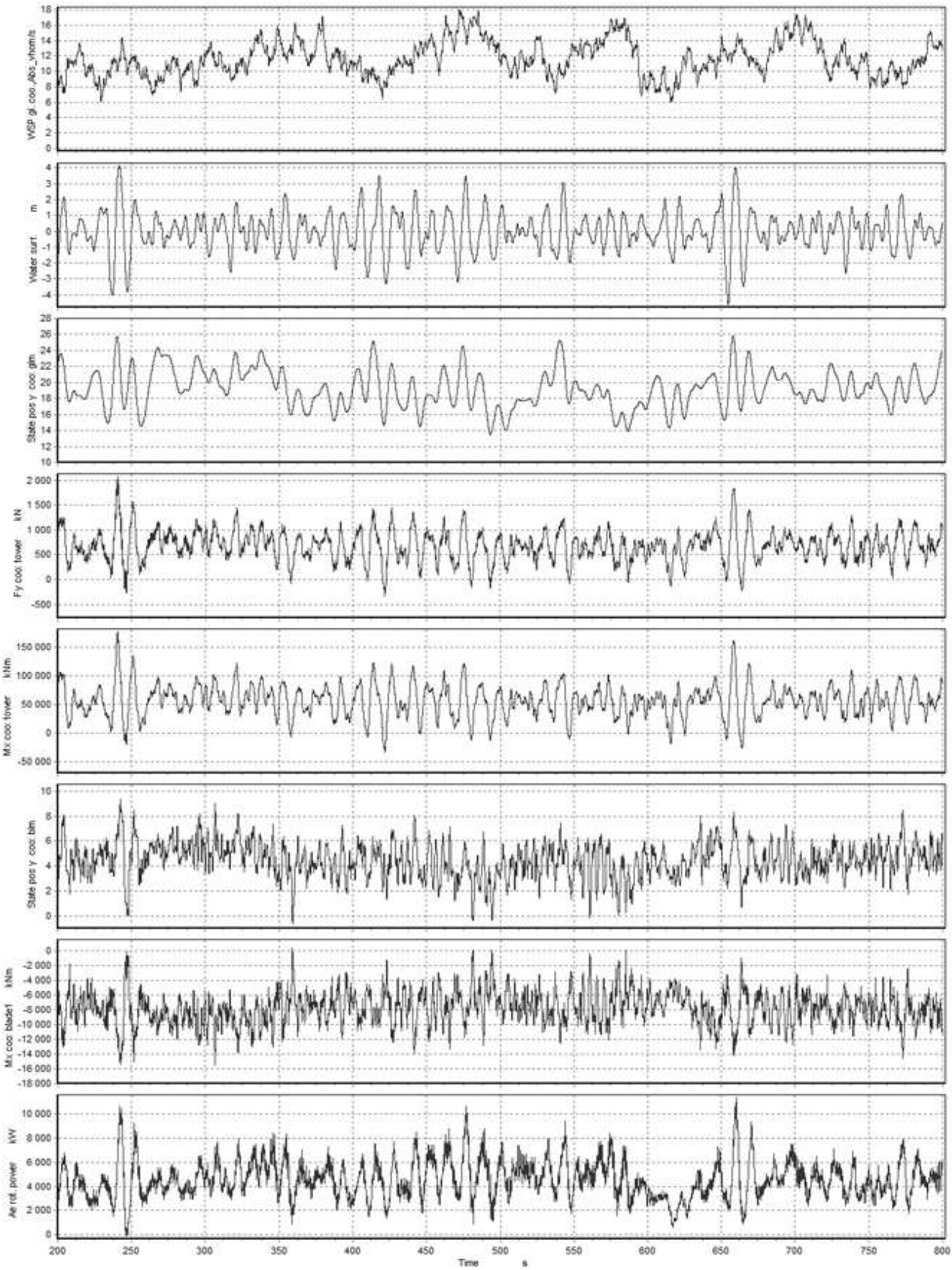

Figure 28: Time series of selected parameters from DLC 1.1, simulation 8. From the top: #1 Absolute horizontal wind speed, #2 water surface level, #3 horizontal displacement of tower in global y-direction at hub height, #4 shear force between nacelle and tower, #5 bending moment between tower and substructure, #6 out-of-plane blade tip deflection, #7 out-of-plane blade root bending moment, #8 rotor power.

When it comes to comparison of the different load cases, the results depend on what part of the wind turbine that is being evaluated; the rotor blades or the substructure/tower. The design driver for the rotor blades seems to be the production load cases (DLC 1.x), in particular the values from DLC 1.1 that is extrapolated to a 50 years return period. The extrapolated out-of-plane blade tip deflection of 12.3 m exceeds the critical deflection value, which for the described values of overhang, shaft tilt, precone and tower diameter is about 11.0 m. This suggests that the out-of-plane stiffness of the blades should be increased to prevent them from crashing into the tower.

While the production load cases determine the design of the rotor, the largest structural loads in the substructure/tower are measured in simulations of DLC 6.1. This load case consisting of a parked turbine exposed to extreme wind and waves, would therefore govern the design of the substructure and tower. Even though all the results from DLC 1.1 ideally should have been extrapolated to 50 years events, the structural loads would not reach the levels of DLC 6.1. The three extrapolated parameters of DLC 1.1 are all about 40 % higher than its mean values, while the structural loads from DLC 6.1 are more than twice as large as those from DLC 1.1.

It should be emphasized that the offshore wind turbine standard IEC 61400-3 describes a number of design load cases that should be evaluated during a design process, which have been ignored in this thesis. These include mainly a variety of fault conditions, in addition to several fatigue analyses. It is possible that some of these load cases would have been more severe to parts of the wind turbine, than the load cases that are simulated here. This applies in particular for the rotor blades, which are exposed to considerable fatigue loads.

Also the magnitude of the responses would increase if a load factor of 1.35 was implemented in the simulations, as specified in IEC 61400. This would however have minor impact on the relative severity of the load cases, as the same load factor would apply to all of those analyzed here. The presence of this factor is therefore unlikely to change any of the conclusions in this thesis. On the other hand, in a real design study for dimensioning purposes, the load factor obviously should be taken into account.

The free decay tests revealed a critically low heave motion period of 15.4 seconds, half the period of other wind turbines of similar concept. Although heave motion is not included in the main parameters that are presented for the different load cases, were measurements of heave performed in all simulations. This revealed considerable motions, especially for the load cases that included extreme waves/sea states. DLC 1.6a, 6.1a and 6.1c all have large waves with periods that is close to resonance with the wind turbine's heave motion period. The results from these simulations were affected by severe heave motions with amplitudes of several meters. However, the motions cannot be considered large enough to void the results of the entire analysis. The values of most of the parameters measured in this thesis are of about the same magnitude as those found in a comparison study of different wind turbine aeroelastic codes, performed on a floating turbine of similar design [24].

Nevertheless, if further analyses of the wind turbine were to be performed, design modifications to increase the heave motion period would be advisable. The best way of doing this is probably by reducing the diameter of the substructure at the water surface line, thus reducing the water crossing area. This would lower the turbine's heave stiffness, and consequently increase the period. The wave induced heave motions would then be minimized, as a high period would make the turbine's motions mass dominated [17].

6 Conclusion

The analysis shows that the peak response under production conditions coincides with the largest wave events. The greatest internal forces of the tower correspond in time with the maximum hub height displacement. The maximum rotor loads occur as the rotor disk area moves into the wind, after the wave initiated displacement.

For a parked turbine exposed to extreme wind and wave conditions, the wind's relative contribution to the total response is enhanced. The maximum loads are then typically observed during unfavorable combinations of strong wind gusts and large waves.

Of the two above mentioned scenarios, the production conditions seem to yield the highest rotor loads, and therefore govern the design of the rotor blades. The opposite is true for the tower and substructure, these experience the highest loads as the turbine is parked and exposed to extreme environmental conditions.

If further analyses were to be performed, the diameter of the substructure at the water surface line could have been decreased. This would increase the heave motion period, and minimize the wave induced heave motion.

References

[1]: Mathew S.: *Wind Energy Fundamentals, Resource Analysis and Economics*, Springer Berlin Heidelberg, 2006

[2]: Breton S.P., Moe G.: *Status, plans and technologies for offshore wind turbines in Europe and North America,* Department of Civil and Transport Engineering, Norwegian University of Science and Technology, Trondheim, 2009

[3]: Jonkman J., Buhl M.L.: *Loads Analysis of a Floating Offshore Wind Turbine Using Fully Coupled Simulation,* WindPower 2007 Conference & Exhibition, Los Angeles, 2007

[4]: Sway AS: http://sway.no/?page=166&show=177, checked 11 June, 2010

[5]: Nielsen F.G.: *Some challenges related to dynamic response of floating offshore wind turbines*, NORCOWE opening Seminar, Bergen, 2009

[6]: Bratland S.: *Hywind – The world's first floating wind turbine*, Powering the future – Marine energy opportunities conference, Lisboa, 2009

[7]: Nielsen F.G., Hanson T.D., Skaare B.: *Integrated dynamic analysis of floating offshore wind turbines*, OMAE2006 25th International Conference on Offshore Mechanics and Arctic Engineering, 2006

[8]: Jonkman J., Butterfield S., Musial W., Scott G.: *Definition of a 5-MW Reference Wind Turbine for Offshore System Development*, National Renewable Energy Laboratory, 2009

[9]: Burton T., Sharpe D., Jenkins N., Bossanyi E.: *WIND ENERGY HANDBOOK*, John Wiley & Sons Ltd, 2001

[10]: Wicker C.: *Global circulation,* www.weatherwizkids.com/globalcirculation.gif, checked 11 June, 2010

[11]: Manwell J.F., McGowan J.G., Rogers A.L.: *Wind Energy Explained, Theory, Design and Application*, John Wiley & Sons Ltd, 2002

[12]: International Electrotechnical Commission: *INTERNATIONAL STANDARD IEC 61400-1 Third edition, Wind Turbines -Part 1: Design requirements*, International Electrotechnical Commission, 2005

[13]: International Electrotechnical Commission: *INTERNATIONAL STANDARD IEC 61400-3 Edition 1.0, Wind Turbines -Part 3: Design requirements for offshore wind turbines*, International Electrotechnical Commission, 2009

[14]: Ingram, G.: *Wind Turbine Blade Analysis using the Blade Element Momentum Method. Version 1.0*, School of Engineering, Durham University, 2005

[15]: DNV/Risø: *Guidelines for Design of Wind Turbines, 2nd Edition*, Det Norske Veritas and Risø National Laboratory, 2002

[16]: Gudmestad O. T.: *MOM260 Marine Technology*, *Lecture notes,* University of Stavanger, 2009

[17]: Gudmestad O. T.: *MOM420 Marine Operations*, *Lecture notes,* University of Stavanger, 2009

[18]: Jonkman J.: *OC3 Phase IV –Model,* IEA Annex XXIII OC3 Meeting, 2009

[19]: Rao S. S.: *Mechanical Vibrations*, Prentice Hall, 2005

[20]: Freudenreich K., Argyriadis K.: *The Load Level of Modern Wind Turbines according to IEC61400-1*, IOP Publishing Ltd, 2007

[21]: Genz R., Nielsen K. B., Madsen P. H.: *An investigation of load extrapolation according toIEC 61400-1 Ed. 3*, EWEC 2006 proceedings, 2006

[22]: Larsen T. J.: *How 2 HAWC2, the user's manual, Version 3-9*, Risø National Laboratory,Technical University of Denmark, 2009

[23]: Larsen T. J., Hanson T. D.: *A method to avoid negative damped low frequent tower vibrations for a floating, pitch controlled wind turbine.*, IOP Publishing Ltd, 2007

[24]: Jonkman J., et al: *Offshore Code Comparison Collaboration within IEA Wind Task 23: Phase IV Results Regarding Floating Wind Turbine Modeling*, European Wind Energy Conference and Exhibition (EWEC) 2010, 2010

Appendix

A1 Structural input parameters

The structural properties of the wind turbine are given by a set of 19 parameters, defined across the length of each main body (tower, hub, blades etc.). An explanation of these parameters is given in a presentation from Risø DTU:

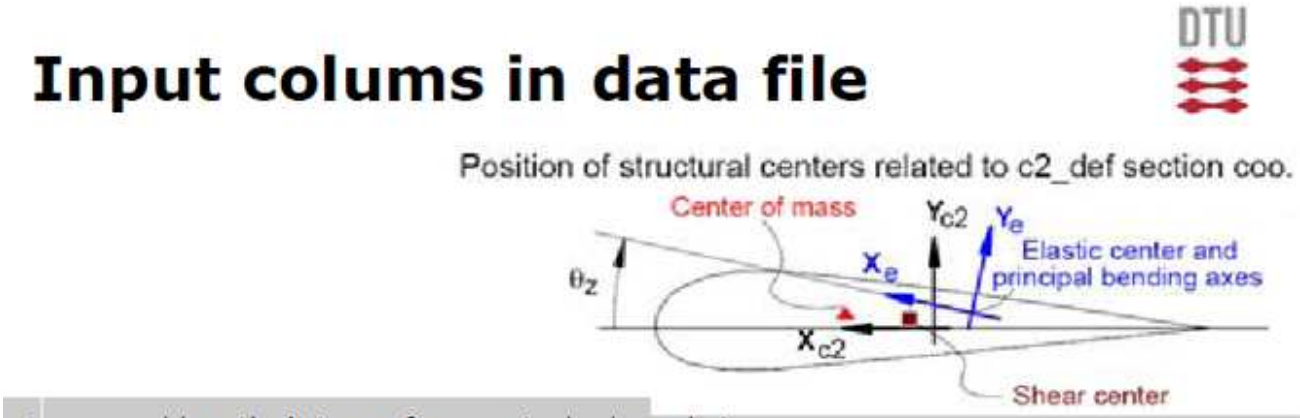

1	r, curved length distance from main_body node1
2	m, mass per unit length [kg/m]
3	xm, xc2-coordinate from C1/2 to mass center [m]
4	ym, yc2-coordinate from C1/2 to mass center [m]
5	rix, radius of inertia related to elastic center. Corresponds to rotation about principal bending xe axis [m]
6	riy, radius of inertia related to elastic center. Corresponds to rotation about principal bending ye axis [m]
7	xs, xc2-coordinate from C1/2 to shear center [m]
8	ys, yc2-coordinate from C1/2 to shear center [m]
9	E, modulus of elasticity [N/m2]
10	G, shear modulus of elasticity [N/m2]
11	Ix, area moment of inertia with respect to principal bending xe axis [N/m4]
12	Iy, area moment of inertia with respect to principal bending ye axis [N/m4]
13	K, torsional stiffness constant with respect to ze axis at the shear center [m4/rad]. For a circular section only this is identical to the polar moment of inertia.
14	kx shear factor for force in principal bending xe direction [-]
15	ky, shear factor for force in principal bending ye direction [-]
16	A, cross sectional area [m2]
17	structural pitch about zc2 axis. This is the angle between the xc2 -axis defined with the c2_def command and the 1st main principal bending axis xe.
18	xe, xc2-coordinate from C1/2 to center of elasticity [m]
19	ye, yc2-coordinate from C1/2 to center of elasticity [m]

Figure A1: Explanation of the structural input parameters used in HAWC2, from a presentation made by Risø DTU.

The structural input parameters of all the main bodies of the wind turbine, i.e. the substructure, tower, shaft, hub and blades, are presented in table A1-A5.

Substructure

#1	#2	#3	#4	#5	#6
0	13196.5	0	0	2.10021	2.10021
92.57	13196.5	0	0	2.10021	2.10021
94.79	11972.9	0	0	1.98353	1.98353
97.01	10740.8	0	0	1.86685	1.86685
99.22	9517.14	0	0	1.75018	1.75018
100	9517.14	0	0	1.75018	1.75018
110	9517.14	0	0	1.75018	1.75018

#7	#8	#9	#10	#11	#12
0	0	2.10E+11	8.08E+10	9.82305	9.82305
0	0	2.10E+11	8.08E+10	9.82305	9.82305
0	0	2.10E+11	8.08E+10	8.19494	8.19494
0	0	2.10E+11	8.08E+10	6.56682	6.56682
0	0	2.10E+11	8.08E+10	4.93871	4.93871
0	0	2.10E+11	8.08E+10	4.93871	4.93871
0	0	2.10E+11	8.08E+10	4.93871	4.93871

#13	#14	#15	#16	#17	#18	#19
19.6461	0.5	0.5	1.553	0	0	0
19.6461	0.5	0.5	1.553	0	0	0
16.3899	0.5	0.5	1.409	0	0	0
13.1336	0.5	0.5	1.264	0	0	0
9.87745	0.5	0.5	1.12	0	0	0
9.87745	0.5	0.5	1.12	0	0	0
9.87745	0.5	0.5	1.12	0	0	0

Table A1: Structural input parameters of the 110 m tall substructure.

Tower

#1	#2	#3	#4	#5	#6
0	4306.51	0	0	2.11179	2.11179
7.76	4030.44	0	0	2.03676	2.03676
15.52	3763.45	0	0	1.96176	1.96176
23.28	3505.52	0	0	1.88673	1.88673
31.04	3256.66	0	0	1.81168	1.81168
38.8	3016.86	0	0	1.73668	1.73668
46.56	2786.13	0	0	1.66167	1.66167
54.32	2564.46	0	0	1.58661	1.58661
62.08	2351.87	0	0	1.51162	1.51162
69.84	2148.34	0	0	1.43659	1.43659
77.59	1953.87	0	0	1.36157	1.36157
77.6	0.001	0	0	1.36157	1.36157
79.13	0.001	0	0	1.36157	1.36157
79.14	0.001	0	0	3.3	3.3
79.56	0.001	0	0	3.3	3.3

#7	#8	#9	#10	#11	#12
0	0	2.10E+11	8.08E+10	2.25948	2.25948
0	0	2.10E+11	8.08E+10	1.96705	1.96705
0	0	2.10E+11	8.08E+10	1.70395	1.70395
0	0	2.10E+11	8.08E+10	1.4681	1.4681
0	0	2.10E+11	8.08E+10	1.25752	1.25752
0	0	2.10E+11	8.08E+10	1.07048	1.07048
0	0	2.10E+11	8.08E+10	0.90505	0.90505
0	0	2.10E+11	8.08E+10	0.75948	0.75948
0	0	2.10E+11	8.08E+10	0.63224	0.63224
0	0	2.10E+11	8.08E+10	0.52162	0.52162
0	0	2.10E+11	8.08E+10	0.42614	0.42614
0	0	2.10E+11	8.08E+10	1000	1000
0	0	2.10E+11	8.08E+10	1000	1000
0	0	2.10E+11	8.08E+10	1000	1000
0	0	2.10E+11	8.08E+10	1000	1000

Table A2a: Structural input parameters of the 80 m tall tower. The tower top mass is placed on its own structure.

#13	#14	#15	#16	#17	#18	#19
4.51897	0.5	0.5	0.507	0	0	0
3.93413	0.5	0.5	0.474	0	0	0
3.40787	0.5	0.5	0.443	0	0	0
2.93616	0.5	0.5	0.412	0	0	0
2.5151	0.5	0.5	0.383	0	0	0
2.14093	0.5	0.5	0.355	0	0	0
1.81005	0.5	0.5	0.328	0	0	0
1.519	0.5	0.5	0.302	0	0	0
1.26444	0.5	0.5	0.277	0	0	0
1.04321	0.5	0.5	0.253	0	0	0
0.85226	0.5	0.5	0.23	0	0	0
256.994	0.5	0.5	1000	0	0	0
256.994	0.5	0.5	1000	0	0	0
256.994	0.5	0.5	1000	0	0	0
256.994	0.5	0.5	1000	0	0	0

Table A2b: Structural input parameters of the 80 m tall tower. The tower top mass is placed on its own structure.

Shaft

#1	#2	#3	#4	#5	#6
0	1	0	0	0.2	0.2
5.0191	1	0	0	0.2	0.2

#7	#8	#9	#10	#11	#12
0	0	2.10E+11	8.10E+10	1.00E+02	1.00E+02
0	0	2.10E+11	8.10E+10	1.00E+02	1.00E+02

#13	#14	#15	#16	#17	#19	#20
0.05376	0.52	0.52	0.59	0	0	0
0.05376	0.52	0.52	0.59	0	0	0

Table A3: Structural input parameters of the shaft.

Hub

#1	#2	#3	#4	#5	#6
0	0.00001	0	0	1.433	1.433
1	0.00001	0	0	1.433	1.433
1.01	39000	0	0	1.433	1.433
1.49	39000	0	0	1.433	1.433

Table A4a: Structural input parameters of the hub.

#7	#8	#9	#10	#11	#12
0	0	2.10E+11	8.07E+10	1.29E+00	1.29E+00
0	0	2.10E+11	8.07E+10	1.29E+00	1.29E+00
0	0	2.10E+11	8.07E+10	1.29E+00	1.29E+00
0	0	2.10E+11	8.07E+10	1.29E+00	1.29E+00

#13	#14	#15	#16	#17	#18	#19
5.56E+00	5.00E-01	0.5	9.96E-01	0.00E+00	0	0
5.56E+00	5.00E-01	0.5	9.96E-01	0.00E+00	0	0
5.56E+00	5.00E-01	0.5	9.96E-01	0.00E+00	0	0
5.56E+00	5.00E-01	0.5	9.96E-01	0.00E+00	0	0

Table A4b: Structural input parameters of the hub.

Blades

#1	#2	#3	#4	#5	#6
0.00E+00	715.02	0	0	1.4329	1.4329
2.00E-01	715.02	0	0	1.4329	1.4329
1.20E+00	814.46	0.023	0	1.4114	1.3787
2.20E+00	779.91	0.015185	0	1.3046	1.4142
3.20E+00	779.37	0.020771	0	1.1808	1.4859
4.20E+00	623.99	0.053098	0	1.0946	1.4733
5.20E+00	474.21	0.10216	0	1.0144	1.424
6.20E+00	446.59	0.1441	0	0.94452	1.3999
7.20E+00	421.93	0.19379	0	0.87764	1.3655
8.20E+00	402.37	0.2352	0	0.82741	1.2841
9.20E+00	420.9	0.29578	0	0.75965	1.2605
1.02E+01	448.98	0.31078	0	0.67846	1.2768
1.12E+01	438.97	0.30459	0	0.59155	1.3671
1.22E+01	427.77	0.26727	0	0.53156	1.4802
1.32E+01	401.69	0.27417	0	0.49056	1.4328
1.42E+01	371.57	0.31606	0	0.45589	1.3278
1.52E+01	368.05	0.31747	0	0.42509	1.2982
1.62E+01	364.96	0.32056	0	0.40489	1.2587
1.82E+01	357.37	0.32672	0	0.36722	1.1731
2.02E+01	347.54	0.3421	0	0.33157	1.0968
2.22E+01	339.1	0.33435	0	0.29304	1.0396
2.42E+01	330.5	0.32595	0	0.25571	0.98261
2.62E+01	310.4	0.35419	0	0.21267	0.89483
2.82E+01	302.38	0.33463	0	0.17216	0.82411
3.02E+01	277.34	0.33984	0	0.14187	0.74459
3.22E+01	266.66	0.32462	0	0.11502	0.711
3.42E+01	254.51	0.30262	0	0.091652	0.67159

Table A5a: Structural input parameters of the blades.

3.62E+01	232.36	0.28762	0	0.078511	0.60963
3.82E+01	210.94	0.26162	0	0.066284	0.57837
4.02E+01	188.94	0.22362	0	0.055369	0.54353
4.22E+01	173.87	0.13362	0	0.044026	0.59781
4.42E+01	162.62	0.10762	0	0.040237	0.55171
4.62E+01	146.32	0.12662	0	0.03698	0.50191
4.82E+01	136.44	0.10962	0	0.032873	0.47312
5.02E+01	112.96	0.11663	0	0.032024	0.42087
5.22E+01	104.03	0.090626	0	0.028459	0.38969
5.42E+01	95.044	0.064628	0	0.023538	0.36465
5.52E+01	87.412	0.052592	0	0.024544	0.36404
5.62E+01	76.781	0.12521	0	0.023423	0.27715
5.72E+01	72.427	0.10983	0	0.020886	0.26964
5.77E+01	69.786	0.097601	0	0.021278	0.25768
5.82E+01	62.494	0.14131	0	0.018359	0.19472
5.87E+01	58.886	0.13109	0	0.013373	0.17437
5.92E+01	55.273	0.11984	0	0.013803	0.15617
5.97E+01	51.724	0.11059	0	0.014269	0.13908
6.02E+01	48.253	0.10318	0	0	0.12182
6.07E+01	43.884	0.096321	0	0	0.096744
6.12E+01	12.062	0.072459	0	0	0.083577
6.15E+01	10.867	0.060136	0	0	0.069609

Table A5b: Structural input parameters of the blades.

#7	#8	#9	#10	#11	#12
0	0	1.40E+10	1.00E+09	1.2936	1.2938
0	0	1.40E+10	1.00E+09	1.2936	1.2938
0	0	1.40E+10	1.00E+09	1.3875	1.397
0.018185	0	1.40E+10	1.00E+09	1.2469	1.3927
0.063771	0	1.40E+10	1.00E+09	1.092	1.4135
0.1121	0	1.40E+10	1.00E+09	0.77017	1.0613
0.16716	0	1.40E+10	1.00E+09	0.51641	0.73004
0.2211	0	1.40E+10	1.00E+09	0.45068	0.65319
0.27779	0	1.40E+10	1.00E+09	0.39488	0.57594
0.3372	0	1.40E+10	1.00E+09	0.35572	0.49175
0.40378	0	1.40E+10	1.00E+09	0.35263	0.50066
0.46878	0	1.40E+10	1.00E+09	0.33512	0.51198
0.52659	0	1.40E+10	1.00E+09	0.2821	0.5194
0.57527	0	1.40E+10	1.00E+09	0.24189	0.50584
0.57817	0	1.40E+10	1.00E+09	0.20955	0.44604
0.58106	0	1.40E+10	1.00E+09	0.1835	0.36064
0.57647	0	1.40E+10	1.00E+09	0.17062	0.35346
0.57056	0	1.40E+10	1.00E+09	0.16229	0.34343
0.55872	0	1.40E+10	1.00E+09	0.14643	0.32153

Table A5c: Structural input parameters of the blades.

0.5461	0	1.40E+10	1.00E+09	0.13059	0.30315
0.53335	0	1.40E+10	1.00E+09	0.11348	0.28538
0.51895	0	1.40E+10	1.00E+09	0.097281	0.26791
0.50419	0	1.40E+10	1.00E+09	0.078741	0.24622
0.48863	0	1.40E+10	1.00E+09	0.062557	0.22422
0.47284	0	1.40E+10	1.00E+09	0.048664	0.1953
0.45762	0	1.40E+10	1.00E+09	0.038194	0.18249
0.44262	0	1.40E+10	1.00E+09	0.029207	0.16672
0.42762	0	1.40E+10	1.00E+09	0.022467	0.13062
0.41262	0	1.40E+10	1.00E+09	0.017045	0.11315
0.39762	0	1.40E+10	1.00E+09	0.012563	0.094526
0.38262	0	1.40E+10	1.00E+09	0.0090007	0.084549
0.36762	0	1.40E+10	1.00E+09	0.0076614	0.072869
0.35262	0	1.40E+10	1.00E+09	0.0064914	0.056986
0.33762	0	1.40E+10	1.00E+09	0.0054507	0.050686
0.32263	0	1.40E+10	1.00E+09	0.0043607	0.037014
0.30763	0	1.40E+10	1.00E+09	0.0035343	0.032491
0.29263	0	1.40E+10	1.00E+09	0.0028114	0.028223
0.28359	0	1.40E+10	1.00E+09	0.0024764	0.025266
0.27321	0	1.40E+10	1.00E+09	0.0021721	0.021766
0.26283	0	1.40E+10	1.00E+09	0.0018943	0.020101
0.2516	0	1.40E+10	1.00E+09	0.0017029	0.018694
0.23631	0	1.40E+10	1.00E+09	0.0014021	0.011344
0.22109	0	1.40E+10	1.00E+09	0.0011429	0.0098486
0.20584	0	1.40E+10	1.00E+09	0.00091643	0.008485
0.19059	0	1.40E+10	1.00E+09	0.00072	0.0072593
0.17418	0	1.40E+10	1.00E+09	0.00053929	0.0060764
0.15032	0	1.40E+10	1.00E+09	0.00032857	0.00459
0.12646	0	1.40E+10	1.00E+09	1.79E-05	0.00047214
0.11214	0	1.40E+10	1.00E+09	1.21E-05	0.00035786

Table A5d: Structural input parameters of the blades.

#13	#14	#15	#16	#17	#18	#19
5.5644	0.5	0.5	0.99592	0	0	0
5.5644	0.5	0.5	0.99592	0	0	0
5.4316	0.5	0.5	1.0754	0	0	0
4.994	0.5	0.5	0.97914	0	0.018185	0
4.6666	0.5	0.5	0.95216	0	0.063771	0
3.4747	0.5	0.5	0.71295	0	0.1121	0
2.3235	0.5	0.5	0.49188	0	0.16716	0
1.9079	0.5	0.5	0.432	0	0.2211	0
1.5704	0.5	0.5	0.37711	0	0.27779	0
1.1583	0.5	0.5	0.31862	0	0.3372	0
1.0021	0.5	0.5	0.30924	0	0.40378	0

Table A5e: Structural input parameters of the blades.

0.8559	0.5	0.5	0.31864	0	0.46878	0
0.67227	0.5	0.5	0.33037	0	0.52659	0
0.54749	0.5	0.5	0.35888	0	0.57527	0
0.44884	0.5	0.5	0.31249	0	0.57817	0
0.33592	0.5	0.5	0.24856	0	0.58106	0
0.31135	0.5	0.5	0.23297	0	0.57647	0
0.29194	0.5	0.5	0.2164	0	0.57056	0
0.261	0.5	0.5	0.18321	0	0.55872	0
0.22882	0.5	0.5	0.15484	0	0.5461	0
0.20075	0.5	0.5	0.13436	0	0.53335	0
0.17438	0.5	0.5	0.11569	0	0.51895	0
0.14447	0.5	0.5	0.089127	0	0.50419	0
0.11998	0.5	0.5	0.072939	0	0.48863	0
0.08119	0.5	0.5	0.054209	0	0.47284	0
0.06909	0.5	0.5	0.047071	0	0.45762	0
0.05745	0.5	0.5	0.039714	0	0.44262	0
0.04592	0.5	0.5	0.029913	0	0.42762	0
0.03598	0.5	0.5	0.024434	0	0.41262	0
0.02744	0.5	0.5	0.019308	0	0.39762	0
0.0209	0.5	0.5	0.021286	0	0.38262	0
0.01854	0.5	0.5	0.01711	0	0.36762	0
0.01628	0.5	0.5	0.012652	0	0.35262	0
0.01453	0.5	0.5	0.01045	0	0.33762	0
0.00907	0.5	0.5	0.0069136	0	0.32263	0
0.00806	0.5	0.5	0.0056886	0	0.30763	0
0.00708	0.5	0.5	0.0046186	0	0.29263	0
0.00609	0.5	0.5	0.0039186	0	0.28359	0
0.00575	0.5	0.5	0.0020029	0	0.27321	0
0.00533	0.5	0.5	0.0017936	0	0.26283	0
0.00494	0.5	0.5	0.0015871	0	0.2516	0
0.00424	0.5	0.5	0.00080929	0	0.23631	0
0.00366	0.5	0.5	0.000615	0	0.22109	0
0.00313	0.5	0.5	0.00046	0	0.20584	0
0.00264	0.5	0.5	0.00034071	0	0.19059	0
0.00217	0.5	0.5	0.00024286	0	0.17418	0
0.00158	0.5	0.5	0.00013857	0	0.15032	0
0.00025	0.5	0.5	2.71E-05	0	0.12646	0
0.00019	0.5	0.5	1.64E-05	0	0.11214	0

Table A5f: Structural input parameters of the blades.

A3 Statistical load extrapolations

For each of the extrapolated parameters, a table that makes up the basis for the statistical extrapolation is presented. A figure with a plot of the data, fitted to a line, is also presented. The plots are made with $\ln(x-\gamma)$ along the horizontal axis, and $\ln\left(-\ln\left(1-F_X(x)\right)\right)$ along the vertical axis. Further explanation of the extrapolation method can be found in [17].

DLC 1.1 Out-of-plane blade tip deflection

Interval [m]	# of obs.	Cum. # of obs. (Nx)	Nx/(N+1) (Fx)	ln(-ln(1-Fx))	ln(x - γ)
8.0≤x<8.2	1	1	0.0323	-3.4176	-1.0498
8.2≤x<8.4	3	4	0.1290	-1.9794	-0.5978
8.4≤x<8.6	2	6	0.1935	-1.5366	-0.2877
8.6≤x<8.8	6	12	0.3871	-0.7143	-0.0513
8.8≤x<9.0	3	15	0.4839	-0.4134	0.1398
9.0≤x<9.2	4	19	0.6129	-0.0523	0.3001
9.2≤x<9.4	4	23	0.7419	0.3035	0.4383
9.4≤x<9.6	3	26	0.8387	0.6013	0.5596
9.6≤x<9.8	0	26	0.8387	0.6013	0.6678
9.8≤x<10.0	3	29	0.9355	1.0083	0.7655
10.0≤x<10.2	1	30	0.9677	1.2337	0.8544

Table A6: Basis for statistical extrapolation of out-of-plane blade tip deflection, DLC 1.1.

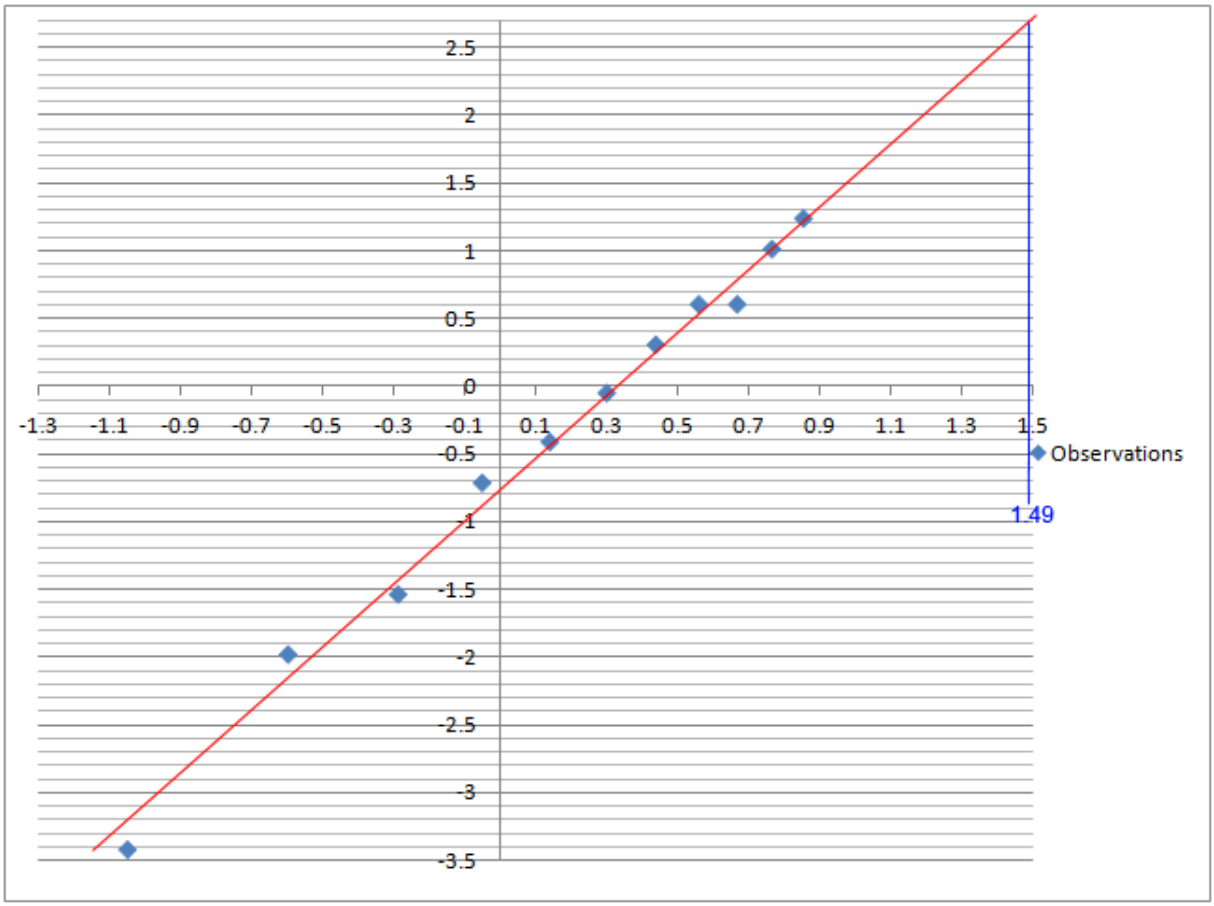

Figure A2: Plot of data using =7.85. The value of 1.49 corresponds to a blade tip deflection of 12.3 m.

DLC 1.1 Out-of-plane blade root bending moment

Interval [kNm]	# of obs.	Cum. # of obs. (Nx)	Nx/(N+1) (Fx)	ln(-ln(1-Fx))	ln(x -)
13 450≤x<13 900	1	1	0.0323	-3.4176	6.5511
13 900≤x<14 350	3	4	0.1290	-1.9794	7.0475
14 350≤x<14 800	5	9	0.2903	-1.0702	7.3778
14 800≤x<15 250	4	13	0.4194	-0.6095	7.6256
15 250≤x<15 700	7	20	0.6452	0.0355	7.8240
15 700≤x<16 150	2	22	0.7097	0.2125	7.9896
16 150≤x<16 600	2	24	0.7742	0.3975	8.1315
16 600≤x<17 050	3	27	0.8710	0.7167	8.2558
17 050≤x<17 500	2	29	0.9355	1.0083	8.3664
17 500≤x<17 950	1	30	0.9677	1.2337	8.4659

Table A7: Basis for statistical extrapolation of out-of-plane blade root bending moment, DLC 1.1.

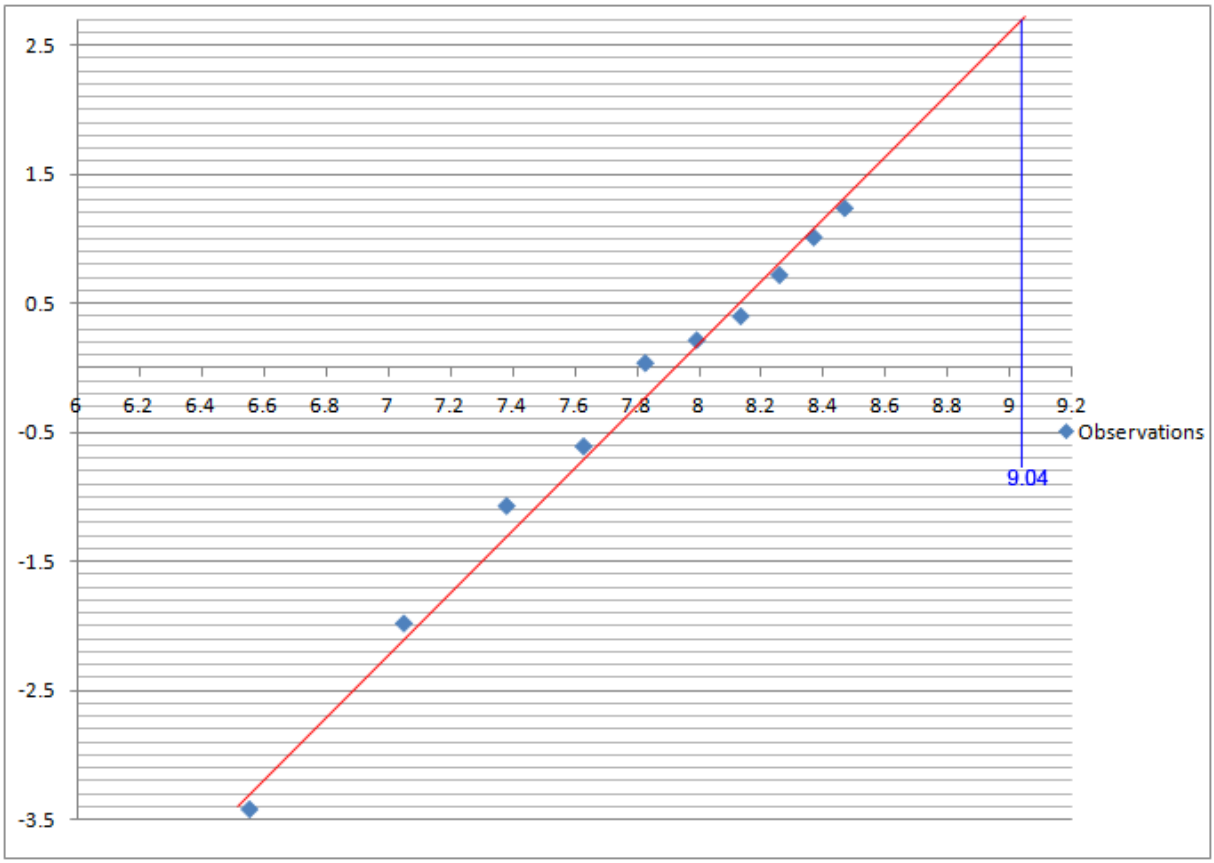

Figure A3: Plot of data using =13 200. The value of 9.04 corresponds to an out-of-plane blade root bending moment of 21 600 kNm.

DLC 1.1 In-plane blade root bending moment

Interval [kNm]	# of obs.	Cum. # of obs. (Nx)	Nx/(N+1) (Fx)	ln(-ln(1-Fx))	ln(x -)
6 160≤x<6 410	1	1	0.0323	-3.4176	6.6333
6 410≤x<6 660	1	2	0.0645	-2.7077	6.9177
6 660≤x<6 910	1	3	0.0968	-2.2849	7.1389
6 910≤x<7 160	1	4	0.1290	-1.9794	7.3199
7 160≤x<7 410	7	11	0.3548	-0.8250	7.4731
7 410≤x<7 660	4	15	0.4839	-0.4134	7.6059
7 660≤x<7 910	6	21	0.6774	0.1235	7.7231
7 910≤x<8 160	3	24	0.7742	0.3975	7.8280
8 160≤x<8 410	3	27	0.8710	0.7167	7.9230
8 410≤x<8 660	2	29	0.9355	1.0083	8.0097
8 660≤x<8 910	1	30	0.9677	1.2337	8.0895

Table A8: Basis for statistical extrapolation of in-plane blade root bending moment, DLC 1.1.

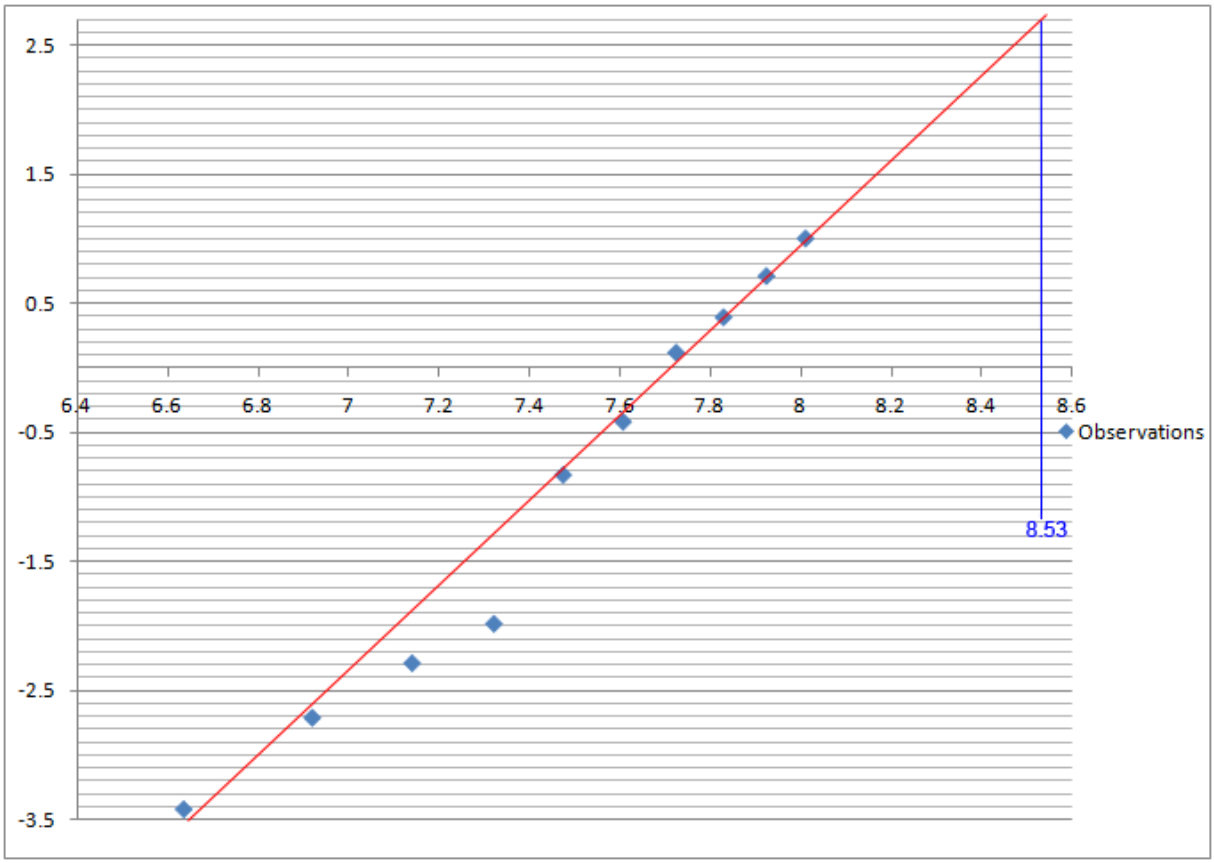

Figure A4: Plot of data using =5 650. The value of 8.53 corresponds to an in-plane blade root bending moment of 10 700 kNm.

DLC 1.1 ONC Out-of-plane blade tip deflection

Interval [m]	# of obs.	Cum. # of obs. (Nx)	Nx/(N+1) (Fx)	ln(-ln(1-Fx))	ln(x -)
8.25≤x<8.50	1	1	0.0323	-3.4176	-1.3863
8.50≤x<8.75	0	1	0.0323	-3.4176	-0.6931
8.75≤x<9.00	5	6	0.1935	-1.5366	-0.2877
9.00≤x<9.25	6	12	0.3871	-0.7143	0.0000
9.25≤x<9.50	7	19	0.6129	-0.0523	0.2231
9.50≤x<9.75	5	24	0.7742	0.3975	0.4055
9.75≤x<10.00	1	25	0.8065	0.4961	0.5596
10.00≤x<10.25	1	26	0.8387	0.6013	0.6931
10.25≤x<10.50	2	28	0.9032	0.8482	0.8109
10.50≤x<10.75	1	29	0.9355	1.0083	0.9163
10.75≤x<11.00	1	30	0.9677	1.2337	1.0116

Table A9: Basis for statistical extrapolation of out-of-plane blade tip deflection, DLC 1.1 ONC.

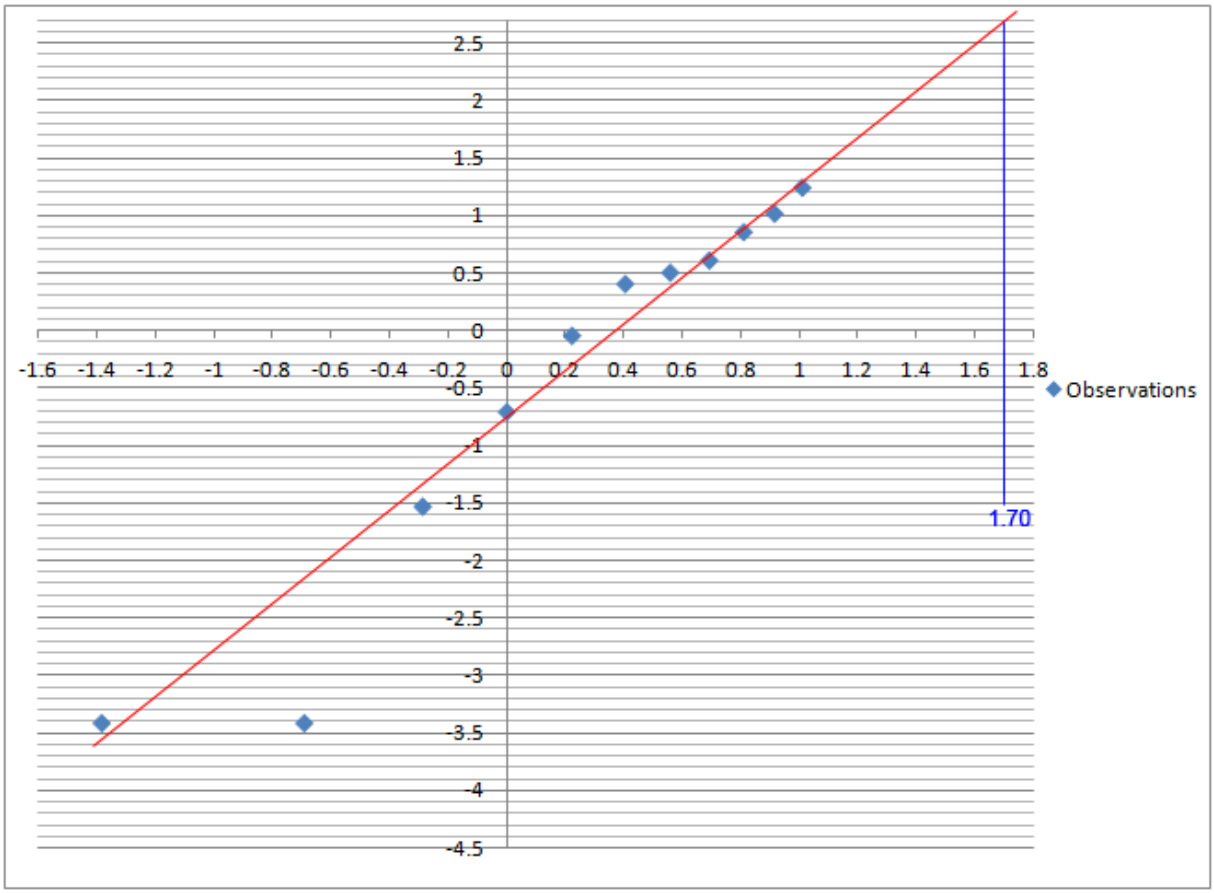

Figure A5: Plot of data using =8.25. The value of 1.70 corresponds to a blade tip deflection of 13.7 m.

DLC 1.1 ONC Out-of-plane blade root bending moment

Interval [kNm]	# of obs.	Cum. # of obs. (Nx)	Nx/(N+1) (Fx)	ln(-ln(1-Fx))	ln(x -)
14 470≤x<14 920	1	1	0.0323	-3.4176	6.0403
14 920≤x<15 370	3	4	0.1290	-1.9794	6.7685
15 370≤x<15 820	7	11	0.3548	-0.8250	7.1854
15 820≤x<16 270	5	16	0.5161	-0.3203	7.4787
16 270≤x<16 720	8	24	0.7742	0.3975	7.7053
16 720≤x<17 170	2	26	0.8387	0.6013	7.8898
17 170≤x<17 620	0	26	0.8387	0.6013	8.0456
17 620≤x<18 070	0	26	0.8387	0.6013	8.1803
18 070≤x<18520	1	27	0.8710	0.7167	8.2990
18520≤x<18970	2	29	0.9355	1.0083	8.4051
18970≤x<19 420	1	30	0.9677	1.2337	8.5011

Table A10: Basis for statistical extrapolation of out-of-plane blade root bending moment, DLC 1.1 ONC.

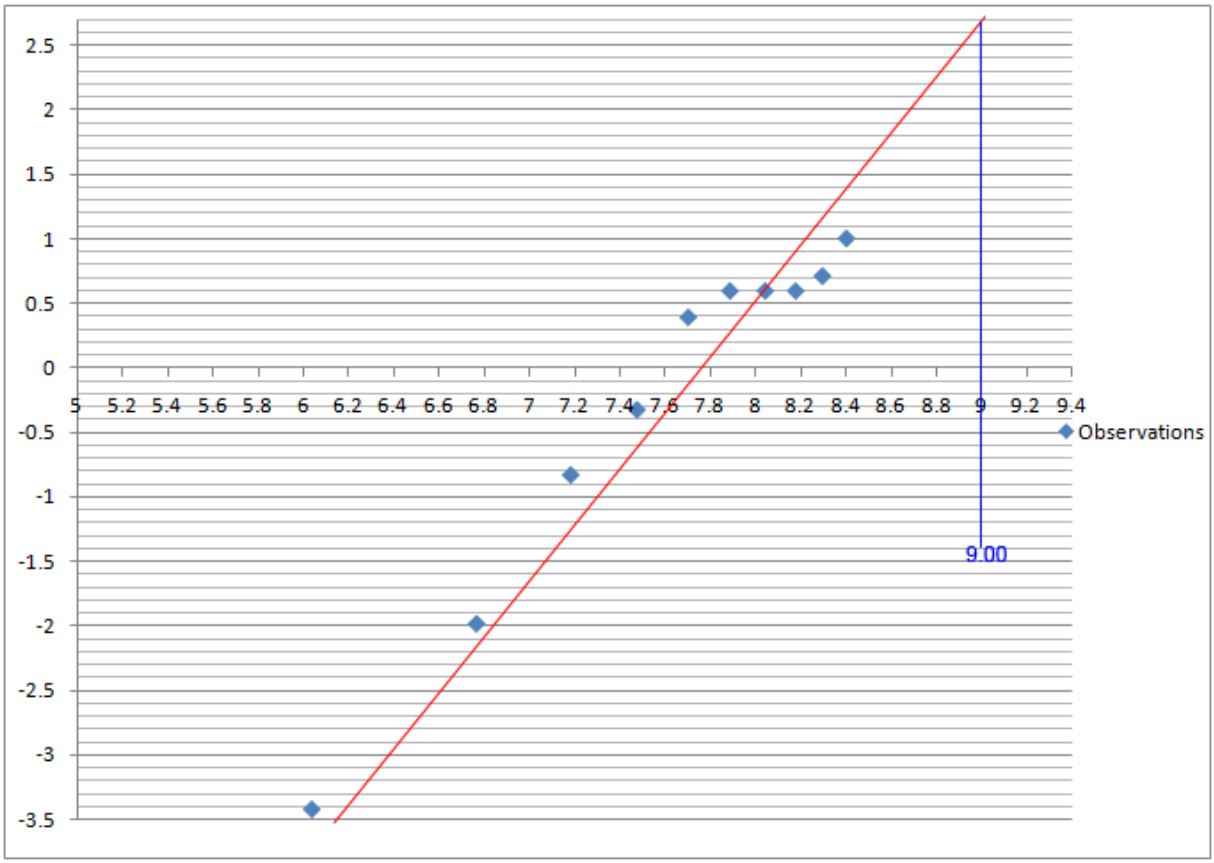

Figur A6: Plot of data using =14 500. The value of 9.00 corresponds to an out-of-plane blade root bending moment of 22 600 kNm.

DLC 1.1 ONC In-plane blade root bending moment

Interval [kNm]	# of obs.	Cum. # of obs. (Nx)	Nx/(N+1) (Fx)	ln(-ln(1-Fx))	ln(x -)
6 150≤x<6 310	1	1	0.0323	-3.4176	4.7005
6 410≤x<6 660	1	2	0.0645	-2.7077	5.5984
6 660≤x<6 910	4	6	0.1935	-1.5366	6.0638
6 910≤x<7 160	7	13	0.4194	-0.6095	6.3801
7 160≤x<7 410	1	14	0.4516	-0.5095	6.6201
7 410≤x<7 660	7	21	0.6774	0.1235	6.8134
7 660≤x<7 910	4	25	0.8065	0.4961	6.9754
7 910≤x<8 160	1	26	0.8387	0.6013	7.1148
8 160≤x<8 410	1	27	0.8710	0.7167	7.2371
8 410≤x<8 660	1	28	0.9032	0.8482	7.3460
8 660≤x<8 910	2	30	0.9677	1.2337	7.4442

Table A11: Basis for statistical extrapolation of in-plane blade root bending moment, DLC 1.1 ONC.

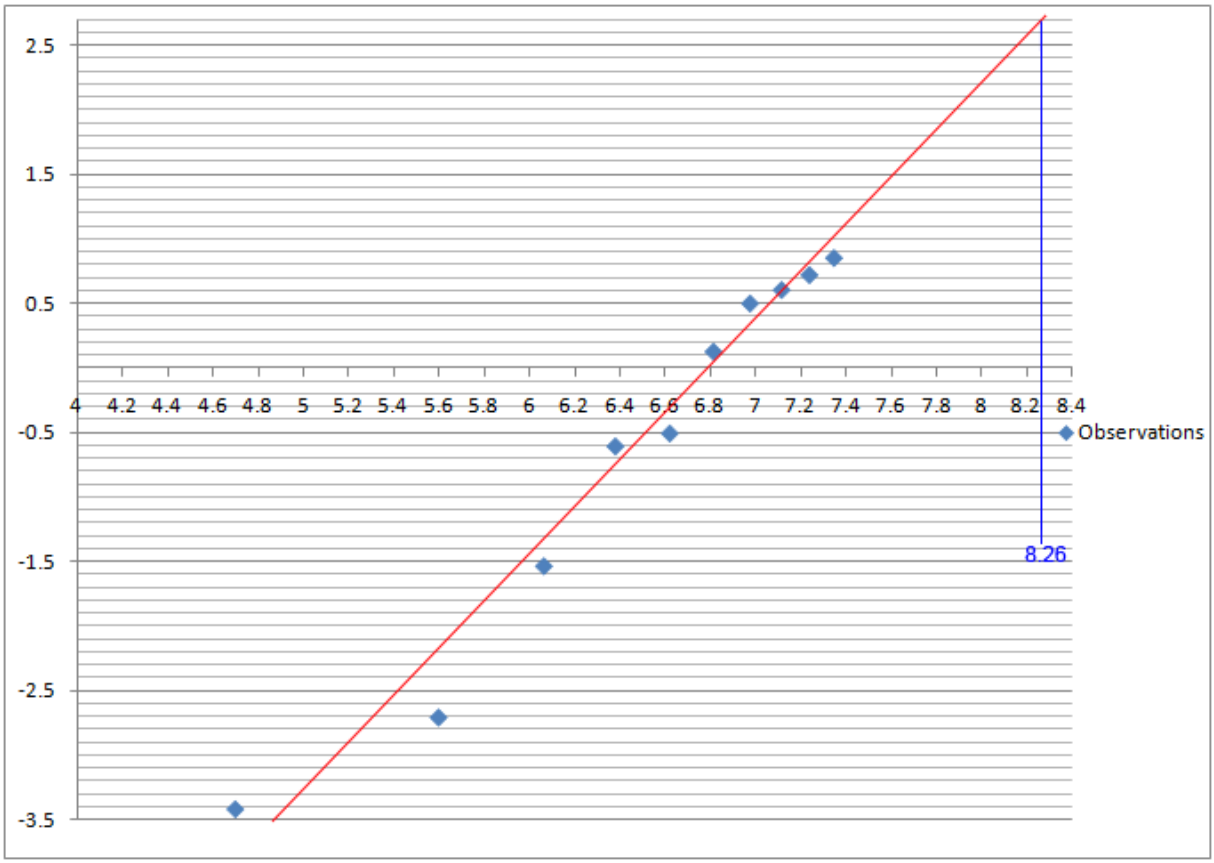

Figure A7: Plot of data using =6 200. The value of 8.26 corresponds to an in-plane blade root bending moment of 10 100 kNm.

A2 Example of HAWC2 main input file

In the following an example of a complete HAWC2 input file is presented. The file is made for a simulation of DLC 1.1. In addition to the main input file, a complete HAWC2 simulation requires several secondary input files, containing e.g. the structural parameters or the pitch controller inputs.

DLC 1.1 main input file

```
begin Simulation;
 time_stop    800.0 ;
  solvertype   1 ;    (newmark)
  on_no_convergence continue ;
  logfile ./log_dlc/DLC11s1.log ;
  animation ./ani_dlc/DLC11s1.dat;
;
  begin newmark;
    deltat    0.025;
   symmetry 2 ;  assymetric solver
  end newmark;
end simulation;
;
begin new_htc_structure;
```

```
  beam_output_file_name  ./log_dlc/DLC11_beam.dat;
  body_output_file_name  ./log_dlc/DLC11_body.dat;
  body_eigenanalysis_file_name ./eigen_dlc/DLC11_body_eigen.dat;
  structure_eigenanalysis_file_name ./eigen_dlc/DLC11_strc_eigen.dat;
;
  begin main_body;        substructure 110m
    name       substructure ;
    type       timoschenko ;
    nbodies    1 ;
    node_distribution     c2_def ;
    concentrated_mass 1 0.0 0.0 0.0 6.524E6 6.524E6 6.524E6 6.524E6 ;
    concentrated_mass 14 0.0 0.0 0.0 1E5 1E5 1E5 1E5 ;
    damping   4.5E-02 4.5E-02 8.0E-01 1.2E-03 1.2E-03 4.5E-04 ;
    begin timoschenko_input;
      filename ./spar/spar_struc.nrl ;
      set 1 1 ;             set subset
    end timoschenko_input;
    begin c2_def;           Definition of centerline (main_body coordinates)
      nsec 14;
      sec 1 0.0 0.0 0.0    0.0 ;  x,y,z,twist
      sec 2 0.0 0.0 -0.1    0.0 ;  x,y,z,twist
      sec 3 0.0 0.0 -10.0    0.0 ;  x,y,z,twist
      sec 4 0.0 0.0 -20.0    0.0 ;  x,y,z,twist
      sec 5 0.0 0.0 -30.0    0.0 ;  x,y,z,twist
      sec 6 0.0 0.0 -40.0    0.0 ;  x,y,z,twist       mooring connection point
      sec 7 0.0 0.0 -46.0    0.0 ;  x,y,z,twist
      sec 8 0.0 0.0 -50.0    0.0 ;  x,y,z,twist
      sec 9 0.0 0.0 -60.0    0.0 ;  x,y,z,twist
      sec 10 0.0 0.0 -70.0    0.0 ;  x,y,z,twist
      sec 11 0.0 0.0 -80.0    0.0 ;  x,y,z,twist
      sec 12 0.0 0.0 -92.57    0.0 ;  x,y,z,twist          cone start
      sec 13 0.0 0.0 -99.22    0.0 ;  x,y,z,twist          cone end
      sec 14 0.0 0.0 -110.0    0.0 ;  x,y,z,twist          substructure flange
    end c2_def ;
  end main_body;
;
  begin main_body;        tower 80m
    name       tower ;
    type       timoschenko ;
    nbodies    1 ;
    node_distribution     c2_def ;
    damping   5.0E-02 5.0E-02 8.0E-01 1.0E-03 1.0E-03 4.5E-04 ;
    concentrated_mass 10 0.0 1.9 0.0 2.4E5 9.126E5 9.126E5 1E5 ;
    begin timoschenko_input;
      filename ./spar/spar_struc.nrl ;
      set 2 1 ;             set subset
    end timoschenko_input;
    begin c2_def;           Definition of centerline (main_body coordinates)
      nsec 10;
      sec 1 0.0 0.0 0.0    0.0 ;  x,y,z,twist
      sec 2 0.0 0.0 -10.0  0.0 ;
      sec 3 0.0 0.0 -20.0  0.0 ;
      sec 4 0.0 0.0 -30.0  0.0 ;
```

```
    sec 5 0.0 0.0 -40.0  0.0 ;
    sec 6 0.0 0.0 -50.0  0.0 ;
    sec 7 0.0 0.0 -60.0 0.0 ;
    sec 8 0.0 0.0 -77.6 0.0 ;
    sec 9 0.0 0.0 -79.14 0.0 ;
    sec 10 0.0 0.0 -79.56 0.0 ;
   end c2_def ;
  end main_body;
;
  begin main_body;
   name       shaft ;
   type       timoschenko ;
   nbodies    1 ;
   node_distribution     c2_def ;
   damping   3.0e-05 3.0e-05 4.0e-02 3.0e-07 3.0e-07 4.5e-03 ;
   concentrated_mass 1 0.0 0.0 0.0 10.0 1E5 1E5 5.026E6 ;
   begin timoschenko_input;
    filename ./data/hawc_st_new2.nrl ;
    set 2 1 ;              set subset   1=flexible,2=stiff
   end timoschenko_input;
   begin c2_def;             Definition of centerline (main_body coordinates)
    nsec 5;
    sec 1 0.0 0.0 0.0     0.0 ; Tower top x,y,z,twist
    sec 2 0.0 0.0 0.1     0.0 ; Generator end
    sec 3 0.0 0.0 1.96256 0.0 ; Gearbox position
    sec 4 0.0 0.0 3.10710 0.0 ; Main bearing
    sec 5 0.0 0.0 5.01910 0.0 ; Rotor centre
   end c2_def ;
  end main_body;
;
  begin  main_body;
   name  hub1  ;
   type  timoschenko  ;
   nbodies  1  ;
   node_distribution  uniform 2  ;
   damping  2.00E-04  2.00E-04  2.00E-03  3.00E-05  3.00E-05  2.00E-04  ;
   begin  timoschenko_input;
    filename  ./data/hawc_st_new2.nrl  ;
    set  3  1  ;
   end  timoschenko_input;
   begin  c2_def;  Definition  of  centerline  (main_body  coordinates)
    nsec  4;
    sec  1  0.00E+00  0.00E+00  0.00E+00  0.00E+00  ;  x,y,z,twist
    sec  2  0.00E+00  0.00E+00  0.50E+00  0.00E+00  ;
    sec  3  0.00E+00  0.00E+00  1.00E+00  0.00E+00  ;
    sec  4  0.00E+00  0.00E+00  1.50E+00  0.00E+00  ;
   end  c2_def  ;
  end  main_body;
;
  begin  main_body;
   name  hub2  ;
   copy_main_body  hub1;
  end  main_body;
```

```
;
 begin  main_body;
  name  hub3  ;
  copy_main_body  hub1;
 end  main_body;
;
 begin main_body;
  name       blade1 ;
  type       timoschenko ;
  nbodies    9 ;
  node_distribution    c2_def ;
  damping   3.0e-2 2.2e-2 4.0e-2 5.9e-4 1.9e-3 5.0e-4 ;
  begin timoschenko_input;
   filename ./data/hawc_st_new2.nrl ;
   set 1 9 ;              set subset      1=flexible with shear flex. , 2=flex without shear flex, 3=stiff
  end timoschenko_input;
  begin c2_def;           Definition of centerline (main_body coordinates)
   nsec 19;
          sec       1       0.000    0.000    0.000    0.000    ;        x,y,z,twist
          sec       2       -0.010   0.000    1.367    -13.308  ;        x,y,z,twist
          sec       3       -0.100   0.000    4.100    -13.308  ;        x,y,z,twist
          sec       4       -0.250   0.000    6.833    -13.308  ;        x,y,z,twist
          sec       5       -0.450   0.000    10.250   -13.308  ;        x,y,z,twist
          sec       6       -0.582   0.000    14.350   -11.480  ;        x,y,z,twist
          sec       7       -0.557   0.000    18.450   -10.162  ;        x,y,z,twist
          sec       8       -0.531   0.000    22.550   -9.011   ;        x,y,z,twist
          sec       9       -0.501   0.000    26.650   -7.795   ;        x,y,z,twist
          sec       10      -0.470   0.000    30.750   -6.600   ;        x,y,z,twist          50%blade          radius
          sec       11      -0.438   0.000    34.850   -5.361   ;        x,y,z,twist
          sec       12      -0.407   0.000    38.950   -4.188   ;        x,y,z,twist
          sec       13      -0.376   0.000    43.050   -3.125   ;        x,y,z,twist
          sec       14      -0.346   0.000    47.150   -2.319   ;        x,y,z,twist
          sec       15      -0.315   0.000    51.250   -1.526   ;        x,y,z,twist
          sec       16      -0.289   0.000    54.667   -0.863   ;        x,y,z,twist
          sec       17      -0.261   0.000    57.400   -0.370   ;        x,y,z,twist
          sec       18      -0.177   0.000    60.133   -0.106   ;        x,y,z,twist
          sec       19      -0.104   0.000    61.500   0.000    ;        x,y,z,twist
  end c2_def ;
 end main_body;
;
 begin main_body;
  name        blade2 ;
  copy_main_body blade1;
 end main_body;
;
 begin main_body;
  name        blade3 ;
  copy_main_body blade1 ;
 end main_body;
;
 begin orientation;
  begin base;
   body  substructure;
```

```
    inipos       0.0 0.0 100.0 ;        initial position of node 1
    body_eulerang 0.0 0.0 0.0;
  end base;
;
  begin relative;
    body1   substructure last;
    body2  tower 1;
    body2_eulerang 0.0 0.0 0.0;
  end relative;
;
  begin relative;
    body1  tower last;
    body2  shaft 1;
    body2_eulerang 90.0 0.0 0.0;
    body2_eulerang 5.0 0.0 0.0;    5 deg tilt
    body2_ini_rotvec_d1 0.0 0.0 -1.0 0.5 ; body initial rotation velocity x,y,z,angle velocity[rad/s]  (body 2 coordinates)
  end relative;
;
  begin relative;
    body1  shaft last;
    body2  hub1 1;
    body2_eulerang -90.0 0.0 0.0;
    body2_eulerang 2.5 0.0 0.0;      2.5deg cone
  end relative;
;
  begin relative;
    body1  shaft last;
    body2  hub2 1;
    body2_eulerang -90.0 0.0 0.0;
    body2_eulerang 0.0 -120.0 0.0;
    body2_eulerang 2.5 0.0 0.0;      2.5deg cone
  end relative;
;
  begin relative;
    body1  shaft last;
    body2  hub3 1;
    body2_eulerang -90.0 0.0 0.0;
    body2_eulerang 0.0 120.0 0.0;
    body2_eulerang 2.5 0.0 0.0;      2.5deg cone
  end relative;
;
  begin relative;
    body1  hub1 last;
    body2  blade1 1;
    body2_eulerang 0.0 0.0 0.0;
  end relative;
;
  begin relative;
    body1  hub2 last;
    body2  blade2 1;
    body2_eulerang 0.0 0.0 0.0;
  end relative;
;
```

```
   begin relative;
     body1  hub3 last;
     body2  blade3 1;
     body2_eulerang 0.0 0.0 0.0;
   end relative;
 end orientation;
;-------------------------------------------------------------------
  begin constraint;
   begin bearing1;                free bearing
     name  shaft_rot ;
     body1 tower last;
     body2 shaft 1;
     bearing_vector 2 0.0 0.0 -1.0;       x=coo (0=global,1=body1,2=body2) vector in body2 coordinates where the free
rotation is present
   end bearing1;
;
   begin fix1;
     body1 substructure last;
     body2 tower 1;
   end fix1;
;
   begin fix1;
     body1 shaft last;
     body2 hub1 1;
   end fix1;
;
   begin fix1;
     body1 shaft last;
     body2 hub2 1;
   end fix1;
;
   begin fix1;
     body1 shaft last;
     body2 hub3 1;
   end fix1;
;
   begin bearing2;                forced bearing
     name pitch1;
     body1 hub1 last;
     body2 blade1 1;
     bearing_vector 2 0.0 0.0 -1.0;       x=coo (0=global,1=body1,2=body2) vector in body2 coordinates where the free
rotation is present
   end bearing2;
;
   begin bearing2;                forced bearing
     name pitch2;
     body1 hub2 last;
     body2 blade2 1;
     bearing_vector 2 0.0 0.0 -1.0;       x=coo (0=global,1=body1,2=body2) vector in body2 coordinates where the free
rotation is present
   end bearing2;
;
   begin bearing2;                forced bearing
     name pitch3;
```

```
    body1 hub3 last;
    body2 blade3 1;
    bearing_vector 2 0.0 0.0 -1.0;       x=coo (0=global,1=body1,2=body2) vector in body2 coordinates where the free
rotation is present
   end bearing2;
 end constraint;
;
end new_htc_structure;
;
begin wind ;
 density              1.225 ; to be checked
 wsp                  11.4  ;
 tint                 0.199 ;
 horizontal_input      1    ;          0=false, 1=true
 windfield_rotations    0.0  0.0  0.0 ;    yaw, tilt, rotation
 center_pos0           0.0 0.0 -90.0 ;
 shear_format          3  0.14  ;0=none,1=constant,2=log,3=power,4=linear
 turb_format           1    ;  0=none, 1=mann,2=flex
 tower_shadow_method    1    ;  0=none, 1=potential flow, 2=jet
 wind_ramp_factor   0.0 50 0 1.0 ;
;
 begin mann;
   create_turb_parameters 29.4 1.0 3.9 1 1.0 ;      L, alfaeps,gamma,seed, highfrq compensation
   filename_u    ./turb_dlc/DLC11s1u.bin ;
   filename_v    ./turb_dlc/DLC11s1v.bin ;
   filename_w    ./turb_dlc/DLC11s1w.bin ;
   box_dim_u    8192 2.0508 ;
   box_dim_v    32 3.125;
   box_dim_w    32 3.125;
   std_scaling   1.0 0.7 0.5 ;
 end mann;
;
 begin tower_shadow_potential;
   tower_offset 0.0 ;
   nsec  2;
   radius     0.0   4.0 ;
   radius    -90.0   1.94 ;
 end tower_shadow_potential;
end wind;
;
begin aero ;
 nblades  3;
 hub_vec shaft -3 ;        rotor rotation vector (normally shaft composant directed from pressure to suction side)
 link 1 mbdy_c2_def blade1;
 link 2 mbdy_c2_def blade2;
 link 3 mbdy_c2_def blade3;
 ae_filename       ./data/hawc2nf_ae.NRL ;
 pc_filename       ./data/hawc_pc.NRL ;
 induction_method   1 ;    0=none, 1=normal
 aerocalc_method    1 ;    0=no aerodynamic, 1=with aerodynamic
 aerosections       30 ;
 ae_sets           1 1 1;
 tiploss_method     1 ;    0=none, 1=prandtl
 dynstall_method    2 ;    0=none, 1=stig øye method,2=mhh method
```

```
end aero ;
;
begin aerodrag ;
 begin aerodrag_element ;
  mbdy_name tower;
  aerodrag_sections uniform 10 ;
  nsec 2 ;
  sec 0.0 0.6 6.0 ;  tower bottom
  sec 79.56 0.6 3.87 ;  tower top
 end aerodrag_element;
;
 begin aerodrag_element ;       Nacelle drag side
  mbdy_name shaft;
  aerodrag_sections uniform 2 ;
  nsec 2 ;
  sec 0.0   0.8 10.0 ;
  sec 5.02  0.8 10.0 ;
 end aerodrag_element;
end aerodrag;
;
begin dll;
 begin hawc_dll;
  filename  ./control/basic_3ba_ct10nl.dll ;
  dll_subroutine regulation ;
  arraysizes  25 15 ;
  begin output;
   general constant 1 ;    inputfile extension
   general time ;                                  1
   constraint bearing1 shaft_rot 1 only 2;   speed generator    2
   constraint bearing2 pitch1 1 only 1;                    3
   constraint bearing2 pitch2 1 only 1;                    4
   constraint bearing2 pitch3 1 only 1;                    5
   wind free_wind 1 0.0 0.0 -123.0 ; coordsys
   general constant 0.4885 ;   Kp  pitch                    9
   general constant 0.0306 ;  Ki   pitch                   10
   general constant 0.00 ;      Kd   pitch                11
   general constant 7.688E6 ;  Kp   torque                  12
   general constant 6.901E5  ;  Ki   torque                 13
   general constant 0.0       ;  Kd   torque               14
   general constant 800 ;  generator stoptime
   general constant 0.2 ;    pitch stopdelay
   general constant 8 ;    pitch stop velmax
   general constant 0 ;      stop type (not used)
   general constant -1 ;      cut-in time
   general constant 10 ;   max pitch velocity operation
  end output;
 end hawc_dll;
;
 begin hawc_dll;
  filename  ./control/basic_3ba_ct10nl.dll ;
  dll_subroutine generator ;
  arraysizes  15 15 ;
;   deltat    0.02 ;
```

```
   begin output;
     general time ;
     dll inpvec 1 1; input til h2, dll no 1, plads no 1
     general constant 0.93;       Efficiency factor
     constraint bearing1 shaft_rot 1 only 2;   speed generator
     general constant 1.0 ;
   end output;
;
   begin actions;
     mbdy moment_int shaft 1 -3 shaft tower 10 ;   generator torque LSS
   end actions;
 end hawc_dll;
;
 begin hawc_dll;
   filename  ./control/basic_3ba_ct10nl.dll ;
   dll_subroutine pitchservo ;
   arraysizes  15 15 ;
;    deltat    0.02 ;
   begin output;
     general time ;
     dll inpvec 1 2;
     dll inpvec 1 3;
     dll inpvec 1 4;
     constraint bearing2 pitch1 1 only 1;                    3
     constraint bearing2 pitch2 1 only 1;                    4
     constraint bearing2 pitch3 1 only 1;                    5
   end output;
;
   begin actions;
     constraint bearing2 angle pitch1;
     constraint bearing2 angle pitch2;
     constraint bearing2 angle pitch3;
   end actions;
 end hawc_dll;
end dll;
;
begin force;
 begin dll;
            dll ./DemoDLL/m60.dll;  Name of DLL
            update DemoForceDLL; Name of subroutine
            mbdy substructure;
            node 6;  ode ; Node number (1 is body origin)
  end dll;
end force;
;
begin hydro;
  begin water_properties;
    rho 1025 ; kg/m^3
    gravity 9.816 ; m/s^2
    mwl 0.0 ;
    mudlevel 200 ;
    current 2 0.114 0.5 0;
    water_kinematics_dll ./wkin_dll.dll   ./hydro_dlc/dlc11s1.inp ;
```

```
  end water_properties;
  ;
  begin hydro_element;
    mbdy_name substructure ;
    buoyancy 1;
    update_states 1;
    hydrosections auto 2 ; distribution of hydro calculation points from sec 1 to nsec
    nsec 14;
    sec     0.00      1.000     1.000     83.3      83.3      10.3      0.000 ;
    sec     10.00  1.000  1.000  83.3  83.3      10.3      0.000 ;
    sec     20.00  1.000  1.000  83.3  83.3      10.3      0.000 ;
    sec     30.00  1.000  1.000  83.3  83.3      10.3      0.000 ;
    sec     40.00  1.000  1.000  83.3  83.3      10.3      0.000 ;
    sec     50.00  1.000  1.000  83.3  83.3      10.3      0.000 ;
    sec     60.00  1.000  1.000  83.3  83.3      10.3      0.000 ;
    sec     70.00  1.000  1.000  83.3  83.3      10.3      0.000 ;
    sec     80.00  1.000  1.000  83.3  83.3      10.3      0.000 ;
    sec     92.56  1.000  1.000  83.3  83.3      10.3      0.000 ;
    sec     92.57  1.000  1.000  83.3  83.3      10.3      0.3233 ;
    sec     99.22  1.000  1.000  28.3  28.3      6.0       0.3233 ;
    sec     99.23  1.000  1.000  28.3  28.3      6.0       0.000 ;
    sec     110.00    1.000     1.000     28.3      28.3      6.0       0.000 ;
  end hydro_element;
;
end hydro;
;
begin output;
  filename ./res_dlc/DLC11s1 ;
  buffer 1 ;
  data_format  hawc_binary;
;
  general time;
  mbdy state pos blade1 18 1 blade1;
  mbdy state pos blade2 18 1 blade2;
  mbdy state pos blade3 18 1 blade3;
  mbdy state pos tower 9 1 global;
  mbdy state acc tower 9 1 global;
  mbdy state_rot axisangle tower 9 1 global;
  mbdy state pos substructure 5 1 global;
  mbdy state acc substructure 5 1 global;
  mbdy state_rot axisangle substructure 5 1 global;
  mbdy forcevec blade1 1 1 blade1;
  mbdy momentvec blade1 1 1 blade1;
  mbdy forcevec blade2 1 1 blade2;
  mbdy momentvec blade2 1 1 blade2;
  mbdy forcevec blade3 1 1 blade3;
  mbdy momentvec blade3 1 1 blade3;
  mbdy forcevec tower 9 2 tower;
  mbdy momentvec tower 9 2 tower;
  mbdy forcevec tower 1 1 tower;
  mbdy momentvec tower 1 1 tower;
  mbdy forcevec substructure 13 1 substructure;
  mbdy momentvec substructure 13 1 substructure;
```

```
  mbdy forcevec substructure 12 1 substructure;
  mbdy momentvec substructure 12 1 substructure;
  mbdy forcevec substructure 5 1 substructure;
  mbdy momentvec substructure 5 1 substructure;
  aero omega;
  aero torque;
  aero power;
  aero thrust;
  aero lambda;
  constraint bearing2 pitch1 5;
  constraint bearing2 pitch2 5;
  constraint bearing2 pitch3 5;
  wind free_wind 1 0.0 0.0 -90.0;
  wind free_wind_hor 1 0.0 0.0 -90.0;
  hydro water_surface 0 0;
end output;
;
exit;
```